

## IMPROVED DISTANCES TO TYPE Ia SUPERNOVAE WITH MULTICOLOR LIGHT-CURVE SHAPES: MLCS2k2

SAURABH JHA,<sup>1,2</sup> ADAM G. RIESS,<sup>3</sup> AND ROBERT P. KIRSHNER<sup>4</sup>

Received 2005 October 26; accepted 2006 December 21

### ABSTRACT

We present an updated version of the multicolor light-curve shape method to measure distances to Type Ia supernovae (SNe Ia), incorporating new procedures for  $K$ -correction and extinction corrections. We also develop a simple model to disentangle intrinsic color variations and reddening by dust and expand the method to incorporate  $U$ -band light curves and to more easily accommodate prior constraints on any of the model parameters. We apply this method to 133 nearby SNe Ia, including 95 objects in the Hubble flow ( $cz \geq 2500 \text{ km s}^{-1}$ ), which give an intrinsic dispersion of less than 7% in distance. The Hubble flow sample, which is of critical importance to all cosmological uses of SNe Ia, is the largest ever presented with homogeneous distances. We find that the Hubble flow SNe with  $H_0 d_{\text{SN}} \geq 7400 \text{ km s}^{-1}$  yield an expansion rate that is  $6.5\% \pm 1.8\%$  lower than the rate determined from SNe within that distance, and this can have a large effect on measurements of the dark energy equation of state with SNe Ia. Peculiar velocities of SN Ia host galaxies in the rest frame of the Local Group are consistent with the dipole measured in the cosmic microwave background. Direct fits of SNe Ia that are significantly reddened by dust in their host galaxies suggest that their mean extinction law may be described by  $R_V \simeq 2.7$ , but optical colors alone provide weak constraints on  $R_V$ .

*Subject headings:* cosmology: observations — distance scale — galaxies: distances and redshifts — supernovae: general

*Online material:* color figures

### 1. INTRODUCTION

The cosmological applications of Type Ia supernovae (SNe Ia) result from precise distances to these calibrated candles. It has been well established that the intrinsic luminosity of SNe Ia is correlated with the shape of their optical light curves (Phillips 1993; Hamuy et al. 1995, 1996a; Riess et al. 1995a, 1996a). Determining a precise distance requires well-observed SN Ia light curves in multiple passbands, to constrain the intrinsic luminosity and extinction by dust along the line of sight to each SN Ia.

A number of methods have been developed to measure calibrated distances from SN Ia multicolor light curves, with each enjoying a similar level of success. The first of these was introduced by Phillips (1993), who noted that the parameter  $\Delta m_{15}(B)$ , the amount by which an SN Ia declined in the  $B$  band during the first 15 days after maximum light, was well correlated with SN Ia intrinsic luminosity. The  $\Delta m_{15}$  method was transformed by Hamuy et al. (1996a), in which  $\Delta m_{15}$  became a parameter in a multidimensional fit to six template  $BVI$  light curves spanning a wide range in  $\Delta m_{15}(B)$  as it was originally defined. Phillips et al. (1999) present the current version of this method, which incorporates measurement of the extinction via late-time  $B - V$  color measurements (roughly independent of  $\Delta m_{15}$ ) and  $B - V$  and  $V - I$  measurements at maximum light (for the measured  $\Delta m_{15}$ , determined in an iterative fashion). Updates to this technique are given by Germany et al. (2004) and Prieto et al. (2006), the latter developing a technique to describe a continuous family of light curves parameterized by  $\Delta m_{15}$ .

Tripp & Branch (1999) present a two-parameter method, empirically correlating SN Ia luminosity to  $\Delta m_{15}$  and maximum light  $B - V$  color, but without regard to the source of the color variation (i.e., extinction or intrinsic variation). Parodi et al. (2000) and Reindl et al. (2005) present similar studies, with empirical correlations between SN Ia maximum light magnitudes in  $BVI$ ,  $\Delta m_{15}$ , and color.

Other methods include the stretch correction of Perlmutter et al. (1997), in which the SN Ia intrinsic luminosity is correlated with a simple stretching of the time axis of a fiducial light curve. This method has been presented in detail for the  $B$  band (Goldhaber et al. 2001) and can be extended straightforwardly to  $U$  and  $V$  (with  $R$  and  $I$  posing more difficulty; Nugent et al. 2002; Knop et al. 2003; Nobili et al. 2005; Jha et al. 2006). Guy et al. (2005) use an innovative approach to constrain the spectral energy distribution (SED) of SNe Ia, parameterized continuously as a function of color and stretch, and allow for the generation of light-curve templates in arbitrary passbands. These methods all determine distances by correlating a distance-dependent parameter (such as peak magnitude in a particular passband, or an average magnitude difference between the observations and templates) and one or more distance-independent parameters (such as color, stretch, or  $\Delta m_{15}$ ).

Wang et al. (2003) describe a novel technique that derives distances based on “light curves” as a function of color rather than time, which may have interesting implications for the physics behind the observed correlations. Finally, Tonry et al. (2003) follow a nonparametric approach, by directly fitting an observed multicolor light curve to a library of nearby SNe Ia and deriving an average distance weighted by the goodness of fit to each object in the library.

Here we describe an updated version of the multicolor light-curve shape method, denoted here as MLCS2k2. Riess et al. (1995a) presented the first incarnation of this method (called LCS as it was based only on  $V$ -band data), in which a continuum

<sup>1</sup> Miller Institute and Department of Astronomy, University of California, Berkeley, CA 94720.

<sup>2</sup> Current address: Kavli Institute for Particle Astrophysics and Cosmology, Stanford Linear Accelerator Center, Menlo Park, CA 94025; saurabh@slac.stanford.edu.

<sup>3</sup> Space Telescope Science Institute, Baltimore, MD 21218.

<sup>4</sup> Harvard-Smithsonian Center for Astrophysics, Cambridge, MA 02138.

of template light curves was created based on a “training set” of SNe Ia with known relative distances and the parameter  $\Delta$ , a particular SN’s under- or overluminosity relative to some fiducial value. The luminosity correction,  $\Delta$ , was used as a parameter in a least-squares fit, resulting in a best-fit distance for each SN, along with a quantitative estimate of the uncertainty. The MLCS method, presented by Riess et al. (1996a), gave the details of the model, as well as incorporating *BVRI* light curves and providing an estimate of extinction by dust. Riess et al. (1998b) updated the training set, using reliable distances measured by the Hubble law in favor of other methods, added a quadratic ( $\Delta^2$ ) term to create the template light curves, and included the effects of covariance in the model. The application of this version of MLCS to nearby SNe Ia and the Hubble constant is given by Jha et al. (1999b).

The MLCS approach has some advantages: by using a relatively large training set to define a continuum of templates, the method becomes less sensitive to peculiarities of individual objects. During the training process, the variance and covariance in the residuals determine the uncertainty in the model, and this is then used to determine statistically reliable estimates of goodness of fit and parameter uncertainties when the model is applied to other objects. The model also attempts a physically motivated separation of extinction by dust from intrinsic color variations (rather than empirical correlations with color) and uses all of the light curves (at all epochs) to constrain the extinction. Finally, the model is easily extended, for example, with the inclusion of a quadratic term in  $\Delta$ , or the incorporation of the *U* band presented here. The major disadvantage is that the method requires accurate estimates of luminosity and extinction for the training set sample in order to construct reliable templates.

We have compiled modern multicolor photoelectric and CCD Johnson/Cousins *UBVRI* data from a variety of sources. The precision of SN Ia distances demands high-quality photometry, and we have relied most heavily on large, homogeneous data sets, such as the observations presented by Hamuy et al. (1996b) from the Calán/Tololo survey (29 SNe Ia), as well as those of Riess et al. (1999) and Jha et al. (2006), consisting of 22 and 44 SNe Ia, respectively, from the CfA monitoring campaign. The complete sample we analyze consists of 133 SNe Ia described in Table 1. For a number of objects we have combined data sets from different sources (for some comparisons see Jha et al. 2006); in some cases we had to make subjective assessments of the relative quality of inconsistent data.

The basic framework for MLCS2k2 was laid out by Jha (2002),<sup>5</sup> and it has already been applied to SN Ia cosmology, including the silver and gold samples of Riess et al. (2004). This work showed that the universe underwent a transition from an epoch of deceleration due to dark matter to current acceleration driven by dark energy, whose inferred properties are consistent with the cosmological constant. In addition, Riess et al. (2005) use MLCS2k2 distances to show that various estimates of  $H_0$  from SNe Ia can be reconciled through the use of modern Cepheid and SN data, deriving  $H_0 = 73 \pm 4$  (statistical)  $\pm 5$  (systematic)  $\text{km s}^{-1} \text{Mpc}^{-1}$ . In this paper we focus only on relative distances to nearby SNe, independent of the zero point derived from external measurements (e.g., Cepheid distances to SN Ia hosts; Freedman et al. 2001; Sandage et al. 2006).

<sup>5</sup> Because the basic algorithms were designed in 2002, we continue to refer to this SN distance fitter as MLCS2k2, even though its implementation, applicability, and robustness have evolved substantially since then. Details of the model presented here, as well as recent updates, can be found at <http://astro.berkeley.edu/~saurabh/mlcs2k2/>.

## 2. GROUNDWORK

Comparison of light curves from many SNe Ia requires understanding and correction for a number of effects to put the photometry on a common basis. These include corrections from the observational photometric system to standard passbands, correction for Galactic extinction, correction for time dilation, and the *K*-correction. We have updated a number of these foundations in our development of MLCS2k2.

### 2.1. *K*-Correction

The stretching and shifting of spectra due to the cosmological expansion leads to changes in measured flux observed through a fixed detector passband as a function of redshift. *K*-corrections for SNe Ia in *B* and *V* have been presented by Hamuy et al. (1993), based on spectra of three objects. Kim et al. (1996) provide additional *K*-corrections in *R*, as well as developing a method of “cross filter” *K*-corrections used at high redshift. These methods use a fixed set of spectra to define the *K*-correction for all objects and do not include SED variations arising from intrinsic differences among SNe (either in the detailed spectral features or in the continuum shape) or changes in the SED due to extinction.

Nugent et al. (2002) developed a method that accounts for these variations with a simple, yet effective, “trick” in which both the intrinsic and extinction-related SED variations are affected by adjusting the SED by the  $R_V = 3.1$  extinction law of Cardelli et al. (1989, hereafter CCM89) to match the color of the SN as observed.<sup>6</sup> This procedure is reasonably well motivated; at early times, SNe Ia are in the photospheric phase and the SED is continuum dominated, so that adjustment of the SED by a relatively slowly varying function of wavelength, like the CCM89 extinction law, to match the observed color will do a good job of mimicking the true SED. At late times, much of the color variation is due, in fact, to extinction and so the adjustment is appropriate. Furthermore, the adjustment is done using a color “local” to the spectral region being adjusted, minimizing any adverse effects. The difference in the *K*-correction accounting for these color variations and assuming a constant color for all objects is typically small (generally  $\lesssim 0.1$  mag), but systematic. Nugent et al. (2002) show the efficacy of this color-based procedure.

Our concern in this paper is for accurate *K*-corrections at low redshift ( $z \lesssim 0.1$ ), so we restrict our attention to *K*-corrections within each passband, not the cross filter *K*-correction. We have implemented the Nugent et al. (2002) procedure using a sample of 91 SN Ia spectra covering phases from  $-14$  to  $+92$  days past maximum light, compiled from a number of sources, including archival *International Ultraviolet Explorer* and *Hubble Space Telescope* data, Keck and Lick Observatory SN Ia spectra from UC Berkeley (Filippenko 1997), and unpublished spectra from the CfA SN Ia follow-up program (T. Matheson et al. 2007, in preparation). Of these, 57 spectra extend far enough to the red to cover the *I* passband, while 32 spectra cover the *U* passband in the blue. The number of spectra that cover the *U* band decreases quickly as the spectra are artificially redshifted to calculate the *K*-correction; however, of the 133 SNe Ia described here, the maximum redshift for which there are *U* observations is only  $z \simeq 0.06$ , meaning that that is the extent to which we need to calculate  $K_{UU}$ .

To derive the *K*-corrections, the basic procedure is as follows. For each of *UBVRI* (we adopt the standard Bessell [1990]

<sup>6</sup> Here we use the extinction law to adjust the SED redder or bluer, to match the observed SN color.

TABLE 1  
 SUPERNOVA AND HOST GALAXY DATA

SN Ia	$l^a$ (deg)	$b^a$ (deg)	$cz_{\odot}^b$ (km s <sup>-1</sup> )	$cz_{LG}^b$ (km s <sup>-1</sup> )	$cz_{CMB}^b$ (km s <sup>-1</sup> )	Morphological Type <sup>c</sup>	SN Offsets <sup>d</sup> ("N)	SN Offsets <sup>d</sup> ("E)	$t_1^e$ (days)	Filters	$E(B - V)^f$ (mag)	References
1972E.....	314.84	+30.08	404	190	678	Sd/Irr	-100.0	-38.0	+8.7	UBV	0.056	1
1980N.....	240.16	-56.63	1760	1633	1653	S0	-20.0	+220.0	-1.0	UBVRI	0.021	2
1981B.....	292.97	+64.74	1808	1662	2151	Sbc	+42.0	+39.0	-0.2	UBVR	0.018	3, 4
1981D.....	240.21	-56.69	1760	1633	1653	S0	-100.0	-20.0	-5.3	UBV	0.021	2
1986G.....	309.54	+19.40	547	301	803	S0	-60.0	+120.0	-5.7	UBVRI	0.115	5
1989B.....	241.92	+64.42	703	567	1051	Sb	+50.0	-15.0	-2.5	UBVRI	0.032	6
1990N.....	294.36	+75.98	978	885	1298	Sbc	-1.0	+65.0	-10.4	UBVRI	0.026	7
1990O.....	37.65	+28.35	9193	9340	9175	Sa	-3.9	+21.8	+0.6	BVRI	0.093	8
1990T.....	341.50	-31.53	12112	12025	12013	Sa	-1.9	+24.8	+14.9	BVRI	0.053	8
1990Y.....	232.64	-53.85	11721	11597	11622	E	-5.0	+1.0	+16.2	BVRI	0.008	8
1990af.....	330.81	-42.20	15169	15059	15056	S0	+7.4	-8.0	-3.1	BV	0.035	8
1991M.....	30.36	+45.90	2180	2265	2277	Sc	+60.0	+36.0	+1.8	VRI	0.038	9
1991S.....	214.06	+57.43	16369	16263	16688	Sb	+17.3	+4.4	+10.8	BVRI	0.026	8, 10
1991T.....	292.60	+65.19	1736	1591	2078	Sbc	+44.0	+26.0	-11.1	UBVRI	0.022	7, 10
1991U.....	311.82	+36.20	9503	9292	9801	Sbc	+5.8	-2.2	+10.4	BVRI	0.062	8
1991ag.....	342.56	-31.60	4264	4182	4161	Sb	+22.1	-4.4	+5.6	BVRI	0.062	8
1991bg.....	278.23	+74.46	1060	955	1391	E	-57.0	+2.0	+0.9	BVRI	0.041	11, 12, 13
1992A.....	235.90	-54.06	1877	1747	1781	S0	+62.0	-3.0	-7.0	UBVRI	0.018	10, 14
1992G.....	184.62	+59.84	1565	1541	1827	Sc	-10.0	+27.0	+3.0	VRI	0.020	9
1992J.....	263.55	+23.50	13371	13077	13708	E/S0	+12.0	-11.9	+14.6	BVI	0.057	8
1992K.....	306.28	+16.30	3087	2828	3340	Sb	-15.4	-1.9	+13.6	BVI	0.101	8
1992P.....	295.62	+73.10	7555	7449	7881	Sa	+9.8	-4.3	-0.5	BVI	0.021	8
1992ae.....	332.70	-41.90	22544	22440	22426	E	+4.0	+2.1	+2.5	BV	0.036	8
1992ag.....	312.48	+38.30	7465	7260	7765	Sa	0.0	-3.0	-0.4	BVI	0.097	8
1992al.....	347.33	-38.40	4377	4324	4228	Sb	-12.0	+19.0	-4.9	BVRI	0.034	8
1992aq.....	1.78	-65.30	30519	30536	30254	Sa	-7.1	+2.4	+2.2	BVI	0.012	8
1992au.....	319.11	-65.80	18407	18338	18213	E	+8.9	+21.2	+12.6	BVI	0.017	8
1992bc.....	245.70	-59.60	6056	5933	5936	Sab	-2.0	+16.1	-10.1	BVRI	0.022	8
1992bg.....	274.61	-18.30	10553	10261	10697	Sa	+5.8	-3.4	+4.3	BVI	0.185	8
1992bh.....	267.85	-37.30	13490	13254	13518	Sbc	-3.6	+1.9	-0.6	BVI	0.022	8
1992bk.....	265.01	-48.90	17418	17229	17372	E	+21.1	+11.9	+8.6	BVI	0.015	8
1992bl.....	344.12	-63.90	13101	13076	12871	S0/Sa	-21.8	+15.3	+3.1	BVI	0.011	8
1992bo.....	261.88	-80.30	5666	5636	5435	E/S0	-54.7	-47.3	-7.5	BVRI	0.027	8
1992bp.....	208.83	-51.00	23773	23704	23646	E/S0	-1.4	-5.4	-1.6	BVI	0.069	8
1992br.....	288.01	-59.40	26442	26306	26319	E	-6.3	+3.6	+1.8	BV	0.026	8
1992bs.....	240.02	-55.33	19097	18965	18998	Sb	+3.6	-9.0	+2.5	BV	0.011	8
1993B.....	273.32	+20.46	20866	20563	21191	Sb	+5.4	+0.9	+3.6	BVI	0.079	8
1993H.....	318.22	+30.33	7165	6962	7430	Sb	+12.3	+1.0	-1.1	BVRI	0.060	8, 10
1993L.....	5.95	-64.37	1858	1885	1587	Sc	+1.4	-25.0	+17.3	BVRI	0.014	10
1993O.....	312.41	+28.92	15289	15065	15567	E/S0	+8.4	-14.1	-6.3	BVI	0.053	8
1993ac.....	149.70	+17.21	14800	14959	14784	E	+31.0	-5.3	+7.0	BVRI	0.163	15
1993ae.....	144.62	-63.22	5712	5820	5410	E	+22.7	+16.1	+13.8	BVRI	0.038	15
1993ag.....	268.43	+15.92	14690	14382	15003	E/S0	-6.1	-5.0	-1.7	BVI	0.112	8
1993ah.....	25.88	-76.77	8842	8892	8543	S0	+8.1	-0.9	+11.8	BVI	0.020	8
1994D.....	290.15	+70.14	592	469	928	S0	+7.8	-9.0	-13.5	UBVRI	0.022	10, 16, 17, 18
1994M.....	291.68	+63.03	6943	6788	7289	E	-28.2	+3.4	+3.1	BVRI	0.023	15
1994Q.....	64.38	+39.67	8672	8871	8670	S0	-3.7	-0.1	+10.8	BVRI	0.017	15
1994S.....	187.37	+85.14	4525	4501	4806	Sab	-6.9	-14.0	-4.5	BVRI	0.021	15
1994T.....	318.01	+59.83	10396	10265	10709	Sa	-12.0	+3.8	+0.2	BVRI	0.029	15
1994ae.....	225.34	+59.66	1301	1175	1637	Sc	+6.1	-29.7	-11.6	UBVRI	0.030	10, 19
1995D.....	230.02	+39.65	1966	1774	2300	S0	-87.8	+11.8	-6.5	BVRI	0.058	10, 15
1995E.....	141.99	+30.26	3470	3638	3496	Sb	-20.8	+7.6	-1.9	BVRI	0.027	15
1995ac.....	58.69	-55.04	14990	15157	14635	Sa	-1.4	-0.9	-5.1	BVRI	0.042	10, 15
1995ak.....	169.65	-48.98	6811	6875	6589	Sbc	+0.8	-7.1	+3.6	BVRI	0.038	15
1995al.....	192.17	+50.83	1514	1465	1777	Sbc	-3.1	-14.7	-3.9	UBVRI	0.014	15
1995bd.....	187.11	-21.66	4377	4364	4326	Sa	-1.0	+22.9	-8.4	BVRI	0.498	15
1996C.....	99.59	+65.00	8094	8206	8244	Sa	+13.2	-1.8	+2.4	BVRI	0.013	15
1996X.....	310.23	+35.64	2032	1815	2333	E	-31.7	-51.4	-3.0	UBVRI	0.069	15, 20
1996Z.....	253.60	+22.55	2254	1971	2584	Sb	-69.9	+2.0	+6.1	BVR	0.064	15
1996ab.....	43.15	+56.93	37109	37201	37239	Sa	+0.6	+2.0	+1.0	BV	0.032	15
1996ai.....	101.58	+79.24	873	910	1101	Scd	+2.9	+23.3	-1.1	UBVRI	0.014	15
1996bk.....	111.25	+54.88	1985	2139	2085	S0	-9.7	-18.1	+3.0	BVRI	0.018	15
1996bl.....	116.99	-51.30	10793	10990	10447	Sc	+5.6	-3.2	-2.4	BVRI	0.092	15
1996bo.....	144.46	-48.95	5182	5328	4893	Sc	-2.1	+6.7	-6.2	BVRI	0.077	10, 15

TABLE 1—Continued

SN Ia	$l^a$ (deg)	$b^a$ (deg)	$cz_{\odot}^b$ (km s $^{-1}$ )	$cz_{LG}^b$ (km s $^{-1}$ )	$cz_{CMB}^b$ (km s $^{-1}$ )	Morphological Type $^c$	SN Offsets $^d$ ("N)	SN Offsets $^d$ ("E)	$t_1^e$ (days)	Filters	$E(B - V)^f$ (mag)	References
1996bv.....	157.33	+17.97	4996	5119	5013	Sa	+2.0	-2.0	+5.1	<i>BVRI</i>	0.105	15
1997E.....	140.20	+25.81	4001	4184	3997	S0	+57.0	-32.0	-2.6	<i>UBVRI</i>	0.124	21
1997Y.....	124.77	+62.37	4806	4911	4964	Sb	+2.0	-8.0	+2.2	<i>UBVRI</i>	0.017	21
1997bp.....	301.15	+51.21	2492	2301	2831	Sd/Irr	-20.0	-15.0	-2.1	<i>UBVRI</i>	0.044	10, 21
1997bq.....	136.29	+39.48	2780	2943	2839	Sbc	-60.0	+50.0	-10.3	<i>UBVRI</i>	0.024	21
1997br.....	311.84	+40.32	2085	1884	2391	Sd/Irr	+52.0	-21.0	-8.7	<i>UBVRI</i>	0.113	10, 21, 22
1997cn.....	9.14	+69.51	4855	4846	5092	E	-12.0	+7.0	+5.4	<i>UBVRI</i>	0.027	21, 23
1997cw.....	113.09	-49.48	5133	5342	4782	Sab	+4.0	+8.0	+12.0	<i>UBVRI</i>	0.073	21
1997dg.....	103.61	-33.98	9238	9507	8890	...	0.0	+2.0	+0.8	<i>UBVRI</i>	0.078	21
1997do.....	171.00	+25.26	3034	3084	3140	Sbc	-4.0	-3.0	-6.1	<i>UBVRI</i>	0.063	21
1997dt.....	87.56	-39.12	2194	2451	1828	Sbc	+1.0	-9.0	-7.9	<i>UBVRI</i>	0.057	21
1998D.....	63.78	+72.91	3765	3825	3962	Sa	-7.0	-26.0	+32.4	<i>UBVRI</i>	0.015	21
1998V.....	43.94	+13.34	5268	5464	5148	Sb	+21.0	-21.0	+2.7	<i>UBVRI</i>	0.196	21
1998ab.....	124.86	+75.19	8134	8181	8354	Sc	+12.0	+2.0	-7.4	<i>UBVRI</i>	0.017	21
1998aq.....	138.83	+60.26	1184	1274	1354	Sb	+7.0	-18.0	-10.1	<i>UBVRI</i>	0.014	19
1998bp.....	43.64	+20.48	3127	3312	3048	E	+13.0	-1.0	-1.5	<i>UBVRI</i>	0.076	21
1998bu.....	234.41	+57.01	855	702	1204	Sab	+55.0	+4.0	-7.7	<i>UBVRI</i>	0.025	24, 25
1998co.....	41.52	-44.94	5418	5573	5094	S0	+5.0	+2.0	+3.0	<i>UBVRI</i>	0.043	21
1998de.....	122.03	-35.24	4990	5228	4671	S0	+3.0	+72.0	-8.6	<i>UBVRI</i>	0.057	21, 26
1998dh.....	82.82	-50.64	2678	2892	2307	Sbc	+10.0	-54.0	-7.8	<i>UBVRI</i>	0.068	21
1998dk.....	102.85	-62.16	3963	4128	3609	Sc	+3.0	+5.0	+18.9	<i>UBVRI</i>	0.044	21
1998dm.....	145.97	-67.40	1968	2061	1668	Sc	-37.0	-14.0	+9.9	<i>UBVRI</i>	0.044	21
1998dx.....	77.67	+26.67	16197	16459	16102	Sb	-12.0	+21.0	+1.2	<i>UBVRI</i>	0.041	21
1998ec.....	166.29	+20.71	5966	6043	6032	Sb	-20.0	-9.0	+13.3	<i>UBVRI</i>	0.085	21
1998ef.....	125.88	-30.56	5319	5558	5020	Sa	-2.0	+6.0	-7.3	<i>UBVRI</i>	0.073	21
1998eg.....	76.46	-42.06	7423	7662	7056	Sc	-25.0	-26.0	-0.1	<i>UBVRI</i>	0.123	21
1998es.....	143.18	-55.18	3168	3301	2868	S0/Sa	+11.0	0.0	-11.0	<i>UBVRI</i>	0.032	21, 27
1999X.....	186.58	+39.59	7503	7474	7720	...	+6.0	+4.0	+14.0	<i>UBVRI</i>	0.032	21
1999aa.....	202.72	+30.31	4330	4227	4572	Sc	+28.0	+1.0	-10.1	<i>UBVRI</i>	0.040	10, 21, 27, 28
1999ac.....	19.88	+39.94	2848	2904	2943	Scd	-30.0	+24.0	-14.4	<i>UBVRI</i>	0.046	21, 27
1999aw.....	260.24	+47.45	11392	11168	11763	...	0.0	0.0	-8.2	<i>BVRI</i>	0.032	29
1999by.....	166.91	+44.11	657	704	827	Sb	+91.0	-96.0	-10.9	<i>UBVRI</i>	0.016	27, 30
1999cc.....	59.66	+48.74	9392	9549	9452	Sc	+2.0	+17.0	-2.7	<i>UBVRI</i>	0.023	21, 31
1999cl.....	282.26	+76.50	2281	2187	2605	Sb	+23.0	-46.0	-6.5	<i>UBVRI</i>	0.038	21, 31
1999cp.....	334.85	+52.71	2845	2737	3115	Scd	+23.0	-52.0	-7.4	<i>BVRI</i>	0.024	28
1999cw.....	101.77	-67.91	3725	3863	3380	Sab	-2.0	+21.0	+24.0	<i>UBVRI</i>	0.036	21
1999da.....	89.73	+32.64	3806	4059	3748	E	+1.0	-71.0	-8.7	<i>BVRI</i>	0.056	27, 32
1999dk.....	137.35	-47.46	4485	4654	4181	Sc	+26.0	+4.0	-0.9	<i>UBVRI</i>	0.054	10, 32
1999dq.....	152.83	-35.87	4295	4436	4060	Sc	-6.0	-4.0	-10.6	<i>UBVRI</i>	0.110	21, 27
1999ee.....	6.50	-55.93	3422	3451	3163	Sbc	-10.0	+10.0	-9.5	<i>UBVRI</i>	0.020	33
1999ef.....	125.72	-50.09	11733	11920	11402	Scd	-10.0	+20.0	+6.8	<i>UBVRI</i>	0.087	21
1999ej.....	130.44	-28.95	4114	4344	3831	S0/Sa	-20.0	+18.0	+5.3	<i>UBVRI</i>	0.071	21
1999ek.....	189.40	-8.23	5253	5221	5278	Sbc	-12.0	-12.0	-2.8	<i>UBVRI</i>	0.561	21, 34
1999gd.....	198.83	+33.98	5535	5451	5775	...	+17.0	+7.0	+3.5	<i>UBVRI</i>	0.041	21
1999gh.....	255.04	+23.73	2302	2019	2637	E	+16.0	+52.0	+7.4	<i>UBVRI</i>	0.058	21
1999gp.....	143.25	-19.50	8018	8215	7806	Sb	+10.0	-11.0	-13.0	<i>UBVRI</i>	0.056	21, 27, 32
2000B.....	166.35	+22.79	5901	5976	5977	E	+19.0	-14.0	+15.7	<i>UBVRI</i>	0.068	21
2000E.....	100.89	+14.84	1415	1711	1257	Sbc	-26.7	-6.3	-15.5	<i>UBVRI</i>	0.364	35
2000bh.....	293.74	+40.33	6905	6666	7248	...	-11.0	-8.0	+5.4	<i>BVRI</i>	0.048	36
2000bk.....	295.29	+55.23	7628	7444	7976	S0	-10.0	+61.0	+12.3	<i>BVRI</i>	0.025	32
2000ca.....	313.20	+27.83	7080	6857	7352	Sbc	+4.7	+0.6	-2.3	<i>UBVRI</i>	0.067	36
2000ce.....	149.10	+32.00	4888	5025	4946	Sb	+17.0	+15.0	+7.0	<i>UBVRI</i>	0.057	21, 32
2000cf.....	99.88	+42.16	10920	11137	10930	...	+4.0	+3.0	+3.2	<i>UBVRI</i>	0.032	21, 31
2000cn.....	53.44	+23.31	7043	7257	6958	Scd	-7.0	-7.0	-7.8	<i>UBVRI</i>	0.057	21
2000cx.....	136.50	-52.48	2379	2536	2068	S0	-109.0	-23.0	-8.4	<i>UBVRI</i>	0.082	10, 21, 37, 38
2000dk.....	126.83	-30.34	5228	5465	4931	E	+9.0	-5.0	-4.5	<i>UBVRI</i>	0.070	21
2000fa.....	194.17	+15.48	6378	6313	6533	Sd/Irr	+4.0	+7.0	-10.1	<i>UBVRI</i>	0.069	21
2001V.....	218.92	+77.73	4539	4478	4846	Sb	+28.0	+52.0	-12.9	<i>UBVRI</i>	0.020	39
2001ay.....	35.98	+68.83	9067	9108	9266	Sb	+9.0	-10.0	-3.0	<i>UBVRI</i>	0.019	40
2001ba.....	285.39	+28.03	8819	8537	9152	Sb	-22.0	+19.0	-3.5	<i>BVI</i>	0.064	36
2001bt.....	337.32	-25.87	4388	4275	4332	Sb	+17.1	-14.1	-8.0	<i>BVRI</i>	0.065	34
2001cn.....	329.65	-24.05	4647	4498	4628	Sc	-17.9	-2.6	+4.7	<i>UBVRI</i>	0.059	34
2001cz.....	302.11	+23.29	4612	4350	4900	Sbc	-31.4	-0.6	-6.3	<i>BVRI</i>	0.092	34
2001el.....	251.52	-51.40	1168	1002	1102	Scd	+19.0	-22.0	-10.7	<i>UBVRI</i>	0.014	41

TABLE 1—*Continued*

SN Ia	$l^a$ (deg)	$b^a$ (deg)	$cz_\odot^b$ (km s <sup>-1</sup> )	$cz_{LG}^b$ (km s <sup>-1</sup> )	$cz_{CMB}^b$ (km s <sup>-1</sup> )	Morphological Type <sup>c</sup>	SN Offsets <sup>d</sup> ("N)	SN Offsets <sup>d</sup> ("E)	$t_1^e$ (days)	Filters	$E(B - V)^f$ (mag)	References
2002bf.....	156.46	+50.08	7254	7327	7418	Sb	+4.0	+0.6	-9.9	<i>BVRI</i>	0.011	42
2002bo.....	213.04	+54.85	1293	1184	1609	Sa	-14.2	+11.6	-13.4	<i>UBVRI</i>	0.025	34, 43, 44
2002cx.....	318.71	+69.14	7184	7085	7494	...	-18.0	+11.0	-5.3	<i>BVRI</i>	0.032	45
2002er.....	28.67	+25.83	2568	2681	2563	Sc	+4.7	-12.3	-7.5	<i>UBVRI</i>	0.157	46
2003du.....	101.18	+53.21	1912	2081	1992	Sd/Irr	-13.5	-8.8	-4.7	<i>BVRI</i>	0.010	42

<sup>a</sup> Host galaxy galactic longitude and latitude, from the NASA/IPAC Extragalactic Database (NED); see <http://nedwww.ipac.caltech.edu>.

<sup>b</sup> Host galaxy heliocentric radial velocities are taken from NED; they are transformed to the Local Group and CMB rest frames using the formulae also provided by NED; see [http://nedwww.ipac.caltech.edu/help/velc\\_help.html#notes](http://nedwww.ipac.caltech.edu/help/velc_help.html#notes).

<sup>c</sup> NED host galaxy morphological type.

<sup>d</sup> Positional offset relative to host galaxy nucleus, from the IAU List of Supernovae; see <http://cfa-www.harvard.edu/iau/lists/Supernovae.html>.

<sup>e</sup> Epoch of the first photometric observation, relative to  $B$  maximum light, in the SN rest frame.

<sup>f</sup> Milky Way dust reddening, from Schlegel et al. (1998).

REFERENCES.—(1) Leibundgut et al. 1991; (2) Hamuy et al. 1991; (3) Buta & Turner 1983; (4) Tsvetkov 1982; (5) Phillips et al. 1987; (6) Wells et al. 1994; (7) Lira et al. 1998; (8) Hamuy et al. 1996b; (9) Ford et al. 1993; (10) Altavilla et al. 2004; (11) Filippenko et al. 1992; (12) Leibundgut et al. 1993; (13) Turatto et al. 1996; (14) N. Suntzeff 2005, private communication; (15) Riess et al. 1999; (16) Richmond et al. 1995; (17) Patat et al. 1996; (18) Meikle et al. 1996; (19) Riess et al. 2005; (20) Salvo et al. 2001; (21) Jha et al. 2006; (22) Li et al. 1999; (23) Turatto et al. 1998; (24) Suntzeff et al. 1999; (25) Jha et al. 1999b; (26) Modjaz et al. 2001; (27) W. Li 2005, private communication; (28) Krisciunas et al. 2000; (29) Strolger et al. 2002; (30) Garnavich et al. 2004; (31) Krisciunas et al. 2006; (32) Krisciunas et al. 2001; (33) Stritzinger et al. 2002; (34) Krisciunas et al. 2004b; (35) Valentini et al. 2003; (36) Krisciunas et al. 2004a; (37) Li et al. 2001; (38) Candia et al. 2003; (39) K. Mandel et al. 2007, in preparation; (40) K. Krisciunas 2005, private communication; (41) Krisciunas et al. 2003; (42) Leonard et al. 2005; (43) Szabó et al. 2003; (44) Benetti et al. 2004; (45) Li et al. 2003; (46) Pignata et al. 2004.

passbands), we choose standard colors including that passband (specifically, for  $U$ :  $U - B$ ;  $B$ :  $U - B$  and  $B - V$ ;  $V$ :  $B - V$ ,  $V - R$ , and  $V - I$ ;  $R$ :  $V - R$  and  $R - I$ ;  $I$ :  $V - I$  and  $R - I$ ). Then for a particular combination of passband and color, we calculate  $K$ -corrections in that passband, such that the spectra are forced to take on a range of observed colors, using the CCM89 extinction law to adjust the spectra to any particular color. Thus, we tabulate the  $K$ -correction as a function of three parameters: epoch (i.e., days after maximum light), redshift, and color. We measure the colors in the observer frame, so that, for example, to determine the  $K$ -correction in the  $V$  band for an SN at maximum light at redshift  $z = 0.05$  with an observed  $B - V = 0.0$  mag, we have taken our maximum light spectra, redshifted them to  $z = 0.05$ , adjusted them using the CCM89 extinction law to have  $B - V = 0.0$  as measured with synthetic photometry, and calculated the  $K$ -correction for that adjusted spectrum. In this example, the answer is  $K_{VV} = -0.04 \pm 0.02$  mag, where the uncertainty is measured from the scatter among the individual spectra about a smooth curve. If the observed color had been redder, e.g.,  $B - V = 0.5$  mag, then  $K_{VV} = 0.06 \pm 0.01$  mag.

The advantage of calculating the  $K$ -correction as a function of observer-frame color (as opposed to the SN rest-frame color) is that no iteration is then required: the measured color directly determines the SN SED in the observer frame. However, in other applications, for example, if one wants to transform rest-frame templates (with known rest-frame colors) to the observer frame, it is more convenient to tabulate the  $K$ -correction as a function of rest-frame color. For the present sample, all SNe have well-measured (to better than  $\sim 0.1$  mag) observer-frame colors, so we can apply the  $K$ -corrections to the data directly and expediently fit the SN in the rest frame. Although not used here, we are also developing an implementation of MLCS2k2 to take rest-frame model light curves, convert them into the observer frame, and then fit the observed data directly. That approach is more appropriate, e.g., for high-redshift observations where observer-frame color information is of lower quality and  $K$ -corrections based on the model light-curve colors should be used.

In Figure 1 we show the derived  $K$ -corrections in the  $U$  band. It is interesting to note that the  $K$ -corrections in  $U$  at maximum light are quite significant ( $\sim 0.1$  mag), even for very modest redshifts. Ignoring the  $K$ -correction would lead to spurious corre-

lations of SN parameters (including those that are nominally distance independent, such as decline rate or color) with redshift and distance.

Nugent et al. (2002) caution against using the CCM89 extinction law adjustment procedure applied to normal SN Ia spectra in determining  $K$ -corrections for SN 1991bg-like objects, whose strong Ti II spectral features dominate the photometric colors (particularly in  $B$ ), even at early times. We have calculated  $K$ -corrections independently for this class of SNe Ia, a small minority of the entire sample, using a separate spectral sample consisting of only SN 1991bg-like objects. The affected objects are SN 1986G, SN 1991bg, SN 1992K, SN 1992bo, SN 1993H, SN 1997cn, SN 1998bp, SN 1998de, SN 1999by, SN 1999da, and SN 1999gh.

## 2.2. Extinction

Extinction by dust along the line of sight to an SN Ia is recognized by its reddening effect on the SN colors. As discussed by Phillips et al. (1999) and Nugent et al. (2002), the evolution of the SN Ia SED over time leads to variations in the observed extinction in any given passband. Furthermore, the extinction itself alters the SED such that the reddening is a nonlinear function of the total extinction. These effects are small (typically at the level of a few hundredths of a magnitude) but systematically affect the observed light curves in a way that can impact the luminosity/light-curve shape relationship and derived distances. In this section we describe in some detail the methods we have used to account for host galaxy extinction in MLCS2k2.

The dust extinction along a particular line of sight is typically parameterized by the extinction in a given band  $X$ ,  $A_X$ , and by the amount of reddening, given by the color excess, typically  $E(B - V)$ . Following Phillips et al. (1999) and Nugent et al. (2002), we distinguish between the “true” reddening  $E(B - V)_{\text{true}}$ , which depends only on the dust itself (and is calculated from the effects of that dust on idealized stellar spectra; CCM89), and the “observed” reddening  $E(B - V)_{\text{obs}} \equiv A_B - A_V$ , which varies with time as the SN spectrum evolves. From these, we can construct the ratio  $R_X^{\text{true}} \equiv A_X/E(B - V)_{\text{true}}$ , which varies in time as the numerator varies, and  $R_X^{\text{obs}} \equiv A_X/E(B - V)_{\text{obs}}$ , for which both the numerator and denominator vary in time. We have calculated both of these ratios similarly to Phillips et al.

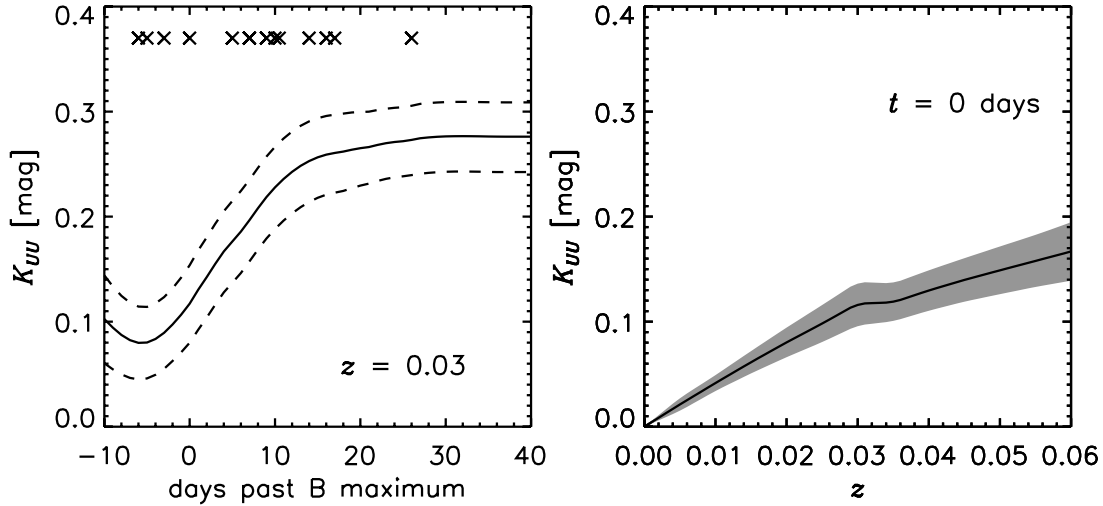


FIG. 1.— $K$ -corrections in the  $U$  band. The left panel shows  $K_{UU}$  as a function of SN age at a redshift of  $z = 0.03$ . The solid line corresponds to an observed maximum light  $U - B = -0.35$  (corresponding to an SN rest-frame color at maximum light  $U - B = -0.50$ ). The dashed lines above and below the solid line correspond to SNe Ia that are 0.2 mag redder and bluer, respectively, in  $U - B$  at all epochs. The crosses indicate the phases of the spectra used in the calculation. The right panel shows  $K_{UU}$  at maximum light as a function of redshift, assuming a rest-frame color of  $U - B = -0.50$ . The shaded region indicates the  $K$ -correction uncertainty. The “kinks” in the right panel occur when individual spectra (out of 32 total) drop out of the  $K$ -correction calculation as their wavelength coverage ceases to encompass the entire  $U$  band.

(1999) and Nugent et al. (2002), by simulating the effects of extinction on the sample of 91 spectra described in § 2.1, using the  $R_V = 3.1$  extinction law of CCM89,<sup>7</sup> as modified by O’Donnell (1994), and synthetic photometry through the Bessell (1990) standard passbands.<sup>8</sup>

We present our calculations of  $R_X^{\text{true}}$  and  $R_X^{\text{obs}}$  in Figures 2 and 3, respectively. We find a good match in general to the results of Nugent et al. (2002) and Phillips et al. (1999), which is not surprising, as we have many of the input spectra in common. The figures show the time variation of these two ratios, as well as its variation over 2 mag in  $E(B - V)_{\text{true}}$ . Both of these ratios have their uses, depending on whether one knows the extinction a priori (for instance, using a Galactic reddening map) or is measuring it from the observed SN colors. Because we have used the SED of SNe Ia themselves to calculate these quantities (and their time variation), it is preferable to use these results rather than those from standard filter tables (e.g., Table 6 of Schlegel et al. 1998).

So far we have restricted ourselves to the standard  $R_V = 3.1$  extinction law of CCM89, but we would like our distance measuring technique to allow for variations in the properties of the dust. CCM89 have shown that in the optical passbands, dust in our Galaxy follows extinction laws that can be expressed in terms of  $R_V$ .<sup>9</sup> Clearly, using extinction laws with different values of  $R_V$  will lead directly to variations in  $R_X^{\text{true}}$  and  $R_X^{\text{obs}}$ . The variation with the total extinction itself adds further complications and makes using these ratios cumbersome. For instance, calculating  $R_I^{\text{obs}} \equiv A_I / (A_B - A_V)$  involves three terms, each varying individually with epoch, total extinction, and extinction law.

To make things simpler, we have chosen to work in the more natural space of  $A_X$  rather than using color excesses to parameterize the extinction. This is convenient because we fit the light curves in each passband directly, rather than fitting color curves,

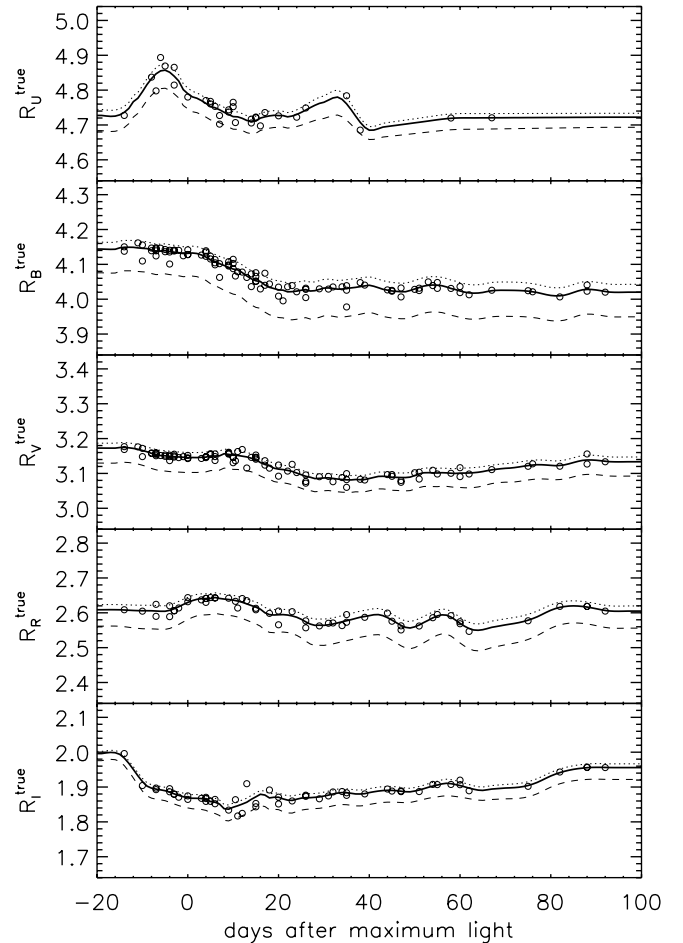


FIG. 2.—Variation of  $R_X^{\text{true}} \equiv A_X / E(B - V)_{\text{true}}$  in  $UBVR I$  as a function of SN phase. The open circles represent the measurement from the individual spectra, and the thick solid line is the smoothed representation. The dotted and dashed lines show the variation of  $R_X^{\text{true}}$  with the total extinction (see Phillips et al. 1999, their Fig. 2). The dashed line corresponds to  $E(B - V)_{\text{true}} = +1.0$  mag relative to the solid line [which was calculated for  $E(B - V)_{\text{true}}$  approaching zero]. The dotted line corresponds to  $E(B - V)_{\text{true}} = -0.5$  mag relative to the solid line (for illustration only, as it would be unphysical unless the extinction zero point for the solid line was significantly underestimated).

<sup>7</sup> We have also explored using the extinction law presented by Fitzpatrick (1999), with similar results.

<sup>8</sup> Previous incarnations of MLCS used extinction coefficients tabulated for the Johnson  $R$  and  $I$  passbands, rather than the Kron/Cousins passbands. We have rectified this here.

<sup>9</sup> We adopt the notation that without a superscript “true” or “obs,”  $R_V$  corresponds to the  $R_V$  of CCM89, i.e., derived from photoelectric measurements of Galactic stars.

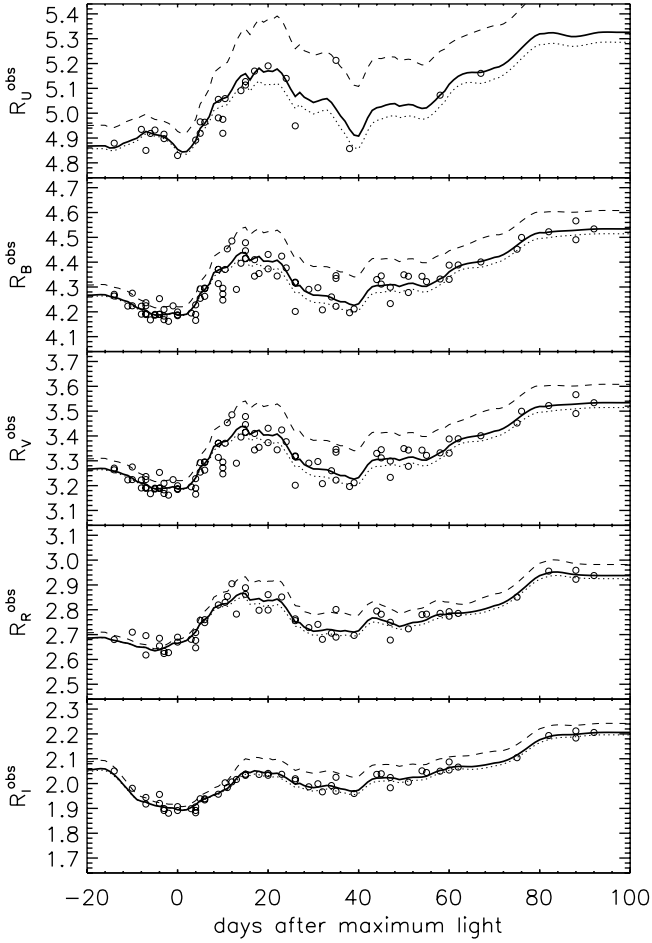


FIG. 3.—Same as Fig. 2, except showing the variation of  $R_X^{\text{obs}} \equiv A_X/E(B-V)_{\text{obs}}$ . Note that the  $y$ -axis ranges have been increased in this figure, to encompass the larger variations in  $R_X^{\text{obs}}$ , and that  $R_B^{\text{obs}} = R_V^{\text{obs}} + 1$  by definition.

an approach that does not require light curves to have multiple color measurements at each epoch. Secondly, the extinction laws themselves are better characterized in ratios of extinctions, e.g.,  $A_B/A_V$ , rather than in ratios of extinctions to color excesses.<sup>10</sup>

The first part of this framework is to separate out the time dependence of the extinction. For each passband  $X$ , we define the quantity

$$\zeta_X \equiv \frac{A_X}{A_X^0}, \quad (1)$$

where we denote quantities that are functions of SN phase in bold [i.e.,  $\zeta_X = \zeta_X(t)$ ] and  $A_X^0$  is defined as the extinction in passband  $X$  at maximum light in  $B$ . Thus,  $\zeta_X(t=0) \equiv 1$  by definition (all times are defined relative to maximum light in  $B$ ). In Figure 4 we show our calculation of  $\zeta_X$  in  $UBVRI$ . The useful result is that  $\zeta_X$  captures all of the time dependence in the extinction and is insensitive to both the total extinction  $E(B-V)_{\text{true}}$  and the extinction law  $R_V$ . This point is also illustrated in Figure 4, where the dark gray bands show the variation in  $\zeta_X$  over the very wide range of 3 mag of  $E(B-V)_{\text{true}}$  and the light gray bands show the variation of a wide range of  $R_V$  from 1.7 to 5.7 [includ-

<sup>10</sup> This point is made explicitly by CCM89, who note that “there are some relationships which emerge more clearly when  $A(\lambda)/A(V)$  is considered than when normalization by  $E(B-V)$  is used.”

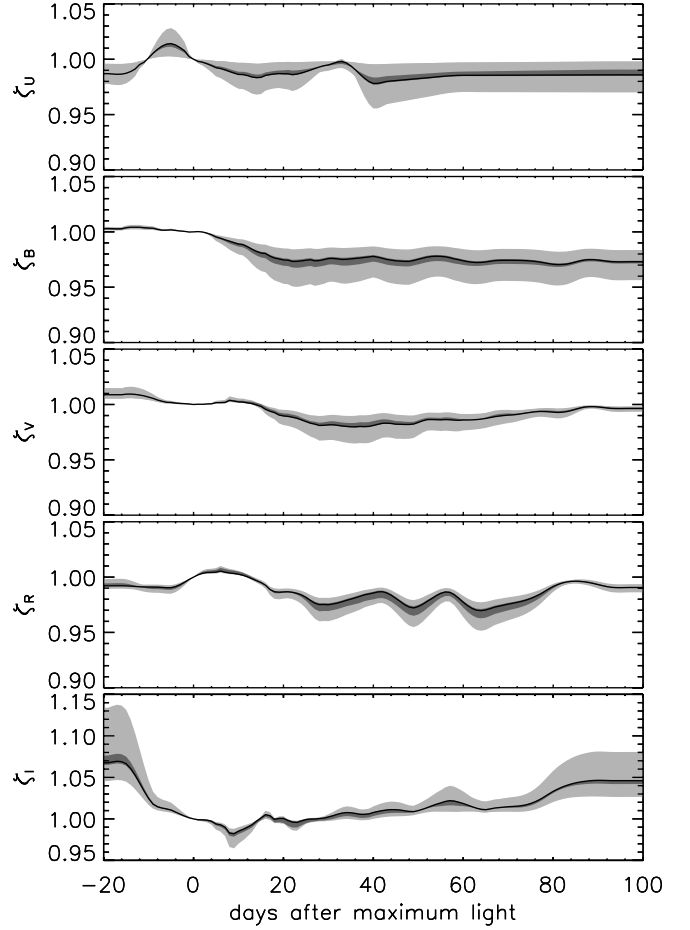


FIG. 4.—Calculation of  $\zeta_X \equiv A_X/A_X^0$  in  $UBVRI$ . The dark solid line shows the result for  $R_V = 3.1$  and  $E(B-V)_{\text{true}}$  approaching zero. The dark gray shaded area shows the range of variation in  $\zeta_X$  over 3 mag in  $E(B-V)_{\text{true}}$ , while the light gray shaded area indicates the variation in  $\zeta_X$  over that reddening range and over the range  $1.7 \leq R_V \leq 5.7$ .

ing the full variation in  $E(B-V)_{\text{true}}$ ]. While the figure shows some differences in  $\zeta_X$  at levels greater than a few percent (for instance, in  $I$  at early times), these are only realized for extreme values of both  $R_V$  and  $E(B-V)_{\text{true}}$ . We can then confidently fix  $\zeta_X$  as shown by the dark solid lines in the figure, independent of the reddening law and total extinction.

With the time dependence separated, we can relate the extinction in any passband at any epoch to the maximum light extinction  $A_X^0$  in that passband. The maximum light extinctions in the different passbands are interrelated, and we can define the relations between these (currently, five) parameters as a function of the total extinction and the reddening law. CCM89 show that the ratio  $A_X/A_V$  is a simple linear function of  $(1/R_V)$ . We have calculated this relationship at maximum light explicitly using our sample of spectra near that epoch and fitted for the coefficients  $\alpha_X$  and  $\beta_X$ , defined by

$$\frac{A_X^0}{A_V^0} = \alpha_X + \frac{\beta_X}{R_V}. \quad (2)$$

The results are presented graphically in Figure 5 and listed in Table 2 (which also shows explicitly the relations for an  $R_V = 3.1$  extinction law). Furthermore, the figure illustrates that  $A_X^0/A_V^0$  is a very weak function of  $E(B-V)_{\text{true}}$  (in most cases the three open circles are indistinguishable), and we are justified in ignoring the dependence on the total extinction.

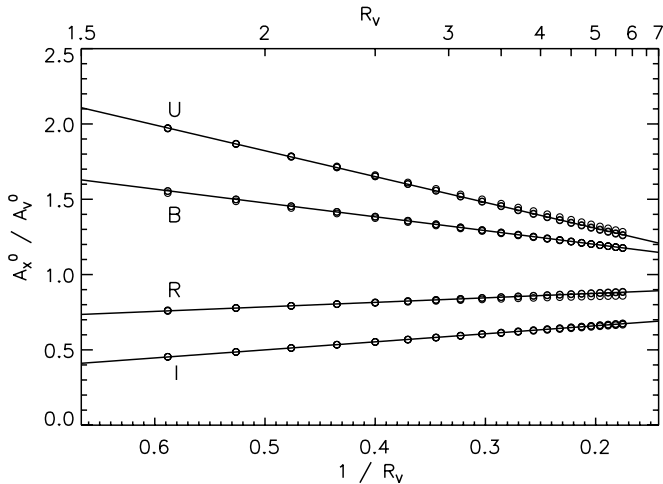


FIG. 5.—Variation of  $A_X^0/A_V^0$  as a function of  $R_V^{-1}$ . The solid lines indicate the best linear fit. The open circles show the calculated points; for each passband and  $R_V$  there are three open circles, with  $E(B - V)_{\text{true}} \simeq -0.5, 0.0$ , and  $+2.5$  mag, showing the small differences in the relations as a function of the total extinction.

In the framework developed, then, we parameterize the extinction by two numbers:  $A_V^0$ , corresponding to the extinction in the  $V$  passband at maximum light, and  $R_V$ , describing the shape of the extinction law. The fixed coefficients  $\alpha_X$  and  $\beta_X$  provide the maximum light extinctions in other passbands, and the vectors  $\zeta_X$  contain the time variation. While the parameterization in terms of  $R_X^{\text{true}}$  and  $R_X^{\text{obs}}$  is still useful for certain tasks (see below), we switch to this new framework in the MLCS2k2 fits.

### 2.3. Separating Reddening and Intrinsic Color

To define the training set that yields our desired template light curves, we need an estimate of the extinction in the host galaxy of each object. Various approaches are possible, e.g., assuming that SNe Ia in early-type host galaxies or the bluest SNe Ia define an extinction-free sample. Knowing the “zero point” of the extinction (i.e., the true, unreddened color of an SN Ia) is not strictly necessary if we are interested only in relative distances (or in tying the SN Ia distances to another set, such as the Cepheid scale), but it becomes essential if we want to use the positivity of the extinction (dust cannot brighten a source or make it appear bluer) as a constraint on our derived distances. We employ the observational results of Lira (1995), who noticed that the late-time ( $t \gtrsim +30$  days)  $B - V$  color evolution of SNe Ia was remarkably similar, regardless of light-curve shape near maximum light. SNe Ia undergoing this transition to the nebular phase also show very similar spectra (see, e.g., Filippenko 1997). Phillips et al. (1999) used this “Lira law,”  $(B - V)_0 = 0.725 - 0.0118(t_V - 60)$ , giving the intrinsic color in terms of the number of days past  $V$  maximum light, to measure extinctions and to constrain the  $B - V$  and  $V - I$  maximum light colors of SNe Ia (as a function of  $\Delta m_{15}$ ). The Lira law as quoted was derived from a fit of late-time photometry of four objects (SN 1992A, SN 1992bc, SN 1992bo, and SN 1994D), estimated to be free of host galaxy extinction. Phillips et al. (1999) estimate that the intrinsic dispersion about the relation is 0.05 mag.

We have attempted to check the Lira relation with another approach. Rather than trying to choose an extinction-free subsample of the data, we use all the data we can. Beginning with the sample of 133 SNe Ia described above, we have corrected the photometry for Galactic extinction, using the reddening maps of Schlegel et al. (1998) and our calculation of  $R_X^{\text{true}}$  above, with

TABLE 2  
MAXIMUM LIGHT EXTINCTION COEFFICIENTS

PASSBAND ( $X$ )	$A_X^0/A_V^0 = \alpha_X + \beta_X/R_V$		
	$\alpha_X$	$\beta_X$	$\alpha_X + \beta_X/3.1$
U.....	0.964	1.716	1.518
B.....	1.016	0.919	1.313
V.....	1.000	0.000	1.000
R.....	0.935	-0.300	0.839
I.....	0.767	-0.534	0.595

the assumption that the Galactic component is described by an  $R_V = 3.1$  extinction law. We have also applied the  $K$ -correction (see § 2.1) and corrected for time dilation to bring the data to the SN rest frame. We have then constructed  $B - V$  color curves for the sample and attempted to measure the late-time color evolution. We find that the Lira late-time  $B - V$  slope of  $-0.0118 \text{ mag day}^{-1}$  does an excellent job of fitting the bulk of the observations.<sup>11</sup> We thus fix this slope and fit a straight line to all the  $B - V$  observations between 32 and 92 days past  $B$  maximum light to determine the intercept,  $BV_{35}$  (which we reference to a fiducial epoch of  $t = +35$  days), and its observational uncertainty  $\sigma_{BV_{35}}$ . Of the 133 objects listed in Table 1, 28 have no useful late-time color information, while an additional 23 have only poor data unsuitable for a good measurement, due to either too few late-time points or points with large uncertainties. The  $BV_{35}$  measurements for the remaining 82 objects are listed in Table 3 and presented in a histogram in Figure 6.

We assume that this distribution is a result of three independent factors: (1) observational uncertainty, (2) an intrinsic  $B - V$  color with an unknown scatter, and (3) reddening by dust in the host galaxy. We then model the distribution of the intrinsic component as a Gaussian with mean  $(B - V)_{+35}$  and standard deviation  $\sigma_{B-V}$  (which subsumes the observational errors) and the distribution of the reddening as an exponential with scale length  $\tau_{E(B-V)}$ , such that the probability density of the reddening peaks at zero and falls to  $1/e$  of the peak at  $\tau_{E(B-V)}$ . The probability distribution function of the sum of these two components is just the convolution of the individual distributions, and we perform a maximum likelihood analysis using each point to determine the best-fit model parameters. The results are also shown in Figure 6, with the convolution overplotted on the histogram and the components inset. The maximum likelihood model parameters are  $(B - V)_{+35} = 1.054 \pm 0.018 \text{ mag}$ ,  $\sigma_{B-V} = 0.062 \pm 0.012 \text{ mag}$ , and  $\tau_{E(B-V)} = 0.138 \pm 0.023 \text{ mag}$ , where the uncertainties were determined by bootstrap resampling of the data set.

There are a couple of cautionary points about this result. First, we have excluded from the fit the very peculiar SN 2000cx (Li et al. 2001), which is a clear outlier in the histogram and whose light curve (but not peak luminosity) is significantly unlike other SNe Ia (Li et al. 2001; Jha et al. 2006). In addition, because the SNe Ia we study were discovered in a variety of SN searches, they do not comprise a complete or well-defined sample and thus may be biased with respect to the true distribution of SN Ia late-time color. In particular, there may be a significant population of heavily obscured SNe Ia that are not present in the sample, leading to an underestimate of  $\tau_{E(B-V)}$ , assuming that an exponential distribution is valid at all (Hatano et al. 1998). While our derived

<sup>11</sup> Using the 31 color curves of highest quality, we find a mean slope of  $-0.0123 \text{ mag day}^{-1}$  with a standard deviation of  $0.0011 \text{ mag day}^{-1}$ .

TABLE 3  
SN Ia LATE-TIME COLORS

SN Ia	$BV_{35}$ (mag)	$\sigma_{BV_{35}}$ (mag)	SN Ia	$BV_{35}$ (mag)	$\sigma_{BV_{35}}$ (mag)
1972E.....	1.092	0.028	1997bp.....	1.305	0.073
1980N.....	1.139	0.027	1997bq.....	1.216	0.026
1981B.....	1.105	0.042	1997br.....	1.362	0.030
1986G.....	1.682	0.029	1997cw.....	1.521	0.042
1989B.....	1.438	0.040	1998V.....	1.123	0.031
1990O.....	1.145	0.044	1998ab.....	1.215	0.029
1990T.....	1.174	0.027	1998aq.....	1.099	0.026
1990Y.....	1.326	0.033	1998bp.....	1.127	0.029
1991S.....	1.177	0.042	1998bu.....	1.384	0.026
1991T.....	1.223	0.028	1998de.....	1.195	0.044
1991ag.....	1.121	0.029	1998dh.....	1.214	0.032
1991bg.....	1.040	0.031	1998dk.....	1.284	0.041
1992A.....	1.036	0.029	1998dm.....	1.461	0.031
1992J.....	1.148	0.048	1998es.....	1.166	0.042
1992K.....	1.045	0.034	1999aa.....	1.075	0.027
1992P.....	1.152	0.031	1999ac.....	1.142	0.029
1992al.....	1.091	0.026	1999aw.....	0.943	0.049
1992bc.....	0.981	0.028	1999by.....	1.067	0.027
1992bg.....	1.095	0.046	1999da.....	1.308	0.074
1992bl.....	1.006	0.046	1999dq.....	1.267	0.037
1992bo.....	1.036	0.072	1999ee.....	1.415	0.026
1993H.....	1.041	0.041	1999ek.....	1.262	0.052
1993L.....	1.283	0.045	1999gd.....	1.490	0.078
1993O.....	1.071	0.029	1999gh.....	1.100	0.026
1993ae.....	1.022	0.029	1999gp.....	1.166	0.035
1993ag.....	1.156	0.050	2000B.....	1.130	0.044
1994D.....	0.970	0.034	2000bh.....	1.176	0.026
1994M.....	1.233	0.029	2000bk.....	1.205	0.027
1994Q.....	1.154	0.039	2000ca.....	1.040	0.029
1994ae.....	1.055	0.027	2000cf.....	1.167	0.026
1995D.....	1.153	0.026	2000cx.....	0.827	0.025
1995E.....	1.857	0.089	2000dk.....	1.007	0.082
1995ac.....	1.117	0.037	2000fa.....	1.159	0.047
1995ak.....	1.331	0.033	2001V.....	1.144	0.026
1995al.....	1.225	0.032	2001bt.....	1.314	0.035
1995bd.....	1.274	0.033	2001cn.....	1.272	0.032
1996C.....	1.107	0.049	2001cz.....	1.221	0.032
1996X.....	1.083	0.035	2001el.....	1.358	0.027
1996bl.....	1.161	0.047	2002bo.....	1.450	0.027
1997E.....	1.111	0.031	2002er.....	1.233	0.030
1997Y.....	1.148	0.031	2003du.....	1.050	0.026

NOTES.—Determined from a linear fit to SN rest-frame  $B - V$  color measurements between 32 and 92 days past  $B$  maximum light, with  $(B - V)(t) = BV_{35} - 0.0118(t - 35)$ . See text for details.

value for  $\tau_{E(B-V)}$  is valid for the sample we study and whose distances we derive in this paper, other SN surveys with flux- or volume-limited samples, or searches in infrared, may find differing numbers of heavily extinguished SNe Ia and different estimates of  $\tau_{E(B-V)}$ .<sup>12</sup>

Fortunately, we are chiefly interested in  $(B - V)_{+35}$  and  $\sigma_{B-V}$ , and it is unlikely that our estimates of these are significantly biased. Our results with this maximum likelihood method are in good accord with the Lira relation [which predicts  $(B - V)_{+35} \simeq 1.044$ ] and its estimated dispersion. Our approach has the advantage of using all normal SNe Ia to determine the intrinsic color zero point, rather than just the bluest objects. As Figure 6 shows, in addition to having low reddening, the bluest

<sup>12</sup> If, for example, we truncate the observed distribution to eliminate the reddest objects with  $BV_{35} \geq 1.5$  mag, the derived scale length is  $\tau = 0.104 \pm 0.021$  mag.

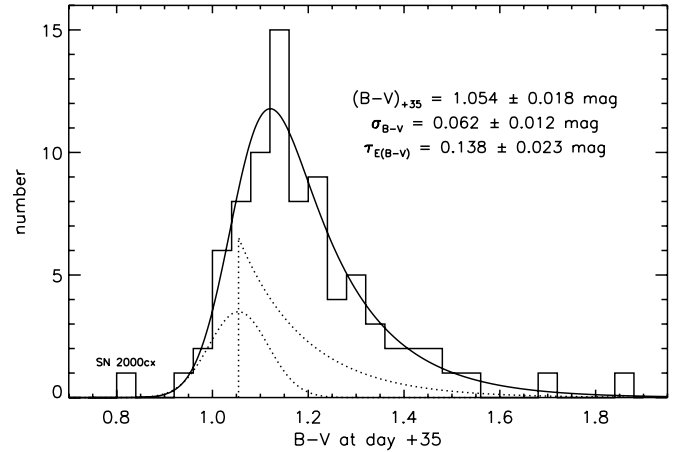


FIG. 6.—Histogram of 82 SNe Ia with well-measured late-time  $B - V$  color evolution. The data were corrected for Galactic extinction and the  $K$ -correction and referenced to +35 days after  $B$  maximum, adopting a late-time color evolution slope of  $-0.0118$  mag day $^{-1}$ . The maximum likelihood fit model is shown as the solid line; it is the convolution of the dotted lines shown (at an arbitrary scale for clarity). SN 2000cx, a clear outlier, was not included in the fit.

objects are also intrinsically bluer than the mean unreddened color. Part of the “intrinsic” color scatter,  $\sigma_{B-V}$ , is due to observational uncertainty in the color measurement. Based on our color measurements, with an average uncertainty of 0.037 mag, we can remove this component and estimate the true intrinsic color scatter  $\sigma_{(B-V)_{\text{int}}} = 0.049$  mag.<sup>13</sup>

Our model then establishes independent distributions for both the intrinsic color of SNe Ia and the reddening. Intrinsically, SNe Ia at 35 days past maximum (and even later times, if corrected by the Lira slope to the reference +35 day epoch) have a  $B - V$  color distribution that can be described by a Gaussian with a mean of 1.054 mag and standard deviation of 0.049 mag. In our sample, the distribution of host galaxy reddening by dust  $E(B - V)$  is well described by an exponential with a scale length of 0.138 mag. The observed color is the sum of the intrinsic color and the reddening.

A straightforward application of Bayes’s theorem yields the prescription to turn the model around: determining estimates of the reddening (and intrinsic color) from a measurement of the observed color. For notational simplicity, we define  $E \equiv E(B - V)$  as the host galaxy reddening,  $L$  as the intrinsic late-time  $B - V$  color, and  $O$  as the observed late-time  $B - V$  color, with  $O = E + L$ . Bayes’s theorem says that the conditional probability  $p(E|O) \propto p(O|E)p(E)$ , where  $p(E)$  is just the reddening distribution derived above,  $p(E) \propto \exp(-E/0.138)$ , for  $E \geq 0$ . The other term, the probability of measuring an observed color given the reddening,  $p(O|E)$ , is simply equivalent to  $p(L = O - E)$ , the probability that the intrinsic color (which has a Gaussian distribution, as above) is that which added to  $E$  gives the observed color,  $O$ .

The conclusion is that for an SN Ia that has a measured late-time  $B - V$  color  $BV_{35}$  with an observational uncertainty  $\sigma_{BV_{35}}$  (with all quantities measured in magnitudes), the probability

<sup>13</sup> Nobili et al. (2003) suggest that the distribution of  $B - V$  observations of unextinguished SNe Ia near 35 days past maximum can be explained entirely by measurement errors, with no intrinsic component to the dispersion. However, here we have combined late-time data from 32 to 92 days into one measurement using the Lira law, and this combination reduces the observational uncertainty. Even with a conservative estimate of a positive correlation among the late-time data for a given SN, our results require an intrinsic late-time color dispersion with a significance  $\geq 3 \sigma$ .

distribution of the host galaxy reddening  $E(B - V)$ , again called  $E$  for notational simplicity, is given by

$$p(E|BV_{35}, \sigma_{BV_{35}}) \propto \begin{cases} \exp\left(-\frac{(BV_{35} - E - 1.054)^2}{2(\sigma_{BV_{35}}^2 + 0.049^2)}\right) \exp\left(-\frac{E}{0.138}\right), & E \geq 0, \\ 0, & E < 0. \end{cases} \quad (3)$$

This is a generalization of the Bayesian filter of Riess et al. (1996a), where our model now includes the uncertainty caused by the intrinsic scatter in SN Ia late-time color in addition to the observational uncertainty. We use equation (3) with the data in Table 3 to get the initial host galaxy reddening estimates required in training MLCS2k2.

The intrinsic scatter in the late-time colors (0.049 mag) dominates the uncertainty in the mean unreddened color from the maximum likelihood fit (0.018 mag), and thus we strongly urge that “negative” extinction be disallowed in any model. The idea of negative extinctions (because of a color zero point that is estimated redward of the true color zero point) is a convenient fiction, but only if the intrinsic color scatter is smaller than the zero-point uncertainty. Here we have the opposite case; blue SNe Ia (with  $BV_{35} = 1.0$  mag, for example) are blue because of the intrinsic color variation, not because they are the only “truly” unextinguished objects. Thus, “correcting” them with a negative extinction is a mistake. As long as there is no systematic error in the mean unreddened color approaching the level of the intrinsic scatter, the mean of equation (3),  $\int_0^\infty p(E|BV_{35}, \sigma_{BV_{35}})E dE$ , provides an *unbiased* estimate of the host galaxy reddening (see the Appendix for further details).

### 3. MODEL

We are now in a position to define our light-curve model. For each passband,  $X$ , we fit the observed light curves (corrected for Galactic extinction,  $K$ -correction, and time dilation),  $\mathbf{m}_X$ , as follows (bold quantities span the SN rest-frame phase):

$$\mathbf{m}_X(t - t_0) = \mathbf{M}_X^0 + \mu_0 + \zeta_X \left( \alpha_X + \frac{\beta_X}{R_V} \right) A_V^0 + \mathbf{P}_X \Delta + \mathbf{Q}_X \Delta^2, \quad (4)$$

where  $t_0$  is the epoch of maximum light in  $B$ ,  $\mathbf{M}_X^0$  are the absolute magnitudes of the fiducial SNe Ia,  $\mu_0$  is the true distance modulus,  $R_V$  and  $A_V^0$  are the host galaxy extinction parameters (§ 2.2),  $\Delta$  is the luminosity/light-curve shape parameter, and  $\mathbf{P}_X$  and  $\mathbf{Q}_X$  are vectors describing the change in light-curve shape as a (quadratic) function of  $\Delta$ . There are five “free” parameters in the model:  $t_0$ ,  $\mu_0$ ,  $\Delta$ ,  $A_V^0$ , and  $R_V$ . As in previous versions of MLCS, we solve for the optimal vectors  $\mathbf{M}_X^0$ ,  $\mathbf{P}_X$ , and  $\mathbf{Q}_X$  using a training set for which we estimate initial values of the free parameters based on relative distances from the Hubble law.

Given a training set and solution for the optimal vectors, we construct an empirical model covariance matrix  $S$  that incorporates the variance and covariance in the residuals of the training set data from the model (minus the variance and covariance in the training set data themselves). Following Riess et al. (1998b), the diagonal elements of the  $S$  matrix are derived from the variance about the model, while the off-diagonal elements are estimated from two-point correlations (in the same passband

at different epochs, in different passbands at the same epoch, and in different passbands at different epochs).

Armed with the template vectors and the model covariance matrix, we can apply the model. Along with the light-curve observations  $\mathbf{m}_X$ , conscientious observers provide a covariance matrix of “noise,”  $N$ , albeit typically only a diagonal one consisting of the variance of each data point (even though SN light-curve data can be highly correlated, for instance, in the fact that all the light-curve points are usually referenced to the same few field comparison stars). We correct these data for Galactic extinction and incorporate the uncertainty estimate of Schlegel et al. (1998), whereby  $\sigma(E(B - V)_{\text{true}}) \simeq 0.16E(B - V)_{\text{true}}$ , updating both the diagonal and off-diagonal elements of  $N$  (the uncertainties in the Galactic extinction correction are highly correlated but generally small). We also apply the  $K$ -correction (§ 2.1), incorporate the  $K$ -correction uncertainty in the diagonal elements of  $N$  (unfortunately we do not have enough data to estimate the  $K$ -correction correlations), and correct for time dilation.

We find the best-fit model parameters via  $\chi^2$  minimization, with

$$\chi^2 = \mathbf{r}^T C^{-1} \mathbf{r}, \quad (5)$$

where  $\mathbf{r}$  is the vector of residuals (in all bands) for a given set of model parameters and  $C = S + N$ . We use a downhill simplex method (amoeba; Press et al. 1992) to perform the minimization (although linear algebra suffices in solving for  $\mu_0$  and  $A_V^0$ , if the other model parameters are fixed) and determine their best-fit parameters. Because the  $S$  matrix is empirically determined from the training set, application of the model to objects in the training set will necessarily have a minimum reduced  $\chi^2_{\nu}$  ( $\equiv \chi^2$  per degree of freedom) close to unity, but in applying the model to other objects, the minimum  $\chi^2_{\nu}$  still yields useful goodness-of-fit information (indicating how similar the light curves of the new object are to those in the training set, given the nature of the model).

We have also incorporated the ability to add priors on any of the model parameters directly into the fit. The previous versions of MLCS, for instance, used a Bayesian filter requiring the extinction to be nonnegative, but this was enforced after the best fits were determined. The advantage of that approach was convenience and expediency, but at the expense of ignoring correlations among the parameters. Those versions of MLCS used  $\mu_V$ , the distance modulus uncorrected for extinction, as the basic distance model parameter rather than  $\mu_0 = \mu_V - A_V$ , in order to minimize this undesirable correlation, thus making the Bayesian filter simple and effective. However, there are situations in which one might like to include other prior information into the fit. For example, a sparsely sampled light curve may not allow for a good determination of the time of maximum light, but we may have other information about the time of maximum from spectroscopy (Riess et al. 1997b). In the extreme limit of the “snapshot” method (Riess et al. 1998a), spectroscopy could be used to determine prior constraints on both  $t_0$  and  $\Delta$ . Alternately, we may have observations in additional, nonmodeled passbands (such as in the near-infrared), which impose prior constraints on  $A_V^0$  or  $R_V$ . Incorporating priors,  $\hat{p}$ , into the fit is straightforward: we simply adjust the  $\chi^2$  to

$$\chi^2 = \mathbf{r}^T C^{-1} \mathbf{r} - 2 \ln \hat{p}(t_0, \mu_0, \Delta, A_V^0, R_V), \quad (6)$$

taking care to reinterpret this “ $\chi^2$ ” in the proper way when estimating the goodness of the model fit (which depends only on the first term, as opposed to the parameter uncertainties). This

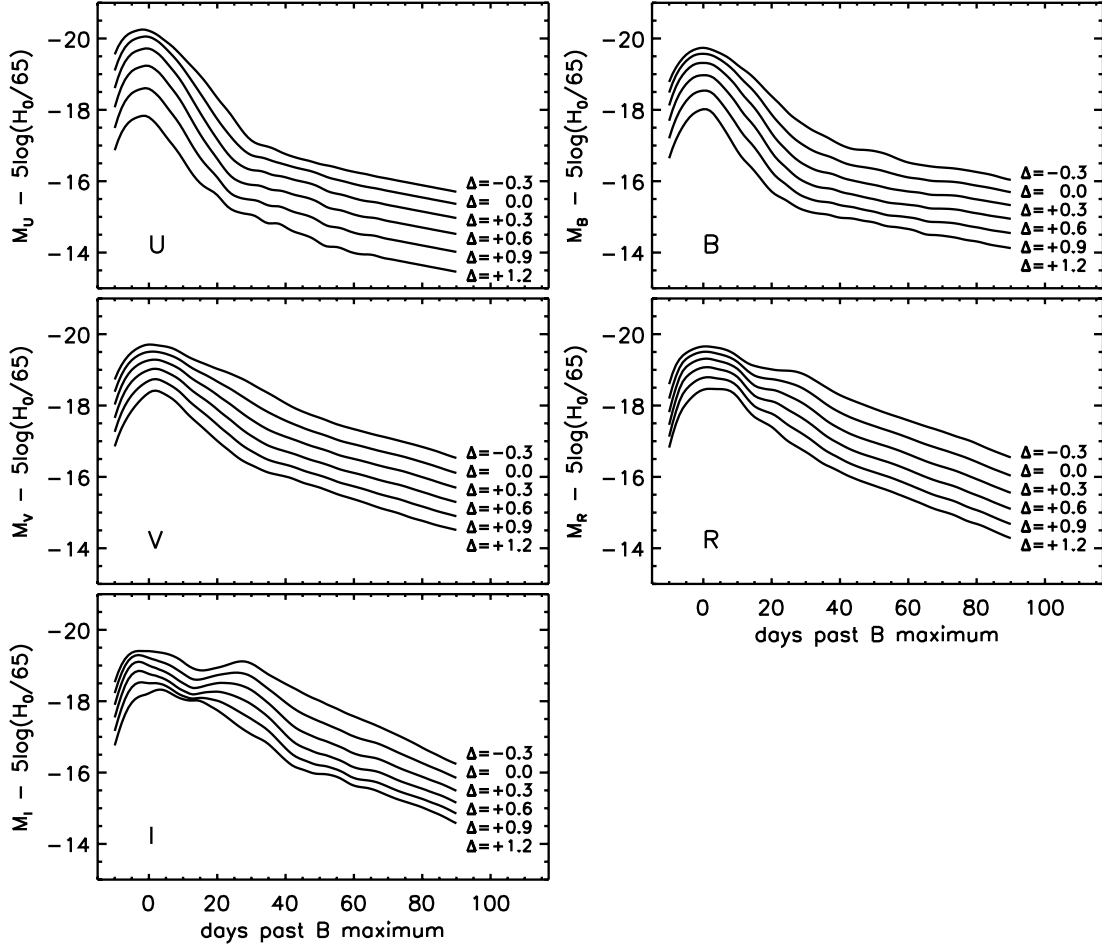


FIG. 7.—MLCS2k2 intrinsic  $UBVR$  light-curve templates,  $M_X = M_X^0 + P_X \Delta + Q_X \Delta^2$ , shown over a range of luminosity and light-curve shape from  $\Delta = -0.3$  (brighter) to  $+1.2$  (fainter).

procedure allows the parameters to be “naturally” filtered during the fit.

#### 4. TRAINING

The training set is the most critical part of the analysis; it requires objects with accurate estimates of the model parameters, in order to construct the template vectors and covariance matrix. As in Riess et al. (1998b), we use the Hubble law to determine precise relative distances; thus, useful objects in the training set need to have recession velocities that are dominated by cosmological expansion, not peculiar motions. The objects also need to have well-measured light curves at maximum light so that  $t_0$  and  $V_{\max}$  (to be used in determining  $\Delta$ , as below) can be reliably determined. Finally, we require accurate host galaxy extinction estimates for the training set objects. This estimate comes from well-sampled  $B$  and  $V$  light curves at the epochs past +35 days when the intrinsic color is not a strong function of luminosity, as described in § 2.3. Ideally, we would also like estimates of the host galaxy extinction law  $R_V$  for each SN, but these are not easily determined a priori, and values based on the SN light curves themselves would require knowledge of the intrinsic colors we are trying to determine! To avoid this conundrum, then, we restrict the initial training sample to objects not very significantly reddened (as determined from the  $B - V$  color at  $\sim 35$  days past maximum), so that variation in  $R_V$  does not have a large effect, allowing us to fix  $R_V = 3.1$  for the initial training set.

Our initial training set consists of 37 SNe Ia, with  $cz \geq 2500$  km s $^{-1}$  (measured in the cosmic microwave background [CMB] frame) and well-sampled light curves beginning earlier than 10 days past maximum light: SN 1990O, SN 1990af, SN 1992P, SN 1992ae, SN 1992al, SN 1992bc, SN 1992bg, SN 1992bl, SN 1992bo, SN 1992bp, SN 1992br, SN 1993H, SN 1993O, SN 1993ag, SN 1994M, SN 1995ac, SN 1996C, SN 1996bl, SN 1997E, SN 1997Y, SN 1997bq, SN 1998V, SN 1998ab, SN 1998bp, SN 1998de, SN 1998es, SN 1999aa, SN 1999ac, SN 1999da, SN 1999gp, SN 2000ca, SN 2000cf, SN 2000dk, SN 2000fa, SN 2001V, SN 2001cz, and SN 2002er. For each SN, we initially calculate  $\Delta$  as the difference between  $V$  magnitude at maximum light (corrected for host galaxy extinction) and the Hubble line given the host galaxy redshift. We assign an uncertainty in  $\Delta$  from the quadrature sum of the uncertainty in the direct fit of  $V_{\max}$ , the extinction uncertainty, and a distance uncertainty based on a peculiar velocity uncertainty of  $\sigma = 300$  km s $^{-1}$ . These initial guesses of  $\Delta$  span a range of over 2 mag, and the sample includes a wide range of over- and under-luminous objects.

From the initial guesses of the model parameters and uncertainties, we derive the best-fit vectors,  $M_X^0$ ,  $P_X$ , and  $Q_X$ , as well as the model covariance matrix  $S$ , all of which are sampled daily over the range  $-10$  days  $\leq t \leq +90$  days past  $B$  maximum, where the data are constraining. With these vectors, we can apply this initial model to our larger sample of SNe, deriving new estimates of  $\Delta$  and  $A_V^0$  while constraining the distance moduli to

their Hubble law estimates (within the uncertainties listed above). Iterating this procedure leads to convergence on a consistent set of model parameters, template vectors, and a model covariance matrix.<sup>14</sup>

In Figure 7 we present the one-parameter family of unreddened template light curves in  $UBVRI$  over a wide range of luminosity, based on the final template vectors derived in the training process. The characteristic result that intrinsically brighter SNe Ia (low  $\Delta$ ) have broader light curves is clearly established in all passbands. We note that while  $\Delta$  is originally estimated by the relative  $V$ -band magnitude difference at maximum light, during the iterative training the meaning of  $\Delta$  changes. It should be viewed simply as a unitless fit parameter that describes the family of light curves and can differ significantly from its original value for a given SN. In particular, it should not be subtracted directly from  $V_{\max}$  to obtain a corrected peak magnitude, although this has been a convenient usage in the past.<sup>15</sup> The fiducial MLCS2k2  $\Delta = 0$  model light curve has  $\Delta m_{15}(B) = 1.07$  (read directly off the  $B$ -band template) and stretch parameter  $s_B = 0.96$  (fitted as described by Jha et al. 2006). The intrinsic absolute  $V$  magnitude at the time of  $B$  maximum light is given by

$$M_V(t=0) = -19.504 + 0.736\Delta + 0.182\Delta^2 + 5 \log\left(\frac{H_0}{65 \text{ km s}^{-1} \text{ Mpc}^{-1}}\right) \text{ mag.} \quad (7)$$

The MLCS2k2 relations also allow us to determine the intrinsic colors of SNe Ia with varying luminosity at any epoch. In Figure 8 we show a sample of the color relations in  $U - B$ ,  $B - V$ , and  $V - I$ , at maximum light and 35 days after maximum. Our fiducial  $\Delta = 0$  SN Ia has  $U - B = -0.47$  mag,  $B - V = -0.07$  mag,  $V - R = 0.00$  mag, and  $V - I = -0.29$  mag, at the time of  $B$  maximum light. The intrinsic dispersion in these colors is captured in the model covariance matrix. Because the intrinsic colors are determined by the model at any epoch, all of the observations can be used to constrain the extinction and  $\Delta$ , weighted by the observational and model uncertainties. This is a more flexible approach than just using late-time or maximum light relations to determine the extinction (e.g., Phillips et al. 1999), or using colors at one specific epoch to determine the intrinsic luminosity and extinction (e.g., at  $t = +12$  days, as suggested by Wang et al. 2005).

## 5. APPLICATION

We have applied the model to our full sample of 133 SNe Ia, employing priors,  $\hat{p}(t_0, \mu_0, \Delta, A_V^0, R_V)$ , via equation (6). Of

<sup>14</sup> In principle, this procedure could artificially decrease the scatter in our distance measurements, if the contribution of individual SNe Ia to the templates “circularly” affected their fits when the model is applied. In practice, however, the templates are derived from a large enough number of objects that this effect is negligible. We have further tested this by applying the model derived only from the initial training set to the remaining objects, as well as by partitioning the full sample and iteratively training the model on one-half of the data, and then applying it to the other half. In all cases the scatter in the Hubble diagram of the objects not used in the training set is significantly decreased, typically from  $\sim 0.5$  to  $\lesssim 0.2$  mag. We thus choose to retain the largest training set sample we can to most robustly determine the templates and, importantly, their associated model uncertainty.

<sup>15</sup> The reason for this is the increased dispersion and shallower slope in SN Ia luminosity at the slowly declining end of the distribution, which has become clear only with the growing samples of SNe Ia now being used to calibrate the luminosity/light-curve shape relationship. The iterative training for MLCS2k2 associates objects with similar light-curve shapes, which leads the model vectors away from their starting point at  $\mathbf{P}_V(t=0) = 1$  and  $\mathbf{Q}_V(t=0) = 0$  to convergence at  $\mathbf{P}_V(t=0) = 0.736$  and  $\mathbf{Q}_V(t=0) = 0.182$ .

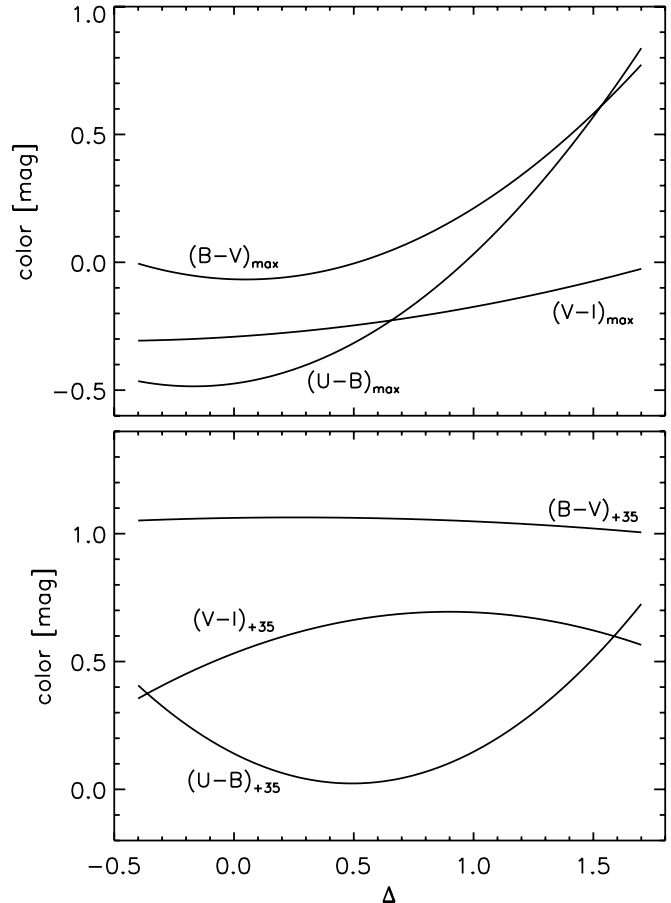


FIG. 8.—MLCS2k2 maximum light (top) and late-time (+35 days; bottom) intrinsic  $U - B$ ,  $B - V$ , and  $V - I$  colors as a function of decreasing intrinsic luminosity (increasing  $\Delta$ ).

course, in applying the model to an SN Ia light curve we impose no prior constraints on the distance modulus,  $\mu_0$ . We require  $t_0$  to be within  $\pm 3$  days of the input estimate used to derive the time-dependent Galactic extinction and  $K$ -corrections; in cases where the fit  $t_0$  is outside this range or otherwise inconsistent with the input value, we start the fit over using the updated estimate for  $t_0$ . We use a uniform prior on  $\Delta$  over the range  $-0.3 \leq \Delta \leq 1.6$ , with a Gaussian roll-off (with  $\sigma = 0.1$ ) on either side of that range; this restricts the fits to the range of  $\Delta$  encompassed by the training set (roughly between  $-0.4$  and  $1.7$ ) and for which the model is valid. We do not see objects in our sample “piling up” at these boundaries, but it will be important to check that application of MLCS2k2 to a new object does not require a fit that extrapolates beyond the training set.

In addition, we constrain the maximum light host galaxy extinction parameter  $A_V^0$  to be nonnegative, as well as incorporate the results of our determination of the SN Ia intrinsic color and reddening distributions (§ 2.3). There we determined that the host galaxy reddening distribution was well described by an exponential with a scale length of  $\tau_{E(B-V)} = 0.138$  mag. Because our MLCS2k2 model parameter is  $A_V^0$ , the maximum light extinction in  $V$ , we need to convert the results based on the late-time  $B - V$  color, multiplying by  $R_V^{\text{obs}}$  [to change from  $E(B - V)$  to  $A_V$ ] and dividing by  $\zeta_V$ . With average late-time values of these quantities, we derive our final prior on the maximum light host galaxy extinction,  $\hat{p}(A_V^0) \propto \exp(-A_V^0/0.457 \text{ mag})$  for  $A_V^0 \geq 0$ . Our results show little sensitivity to the exact value for the exponential scale in the denominator.

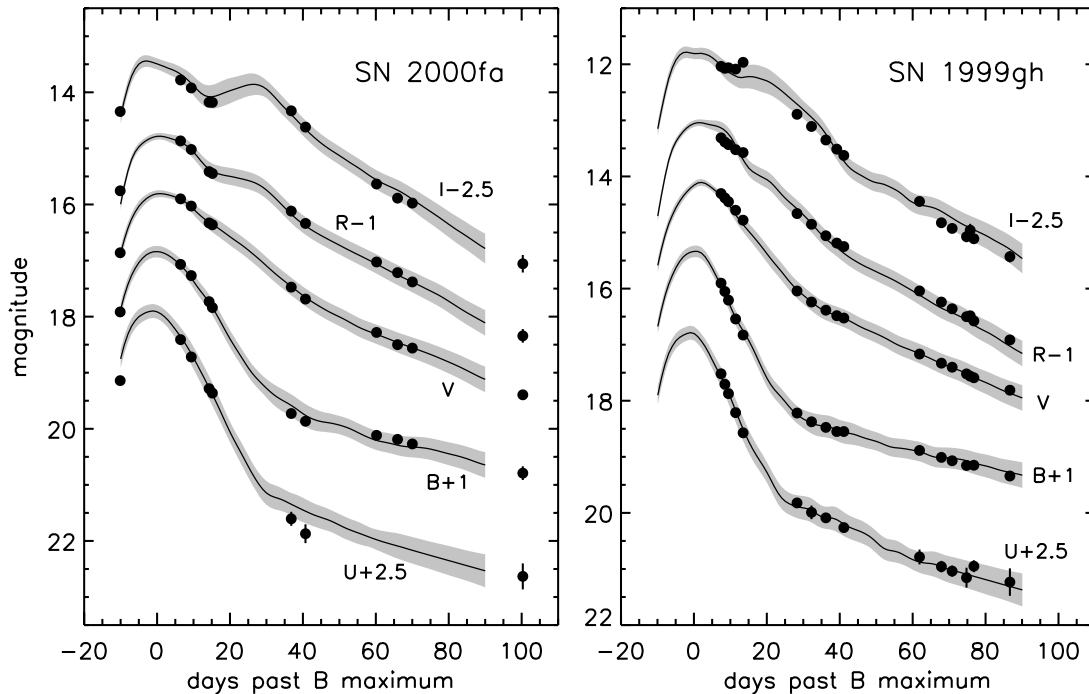


FIG. 9.—MLCS2k2 fits of SN 2000fa and SN 1999gh. The SN rest-frame *UBVRI* photometry (*filled circles*) is shown with the best-fit model light curves (*solid lines*), as well as the model uncertainty (*shaded regions*) derived from the diagonal elements of the model covariance matrix. The SNe are well fitted, even with gaps in the light curves and a lack of observations at maximum light.

Finally, we use a prior constraint on  $R_V$  estimated from its distribution over multiple lines of sight to stars in the Galaxy (CCM89). For  $\hat{p}(R_V)$ , we adopt a functional form that is Gaussian in  $R_V^{-1}$  with a mean  $\langle R_V \rangle = 3.1$  and standard deviation  $(\langle R_V^2 \rangle - \langle R_V \rangle^2)^{1/2} = 0.4$ . The choice of a prior on  $R_V$  has a significant effect on the best-fit parameters of heavily extinguished SNe Ia, and we discuss this issue more fully below (§ 6.4).

To fit the MLCS2k2 model, we first calculate  $\chi^2$  (eq. [6]) over a four-dimensional grid of  $(t_0, \mu_0, \Delta, A_V^0)$ , with a fixed  $R_V = 3.1$ . Because variation in the reddening law has only a very small effect on the measured distance if the extinction is low, we expand this to a five-dimensional grid (including  $R_V$  as a fit parameter) just for those objects that show  $A_V^0 > 0.5$  mag in the initial fit. Although mapping  $\chi^2$  over a large grid is computationally expensive, it allows us to fully explore our nonlinear model and makes evident, for example, objects that could be well fitted in separate regions of parameter space or otherwise have a complicated  $\chi^2$  surface (which can occur especially for SNe Ia with sparse photometry).

In Figure 9 we show example light-curve fits for SN 2000fa and SN 1999gh (Jha et al. 2006), whose light curves are typical in the nearby SN Ia sample. SN 2000fa has a slightly broader light curve than average and is moderately extinguished by dust in its host galaxy, while SN 1999gh is a fast declining, subluminal SN Ia with little host extinction. The shaded regions in the figure show the model uncertainty (more precisely, the square root of the diagonal elements of  $S$ ), which generally dominates the uncertainty in the data.

From the likelihood grid we calculate  $p(t_0, \mu_0, \Delta, A_V^0, R_V) = \exp(-\chi^2/2)$ , the posterior probability density function (pdf). We marginalize this distribution to determine the pdf's of the parameters of interest. Although the full surface is difficult to visualize or present, we show all of the two-dimensional marginalizations of the probability densities for SN 2000fa and SN 1999gh in Figure 10, clearly illustrating bivariate correlations among the model parameters. Finally, in Figure 11 we show the one-

dimensional pdf's for each of the model parameters. Our best estimate of each parameter is given by the *mean* of these distributions (not the mode/peak), and their standard deviations give an estimate of the uncertainty. Note that in some cases these distributions are asymmetric or otherwise non-Gaussian [for example,  $p(A_V^0)$  for SN 1999gh], so the mean and standard deviation do not always provide a complete description. In typical cases, however, the distribution of  $\mu_0$ , the parameter of primary interest, can be well approximated by a Gaussian. While derivative calculations based on these parameters (fitting the Hubble diagram, for example) should formally employ the full pdf, we have found that after combination of just a few objects, the formally correct (but computationally intensive) method yields results indistinguishable from those based on the means and standard deviations.

We present the full results of the MLCS2k2 fits to our SN Ia sample in Table 4. The tabulated values correspond to the means and standard deviations of the posterior pdf for each parameter taken *individually*, i.e., marginalizing over all the other parameters. As such the model derived from setting each parameter to its mean value does not correspond exactly to the true best fit (at which the pdf is maximized), although the difference is typically small. Since we are generally interested in the individual parameter distributions (and the distance modulus in particular), it is more useful to present the fit results in this form.

Two objects, SN 2000cx and SN 2002cx, cannot be fitted by MLCS2k2. Li et al. (2001, 2003) discuss the peculiarity of these objects, whose light curves are distinct from the vast majority of SNe Ia. In addition, SN 1998D and SN 1999cw have poor fits, with very broad or multi-peaked pdf's. Both of these objects have a paucity of data (no more than three photometric points in any filter), and more importantly, the first observations for each object occurred well after maximum light (+32 and +24 days, respectively; see Table 1). This allows for a wide range of models to fit the data well, and the uncertain results are not very informative, but we present them for completeness.

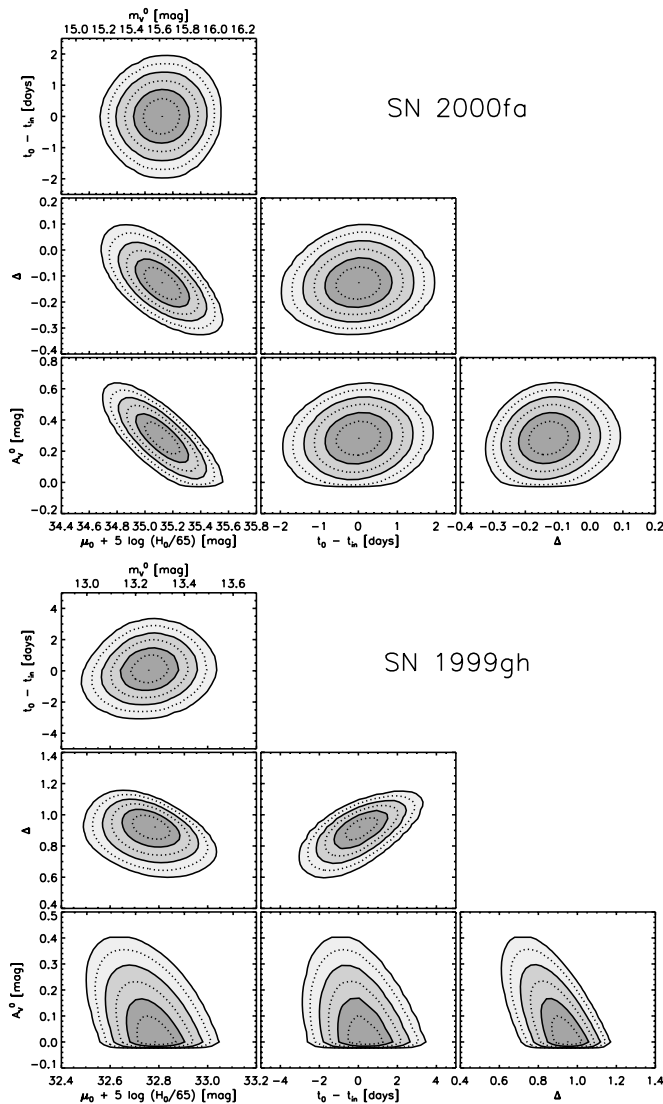


FIG. 10.—Two-dimensional MLCS2k2 probability densities for the fits to SN 2000fa and SN 1999gh. Each panel shows the four-dimensional probability density marginalized over the two remaining parameters. The solid lines and shaded regions indicate 1, 2, and 3  $\sigma$  confidence regions (more precisely, 68.3%, 95.4%, and 99.7% enclosed probability regions), while the dotted lines show  $\frac{1}{2}\sigma$  contours.

Finally, analysis of the distance modulus residuals (see §§ 6.1 and 6.2) leads us to conclude that the  $\mu_0$  (and  $m_V^0$ ) uncertainties listed in Table 4 are slightly underestimated. This is likely due to our less than perfect knowledge of the model covariance matrix  $S$ . In particular, our analysis shows that the objects with the smallest distance uncertainties are the ones that show the strongest evidence for unmodeled variance, suggesting that there is a systematic floor to the distance uncertainty (as opposed to a multiplicative factor to adjust all the uncertainties). We thus recommend that the  $\mu_0$  and  $m_V^0$  uncertainties in Table 4 be increased by adding  $\sigma_{\text{add}} = 0.08$  mag in quadrature to yield a final estimate of  $\sigma(\mu_0)$  and  $\sigma(m_V^0)$ , and we adopt this augmented uncertainty for all subsequent results.<sup>16</sup>

<sup>16</sup> Note that this number shows only the deficiency of our implementation; in a perfect version of a model like MLCS2k2, the average distance uncertainties would match the scatter in the residuals without augmentation. This is because the intrinsic variation of SNe Ia around the model is encapsulated into the model covariance matrix, just not perfectly in our case. Other distance fitters that do not include any model uncertainty often add the standard deviation of the residuals in quadrature to individual distance errors; this would not be correct for MLCS2k2.

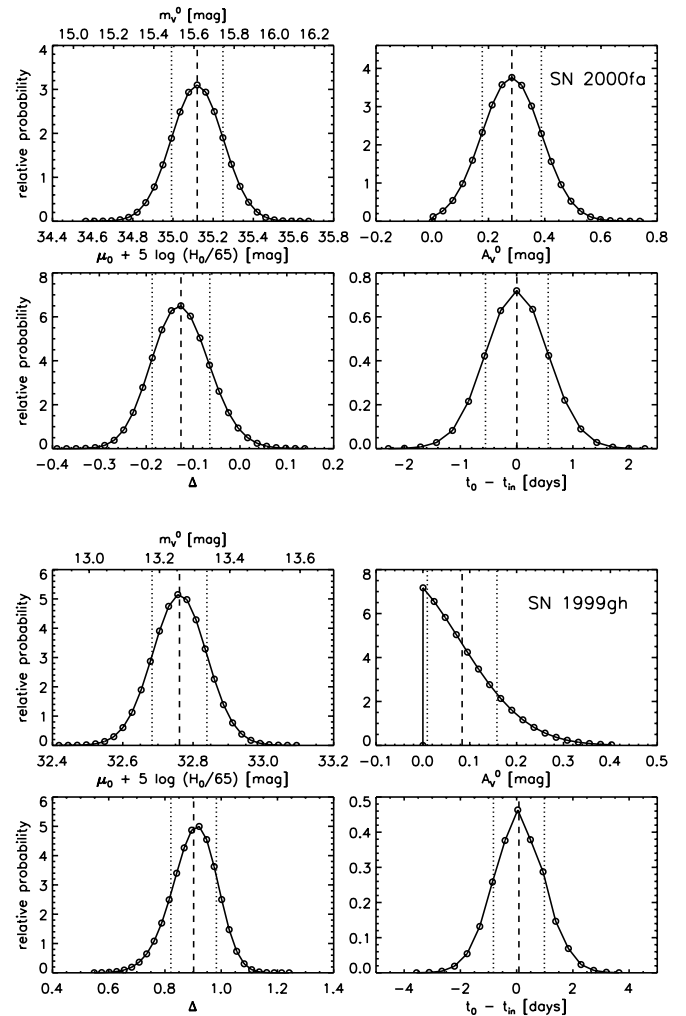


FIG. 11.—MLCS2k2 probability densities for the fits to SN 2000fa and SN 1999gh. Each panel shows the probability distribution for each free parameter, marginalizing over the three remaining parameters. The open circles show the grid points at which the fits were calculated. The distribution mean is denoted by the dashed line, while the dotted lines show one standard deviation about the mean.

## 6. DISCUSSION

### 6.1. Hubble Flow Sample

Constructing a Hubble diagram of nearby SNe Ia (Hubble 1929; Kirshner 2004) requires a Hubble flow sample, for which the measured recession velocities are dominated by the cosmological redshift (as opposed to peculiar motions). We consider objects with  $cz \geq 2500$  km s<sup>-1</sup> in the CMB rest frame to be in the Hubble flow, yielding 101 objects out of our original 133. In addition, we require good distances for these SNe Ia, eliminating SN 2002cx, which could not be fitted by MLCS2k2. Similarly, we further cull the Hubble flow sample to exclude objects whose first observation occurs more than 20 days past maximum light ( $t_1 > 20$  days; see Table 1), eliminating two SNe Ia (SN 1998D and SN 1999cw). Excessive host galaxy extinction also leads to uncertain distances, and we exclude objects with mean  $A_V^0 > 2.0$  mag (another two objects: SN 1995E and SN 1999cl). We explore the consequences of this relatively permissive extinction cut in § 6.4.

We constructed a Hubble diagram of the 96 SNe Ia that passed these cuts and noticed a significant outlier: SN 1999ej in NGC 495 (Friedman et al. 1999;  $cz_{\text{CMB}} = 3831$  km s<sup>-1</sup>) gave

TABLE 4  
MLCS2k2 LIGHT-CURVE FITS

SN Ia	$t_0 - 2,400,000$ (HJD)	$\mu_0 + 5 \log h_{65}$ (mag)	$\Delta$	$A_V^0$ (mag)	$R_V$	$m_V^0$ (mag)	Notes
1972E.....	41446.64 ± 0.96	27.829 ± 0.110	-0.145 ± 0.062	0.068 ± 0.059	3.1	8.324 ± 0.110	
1980N.....	44585.60 ± 0.63	31.602 ± 0.099	+0.032 ± 0.060	0.282 ± 0.082	3.1	12.098 ± 0.099	
1981B.....	44670.95 ± 0.73	31.104 ± 0.140	-0.081 ± 0.060	0.364 ± 0.121	3.1	11.599 ± 0.140	
1981D.....	44680.21 ± 0.53	31.009 ± 0.228	+0.257 ± 0.204	0.631 ± 0.270	3.07 ± 0.37	11.505 ± 0.228	
1986G.....	46561.36 ± 0.24	27.460 ± 0.203	+1.054 ± 0.065	2.227 ± 0.224	2.87 ± 0.27	7.956 ± 0.203	
1989B.....	47564.32 ± 0.59	30.040 ± 0.144	+0.035 ± 0.087	1.330 ± 0.144	2.86 ± 0.29	10.536 ± 0.144	
1990N.....	48081.90 ± 0.17	32.153 ± 0.090	-0.242 ± 0.046	0.174 ± 0.084	3.1	12.648 ± 0.090	
1990O.....	48076.12 ± 1.02	35.814 ± 0.095	-0.150 ± 0.066	0.071 ± 0.063	3.1	16.310 ± 0.095	HF
1990T.....	48083.06 ± 1.16	36.555 ± 0.169	-0.111 ± 0.095	0.200 ± 0.120	3.1	17.050 ± 0.169	HF
1990Y.....	48115.94 ± 1.28	36.221 ± 0.248	+0.036 ± 0.161	0.497 ± 0.150	3.03 ± 0.36	16.717 ± 0.248	HF
1990af.....	48195.86 ± 0.44	36.714 ± 0.160	+0.519 ± 0.113	0.144 ± 0.134	3.1	17.209 ± 0.160	HF
1991M.....	48334.98 ± 1.41	33.516 ± 0.179	+0.191 ± 0.112	0.269 ± 0.174	3.1	14.012 ± 0.179	
1991S.....	48348.17 ± 1.18	37.274 ± 0.131	-0.147 ± 0.074	0.129 ± 0.101	3.1	17.770 ± 0.131	HF
1991T.....	48374.03 ± 0.14	30.776 ± 0.080	-0.220 ± 0.031	0.340 ± 0.070	3.1	11.271 ± 0.080	
1991U.....	48356.18 ± 1.38	35.612 ± 0.167	-0.096 ± 0.086	0.379 ± 0.187	3.1	16.108 ± 0.167	HF
1991ag.....	48414.23 ± 1.45	34.007 ± 0.097	-0.134 ± 0.061	0.060 ± 0.056	3.1	14.503 ± 0.097	HF
1991bg.....	48603.12 ± 0.31	31.418 ± 0.101	+1.404 ± 0.047	0.611 ± 0.123	3.21 ± 0.41	11.913 ± 0.101	
1992A.....	48640.63 ± 0.19	31.654 ± 0.067	+0.447 ± 0.054	0.038 ± 0.032	3.1	12.150 ± 0.067	
1992G.....	48669.96 ± 1.06	32.584 ± 0.141	-0.198 ± 0.047	0.499 ± 0.136	3.07 ± 0.37	13.079 ± 0.141	
1992J.....	48671.64 ± 1.60	36.453 ± 0.265	+0.445 ± 0.236	0.259 ± 0.185	3.1	16.949 ± 0.265	HF
1992K.....	48674.37 ± 1.76	33.207 ± 0.153	+1.378 ± 0.116	0.223 ± 0.144	3.1	13.702 ± 0.153	HF
1992P.....	48719.20 ± 0.86	35.585 ± 0.124	-0.142 ± 0.082	0.136 ± 0.092	3.1	16.081 ± 0.124	HF
1992ae.....	48803.18 ± 1.34	37.731 ± 0.167	+0.051 ± 0.102	0.163 ± 0.141	3.1	18.227 ± 0.167	HF
1992ag.....	48806.95 ± 0.81	35.247 ± 0.151	+0.027 ± 0.077	0.424 ± 0.134	3.1	15.743 ± 0.151	HF
1992al.....	48837.86 ± 0.49	34.125 ± 0.065	-0.144 ± 0.035	0.045 ± 0.038	3.1	14.621 ± 0.065	HF
1992aq.....	48833.33 ± 1.18	38.651 ± 0.117	+0.193 ± 0.116	0.065 ± 0.053	3.1	19.147 ± 0.117	HF
1992au.....	48830.62 ± 1.55	37.379 ± 0.216	+0.292 ± 0.196	0.115 ± 0.097	3.1	17.875 ± 0.216	HF
1992bc.....	48912.06 ± 0.17	34.859 ± 0.042	-0.236 ± 0.030	0.017 ± 0.014	3.1	15.354 ± 0.042	HF
1992bg.....	48915.39 ± 1.23	36.126 ± 0.130	+0.008 ± 0.076	0.130 ± 0.091	3.1	16.622 ± 0.130	HF
1992bh.....	48920.43 ± 0.97	36.899 ± 0.133	-0.051 ± 0.085	0.204 ± 0.114	3.1	17.395 ± 0.133	HF
1992bk.....	48938.95 ± 1.59	37.184 ± 0.170	+0.414 ± 0.157	0.097 ± 0.082	3.1	17.679 ± 0.170	HF
1992bl.....	48946.33 ± 1.14	36.497 ± 0.123	+0.353 ± 0.117	0.061 ± 0.060	3.1	16.993 ± 0.123	HF
1992bo.....	48986.26 ± 0.16	34.742 ± 0.091	+0.595 ± 0.072	0.051 ± 0.049	3.1	15.237 ± 0.091	HF
1992bp.....	48980.41 ± 0.74	37.793 ± 0.106	+0.095 ± 0.092	0.060 ± 0.056	3.1	18.289 ± 0.106	HF
1992br.....	48984.63 ± 1.34	37.977 ± 0.185	+0.888 ± 0.173	0.125 ± 0.115	3.1	18.472 ± 0.185	HF
1992bs.....	48985.05 ± 1.30	37.636 ± 0.161	-0.031 ± 0.089	0.172 ± 0.137	3.1	18.132 ± 0.161	HF
1993B.....	49003.99 ± 1.35	37.779 ± 0.148	-0.115 ± 0.076	0.198 ± 0.119	3.1	18.274 ± 0.148	HF
1993H.....	49068.92 ± 0.46	35.109 ± 0.095	+0.904 ± 0.076	0.139 ± 0.086	3.1	15.605 ± 0.095	HF
1993L.....	49095.40 ± 1.51	31.986 ± 0.305	+0.041 ± 0.198	0.722 ± 0.172	3.04 ± 0.36	12.482 ± 0.305	
1993O.....	49134.40 ± 0.43	37.140 ± 0.095	+0.025 ± 0.070	0.077 ± 0.059	3.1	17.636 ± 0.095	HF
1993ac.....	49269.70 ± 1.19	36.881 ± 0.189	-0.054 ± 0.108	0.377 ± 0.191	3.1	17.377 ± 0.189	HF
1993ae.....	49288.58 ± 1.19	34.468 ± 0.187	+0.401 ± 0.157	0.055 ± 0.055	3.1	14.963 ± 0.187	HF
1993ag.....	49316.67 ± 0.68	37.041 ± 0.131	+0.119 ± 0.089	0.166 ± 0.097	3.1	17.537 ± 0.131	HF
1993ah.....	49302.52 ± 1.33	35.640 ± 0.200	+0.147 ± 0.164	0.136 ± 0.121	3.1	16.135 ± 0.200	HF
1994D.....	49432.47 ± 0.10	31.187 ± 0.067	+0.142 ± 0.035	0.109 ± 0.047	3.1	11.682 ± 0.067	
1994M.....	49473.61 ± 0.90	35.244 ± 0.121	+0.261 ± 0.079	0.226 ± 0.115	3.1	15.739 ± 0.121	HF
1994Q.....	49496.72 ± 1.09	35.759 ± 0.141	-0.140 ± 0.075	0.192 ± 0.121	3.1	16.255 ± 0.141	HF
1994S.....	49518.28 ± 0.50	34.356 ± 0.077	-0.084 ± 0.074	0.054 ± 0.045	3.1	14.852 ± 0.077	HF
1994T.....	49514.54 ± 0.52	36.012 ± 0.112	+0.731 ± 0.103	0.093 ± 0.075	3.1	16.507 ± 0.112	HF
1994ae.....	49684.65 ± 0.15	32.563 ± 0.065	-0.191 ± 0.036	0.070 ± 0.047	3.1	13.058 ± 0.065	
1995D.....	49768.60 ± 0.44	32.813 ± 0.074	-0.186 ± 0.041	0.081 ± 0.060	3.1	13.308 ± 0.074	
1995E.....	49774.67 ± 0.54	33.198 ± 0.178	+0.006 ± 0.057	2.241 ± 0.176	2.85 ± 0.28	13.694 ± 0.178	
1995ac.....	49992.99 ± 0.40	36.511 ± 0.108	-0.231 ± 0.047	0.252 ± 0.107	3.1	17.007 ± 0.108	HF
1995ak.....	50021.16 ± 0.93	34.741 ± 0.138	+0.122 ± 0.065	0.613 ± 0.131	3.12 ± 0.39	15.237 ± 0.138	HF
1995al.....	50028.96 ± 0.44	32.714 ± 0.081	-0.282 ± 0.035	0.177 ± 0.065	3.1	13.209 ± 0.081	
1995bd.....	50086.31 ± 0.24	34.006 ± 0.125	-0.239 ± 0.051	0.523 ± 0.241	3.01 ± 0.35	14.502 ± 0.125	HF
1996C.....	50128.42 ± 0.90	35.947 ± 0.104	-0.104 ± 0.055	0.136 ± 0.091	3.1	16.443 ± 0.104	HF
1996X.....	50190.85 ± 0.33	32.432 ± 0.065	+0.095 ± 0.048	0.061 ± 0.044	3.1	12.927 ± 0.065	
1996Z.....	50215.24 ± 1.46	32.760 ± 0.238	+0.112 ± 0.210	0.609 ± 0.316	3.05 ± 0.36	13.256 ± 0.238	HF
1996ab.....	50224.69 ± 1.07	38.934 ± 0.146	+0.164 ± 0.127	0.098 ± 0.091	3.1	19.430 ± 0.146	HF
1996ai.....	50255.21 ± 0.81	31.151 ± 0.187	-0.098 ± 0.068	3.662 ± 0.185	2.09 ± 0.12	11.647 ± 0.187	
1996bk.....	50368.46 ± 1.02	32.195 ± 0.142	+1.011 ± 0.124	0.711 ± 0.184	3.10 ± 0.38	12.691 ± 0.142	
1996bl.....	50376.32 ± 0.58	36.096 ± 0.113	-0.116 ± 0.064	0.208 ± 0.115	3.1	16.592 ± 0.113	HF
1996bo.....	50386.93 ± 0.30	34.043 ± 0.138	+0.057 ± 0.070	0.938 ± 0.138	3.02 ± 0.35	14.538 ± 0.138	HF

TABLE 4—Continued

SN Ia	$t_0 - 2,400,000$ (HJD)	$\mu_0 + 5 \log h_{65}$ (mag)	$\Delta$	$A_V^0$ (mag)	$R_V$	$m_V^0$ (mag)	Notes
1996bv.....	50403.72 ± 1.27	34.213 ± 0.157	-0.206 ± 0.065	0.547 ± 0.159	3.07 ± 0.37	14.709 ± 0.157	HF
1997E.....	50467.58 ± 0.41	34.105 ± 0.091	+0.341 ± 0.084	0.213 ± 0.104	3.1	14.600 ± 0.091	HF
1997Y.....	50486.88 ± 1.37	34.563 ± 0.104	+0.060 ± 0.078	0.196 ± 0.087	3.1	15.058 ± 0.104	HF
1997bp.....	50548.94 ± 0.52	32.895 ± 0.092	-0.180 ± 0.049	0.537 ± 0.086	2.88 ± 0.31	13.391 ± 0.092	HF
1997bq.....	50557.99 ± 0.18	33.458 ± 0.109	-0.095 ± 0.063	0.513 ± 0.095	3.03 ± 0.35	13.953 ± 0.109	HF
1997br.....	50559.26 ± 0.23	32.248 ± 0.104	-0.303 ± 0.031	0.804 ± 0.112	3.03 ± 0.35	12.743 ± 0.104	
1997cn.....	50586.64 ± 0.77	34.532 ± 0.070	+1.381 ± 0.046	0.071 ± 0.059	3.1	15.027 ± 0.070	HF
1997cw.....	50630.75 ± 0.98	34.075 ± 0.151	-0.179 ± 0.064	1.092 ± 0.145	2.97 ± 0.33	14.570 ± 0.151	HF
1997dg.....	50720.05 ± 0.84	36.149 ± 0.114	-0.006 ± 0.076	0.201 ± 0.102	3.1	16.645 ± 0.114	HF
1997do.....	50766.21 ± 0.45	33.601 ± 0.118	-0.146 ± 0.080	0.312 ± 0.102	3.1	14.097 ± 0.118	HF
1997dt.....	50785.60 ± 0.31	32.723 ± 0.191	-0.126 ± 0.070	1.849 ± 0.198	3.03 ± 0.34	13.219 ± 0.191	
1998D.....	50841.07 ± 2.02	34.089 ± 0.627	+0.571 ± 0.482	0.346 ± 0.186	3.1	14.585 ± 0.627	Poor fit
1998V.....	50891.27 ± 0.84	34.395 ± 0.102	-0.055 ± 0.064	0.209 ± 0.115	3.1	14.891 ± 0.102	HF
1998ab.....	50914.43 ± 0.25	35.213 ± 0.100	-0.118 ± 0.051	0.394 ± 0.082	3.1	15.709 ± 0.100	HF
1998aq.....	50930.80 ± 0.13	31.974 ± 0.046	-0.063 ± 0.036	0.024 ± 0.019	3.1	12.470 ± 0.046	
1998bp.....	50936.39 ± 0.33	33.304 ± 0.075	+1.114 ± 0.057	0.188 ± 0.100	3.1	13.800 ± 0.075	HF
1998bu.....	50952.40 ± 0.23	30.283 ± 0.117	-0.015 ± 0.038	1.055 ± 0.114	3.13 ± 0.36	10.778 ± 0.117	
1998co.....	50987.76 ± 1.32	34.431 ± 0.126	+0.464 ± 0.196	0.301 ± 0.183	3.1	14.926 ± 0.126	HF
1998de.....	51026.69 ± 0.17	34.400 ± 0.082	+1.448 ± 0.036	0.398 ± 0.101	3.1	14.896 ± 0.082	HF
1998dh.....	51029.83 ± 0.22	32.846 ± 0.087	-0.051 ± 0.042	0.471 ± 0.061	2.76 ± 0.27	13.342 ± 0.087	
1998dk.....	51056.58 ± 1.48	33.802 ± 0.219	-0.127 ± 0.134	0.508 ± 0.152	3.10 ± 0.38	14.297 ± 0.219	HF
1998dm.....	51062.03 ± 1.16	33.067 ± 0.178	-0.192 ± 0.073	1.045 ± 0.160	3.08 ± 0.37	13.563 ± 0.178	
1998dx.....	51071.32 ± 0.80	36.917 ± 0.099	+0.190 ± 0.099	0.086 ± 0.065	3.1	17.413 ± 0.099	HF
1998ec.....	51088.41 ± 1.07	35.082 ± 0.161	-0.169 ± 0.077	0.569 ± 0.125	3.01 ± 0.35	15.578 ± 0.161	HF
1998ef.....	51113.99 ± 0.22	34.142 ± 0.105	+0.269 ± 0.083	0.046 ± 0.044	3.1	14.638 ± 0.105	HF
1998eg.....	51110.69 ± 1.23	35.353 ± 0.120	+0.014 ± 0.118	0.224 ± 0.118	3.1	15.849 ± 0.120	HF
1998es.....	51141.89 ± 0.15	33.263 ± 0.078	-0.287 ± 0.030	0.227 ± 0.073	3.1	13.758 ± 0.078	HF
1999X.....	51203.48 ± 1.04	35.546 ± 0.132	-0.181 ± 0.075	0.139 ± 0.095	3.1	16.041 ± 0.132	HF
1999aa.....	51231.97 ± 0.15	34.468 ± 0.042	-0.271 ± 0.028	0.020 ± 0.018	3.1	14.963 ± 0.042	HF
1999ac.....	51250.60 ± 0.17	33.334 ± 0.081	-0.086 ± 0.039	0.308 ± 0.072	3.1	13.830 ± 0.081	HF
1999aw.....	51253.96 ± 0.29	36.551 ± 0.043	-0.369 ± 0.032	0.019 ± 0.018	3.1	17.047 ± 0.043	HF
1999by.....	51309.50 ± 0.14	31.158 ± 0.073	+1.348 ± 0.030	0.170 ± 0.083	3.1	11.653 ± 0.073	
1999cc.....	51315.62 ± 0.46	35.859 ± 0.092	+0.337 ± 0.097	0.148 ± 0.088	3.1	16.355 ± 0.092	HF
1999cl.....	51342.28 ± 0.26	30.604 ± 0.163	+0.031 ± 0.087	2.666 ± 0.160	2.22 ± 0.15	11.099 ± 0.163	
1999cp.....	51363.22 ± 0.26	33.520 ± 0.098	-0.103 ± 0.102	0.072 ± 0.062	3.1	14.015 ± 0.098	HF
1999cw.....	51352.49 ± 1.47	33.363 ± 0.141	-0.306 ± 0.067	0.161 ± 0.073	3.1	13.859 ± 0.141	Poor fit
1999da.....	51370.57 ± 0.17	33.905 ± 0.101	+1.451 ± 0.038	0.233 ± 0.115	3.1	14.400 ± 0.101	HF
1999dk.....	51413.92 ± 0.78	34.273 ± 0.098	-0.233 ± 0.047	0.201 ± 0.094	3.1	14.769 ± 0.098	HF
1999dq.....	51435.70 ± 0.15	33.668 ± 0.067	-0.338 ± 0.024	0.369 ± 0.077	3.1	14.163 ± 0.067	HF
1999ee.....	51469.29 ± 0.14	33.472 ± 0.088	-0.208 ± 0.030	0.797 ± 0.085	2.76 ± 0.27	13.968 ± 0.088	HF
1999ef.....	51457.78 ± 1.27	36.657 ± 0.111	-0.057 ± 0.077	0.051 ± 0.044	3.1	17.153 ± 0.111	HF
1999ej.....	51482.37 ± 0.85	34.459 ± 0.123	+0.302 ± 0.088	0.166 ± 0.099	3.1	14.954 ± 0.123	
1999ek.....	51481.65 ± 0.50	34.360 ± 0.111	+0.050 ± 0.067	0.475 ± 0.251	3.1	14.856 ± 0.111	HF
1999gd.....	51518.40 ± 1.14	34.606 ± 0.167	+0.024 ± 0.073	1.381 ± 0.156	2.99 ± 0.33	15.101 ± 0.167	HF
1999gh.....	51513.53 ± 0.91	32.761 ± 0.078	+0.902 ± 0.081	0.084 ± 0.074	3.1	13.257 ± 0.078	HF
1999gp.....	51550.30 ± 0.17	35.622 ± 0.061	-0.323 ± 0.030	0.076 ± 0.051	3.1	16.118 ± 0.061	HF
2000B.....	51562.85 ± 1.30	34.628 ± 0.216	+0.253 ± 0.190	0.286 ± 0.136	3.1	15.123 ± 0.216	HF
2000E.....	51576.80 ± 0.35	31.721 ± 0.107	-0.277 ± 0.039	0.609 ± 0.189	3.01 ± 0.35	12.216 ± 0.107	
2000bh.....	51636.31 ± 1.47	35.309 ± 0.131	-0.026 ± 0.067	0.138 ± 0.093	3.1	15.805 ± 0.131	HF
2000bk.....	51646.02 ± 1.08	35.390 ± 0.156	+0.613 ± 0.129	0.290 ± 0.148	3.1	15.885 ± 0.156	HF
2000ca.....	51666.12 ± 0.46	35.250 ± 0.060	-0.125 ± 0.048	0.030 ± 0.024	3.1	15.746 ± 0.060	HF
2000ce.....	51667.45 ± 1.01	34.376 ± 0.179	-0.149 ± 0.060	1.761 ± 0.179	2.91 ± 0.30	14.872 ± 0.179	HF
2000cf.....	51672.33 ± 0.83	36.382 ± 0.104	-0.006 ± 0.065	0.194 ± 0.097	3.1	16.878 ± 0.104	HF
2000cn.....	51707.83 ± 0.16	35.153 ± 0.086	+0.716 ± 0.076	0.171 ± 0.109	3.1	15.648 ± 0.086	HF
2000cx.....	...	...	...	...	...	...	Bad fit
2000dk.....	51812.47 ± 0.28	34.408 ± 0.077	+0.578 ± 0.067	0.033 ± 0.032	3.1	14.904 ± 0.077	HF
2000fa.....	51892.25 ± 0.57	35.121 ± 0.128	-0.126 ± 0.061	0.283 ± 0.105	3.1	15.616 ± 0.128	HF
2001V.....	51973.28 ± 0.16	34.187 ± 0.065	-0.280 ± 0.032	0.092 ± 0.052	3.1	14.683 ± 0.065	HF
2001ay.....	52023.96 ± 0.78	35.926 ± 0.102	-0.405 ± 0.045	0.374 ± 0.098	3.1	16.422 ± 0.102	HF
2001ba.....	52034.18 ± 0.54	35.889 ± 0.075	-0.093 ± 0.056	0.041 ± 0.037	3.1	16.385 ± 0.075	HF
2001bt.....	52063.91 ± 0.21	33.952 ± 0.114	+0.071 ± 0.052	0.616 ± 0.111	3.00 ± 0.35	14.447 ± 0.114	HF
2001cn.....	52071.10 ± 0.74	34.130 ± 0.106	+0.007 ± 0.052	0.447 ± 0.100	3.1	14.625 ± 0.106	HF
2001cz.....	52103.89 ± 0.31	34.294 ± 0.111	-0.078 ± 0.054	0.254 ± 0.116	3.1	14.790 ± 0.111	HF
2001el.....	52182.55 ± 0.20	31.544 ± 0.077	-0.193 ± 0.032	0.696 ± 0.059	2.40 ± 0.19	12.040 ± 0.077	

TABLE 4—Continued

SN Ia	$t_0 - 2,400,000$ (HJD)	$\mu_0 + 5 \log h_{65}$ (mag)	$\Delta$	$A_V^0$ (mag)	$R_V$	$m_V^0$ (mag)	Notes
2002bf.....	$52337.87 \pm 0.50$	$35.480 \pm 0.134$	$-0.111 \pm 0.065$	$0.254 \pm 0.131$	3.1	$15.975 \pm 0.134$	HF
2002bo.....	$52356.89 \pm 0.14$	$31.945 \pm 0.105$	$-0.048 \pm 0.041$	$1.212 \pm 0.099$	$2.57 \pm 0.22$	$12.441 \pm 0.105$	
2002cx.....	...	...	...	...	...	...	Bad fit
2002er.....	$52524.84 \pm 0.15$	$33.034 \pm 0.085$	$+0.170 \pm 0.057$	$0.470 \pm 0.112$	3.1	$13.530 \pm 0.085$	HF
2003du.....	$52765.62 \pm 0.50$	$33.189 \pm 0.049$	$-0.247 \pm 0.028$	$0.037 \pm 0.026$	3.1	$13.685 \pm 0.049$	

NOTES.—Values listed are means and standard deviations for each of the parameters, as determined from their one-dimensional probability distributions marginalized over the other parameters. We use the standard notation  $h_{65} \equiv H_0/(65 \text{ km s}^{-1} \text{ Mpc}^{-1})$ . The extinction parameters  $A_V^0$  and  $R_V$  correspond to host galaxy extinction only; Galactic reddening is listed in Table 1. The corrected apparent peak magnitude  $m_V^0$  differs from the distance modulus  $\mu_0$  by an additive constant,  $m_V^0 \equiv \mu_0 + M_V^0$ .

a residual of  $\sim 0.6$  mag relative to the tight locus defined by the other objects. Spectroscopy of SN 1999ej showed it to be a normal SN Ia (Jha et al. 1999a), and the photometric data (Jha et al. 2006), although not plentiful with only four fit points each in *UBVRI*, nonetheless provide a good MLCS2k2 distance with no indication of peculiarity. The solution to this puzzle is that NGC 495 is in a particularly dense region of the group/poor cluster Zw 0107+3212 (whose brightest cluster galaxy is the nearby NGC 507). The cluster has a mean redshift  $cz_{\text{CMB}} \simeq 4690 \text{ km s}^{-1}$  and estimated velocity dispersion  $\sigma$  ranging from 440 to 590  $\text{km s}^{-1}$  (Ramella et al. 2002; Miller et al. 2002). Using this cluster mean redshift instead for SN 1999ej makes it fully consistent with the rest of the sample, suggesting that the observed recession velocity of NGC 495 is strongly affected by its environment, but we have chosen simply to exclude SN 1999ej from the Hubble flow sample. From an NED search, we did not find any independent evidence for large peculiar velocities among the other Hubble flow objects.

Our final Hubble flow sample is the largest compiled to date for SNe Ia in the nearby universe with homogeneous distances. It consists of 95 SNe Ia (denoted HF in Table 4), including 35 out of 44 of the objects presented by Jha et al. (2006), and more than doubles the MLCS Hubble flow sample of Jha et al. (1999b).

The Hubble diagram for this sample is shown in Figure 12, where we have fitted for only one free parameter, the intercept.<sup>17</sup> This intercept is scale dependent but can be expressed several different ways. One relates it to the absolute magnitude of the fiducial SN Ia and provides the derivation for the zero point in equation (7) (which in turn defines the relation between  $\mu_0$  and  $m_V^0$ ):

$$M_V^0 - 5 \log H_0 = m_V^0 - 25 - 5 \log \left( c(1+z) \int_0^z \left[ \Omega_M(1+z')^3 + \Omega_\Lambda \right]^{-1/2} dz' \right), \quad (8)$$

valid for a flat,  $\Omega_M + \Omega_\Lambda = 1$  universe. The weighted fit to the full Hubble flow sample gives  $M_V^0 - 5 \log h_{65} = -19.504 \pm 0.018$  mag (statistical uncertainty only). Alternately, we can fol-

<sup>17</sup> We have adopted an  $\Omega_M = 0.3$ ,  $\Omega_\Lambda = 0.7$  cosmology, which is significant for the more distant objects, and assumed a peculiar velocity uncertainty of  $\pm 300 \text{ km s}^{-1}$ , important for the nearby objects. Including in quadrature the error floor (see § 5) of  $\sigma_{\text{add}} = 0.08$  mag yields a reduced  $\chi^2$  of 1.06 for 94 degrees of freedom. This combination of the peculiar velocity uncertainty and  $\sigma_{\text{add}}$  results in a good fit across the whole Hubble flow sample, as well as selected subsamples.

low the notation of Jha et al. (1999b) and calculate the “intercept of the ridgeline,”  $a_V$ , defined as<sup>18</sup>

$$a_V = \log \left( c(1+z) \int_0^z \left[ \Omega_M(1+z')^3 + \Omega_\Lambda \right]^{-1/2} dz' \right) - 0.2m_V^0, \quad (9)$$

again assuming an  $\Omega_M + \Omega_\Lambda = 1$  universe. The full Hubble flow sample gives a best-fit value and formal uncertainty of  $a_V = 0.7139 \pm 0.0037$ . Unfortunately, we cannot directly compare these intermediate results with the values given by Jha et al. (1999b) because MLCS2k2 uses new template vectors with new magnitude and  $\Delta$  zero points, which uniformly shifts all distances,  $a_V$ , and  $M_V^0$ .

The scatter about the Hubble line in Figures 12 and 13 is  $\sigma = 0.18$  mag ( $\sim 8\%$  in distance). Part of the scatter in the Hubble diagram comes from our inexact knowledge of cosmological redshifts because of galactic peculiar velocities. Our estimate of the peculiar velocity uncertainty of  $\pm 300 \text{ km s}^{-1}$  corresponds to an uncertainty of 0.26 mag for the nearest objects in the Hubble flow sample ( $cz \simeq 2500 \text{ km s}^{-1}$ ), which drops to under 0.02 mag for the most distant object ( $cz = 37,239 \text{ km s}^{-1}$ ).

<sup>18</sup> In Jha et al. (1999b) the intercept of the ridgeline was given as  $a_V = \log cz - 0.2m_V^0$ . Here we explicitly show the dependence on cosmological parameters.

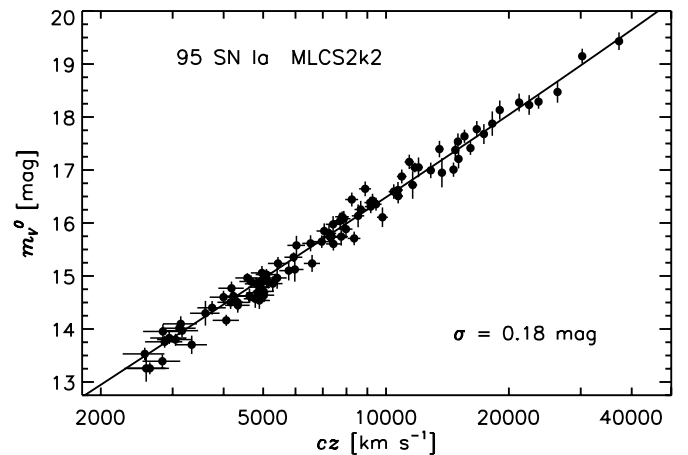


FIG. 12.—Apparent magnitude–redshift relation for our Hubble flow sample of 95 SNe Ia, using MLCS2k2 to correct for host galaxy extinction and intrinsic luminosity differences, and redshifts in the CMB frame. The shape of the solid line is fixed by the inverse square law and (for high  $cz$ ) the adopted  $\Omega_M = 0.3$ ,  $\Omega_\Lambda = 0.7$  cosmology; the intercept is the only free parameter and is determined to  $\pm 0.018$  mag.

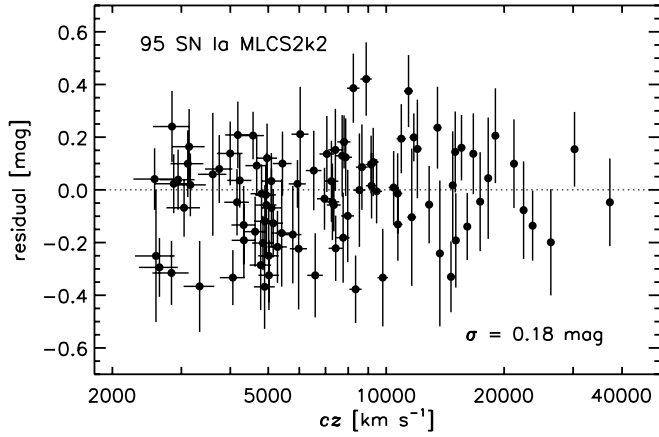


FIG. 13.—Magnitude residuals of the Hubble flow sample after MLCS2k2 correction, relative to the best-fit Hubble line shown in Fig. 12.

The mean peculiar velocity uncertainty for the full sample is 0.11 mag,<sup>19</sup> and subtracting this in quadrature from the overall dispersion implies that the *intrinsic* dispersion in SN Ia distances is at most 0.14 mag ( $\lesssim 7\%$  in distance) for samples similar to the one presented here.

Our Hubble flow sample is the largest ever fitted self-consistently with one technique and comprises data from diverse sources. In addition, we have attempted to limit the number of objects rejected from the sample. We believe that the measured dispersion is more reflective of the true dispersion among SNe Ia as they are currently being observed. Further restricting samples to the best objects (e.g., those with low reddening or close to fiducial luminosity/light-curve shape) clearly provides an avenue to reducing the dispersion, but it is important that these

<sup>19</sup> Because of the inverse dependence on the redshift, this is not the same as the peculiar velocity uncertainty at the mean redshift,  $cz_{\text{CMB}} = 8796 \text{ km s}^{-1}$ , where  $\pm 300 \text{ km s}^{-1}$  corresponds to  $\pm 0.07 \text{ mag}$ .

restrictions be carefully defined to avoid biasing applications of these samples to measuring cosmological parameters such as  $H_0$ ,  $\Omega_\Lambda$ , or  $w$ . For example, Guy et al. (2005) show that the quoted dispersions of 0.08 and 0.07 mag for the color-selected samples presented by Wang et al. (2003) and Wang et al. (2005), respectively, increase to 0.15 and 0.18 mag, when less stringent color cuts are applied. Comparison of MLCS2k2 to other SN Ia distance-fitting techniques based on the scatter in respective Hubble diagrams requires SN samples that are comparable (and ideally identical) in size and scope.

We display the distribution of the Hubble flow residuals versus the measured  $\Delta$  and  $A_V^0$  in Figure 14. No obvious trends are present, although the scatter of the points decreases with increasing  $\Delta$ , meaning that the lower luminosity SNe Ia have a tighter correlation around the luminosity/light-curve shape relationship. If we arbitrarily divide the sample into three bins, with slow decliners ( $\Delta < -0.15$ ), normal SNe Ia ( $-0.15 \leq \Delta \leq 0.3$ ), and fast decliners ( $\Delta > 0.3$ ), the residual dispersions are  $\sigma = 0.21 \text{ mag}$  ( $N = 17$  objects),  $0.18 \text{ mag}$  ( $N = 57$ ), and  $0.14 \text{ mag}$  ( $N = 21$ ), respectively.

In Figure 15 we show correlations in the MLCS2k2 fit parameters ( $\Delta$  and  $A_V^0$ ), as well as the residuals in the Hubble flow sample, with host galaxy morphological type and projected separation. These confirm well-known trends for SNe Ia (e.g., Hamuy et al. 2000 and references therein): slowly declining (low  $\Delta$ , high luminosity) SNe Ia and heavily extinguished SNe Ia are not generally found in early-type galaxies or in the outskirts of their hosts. Note that there are some exceptions, such as SN 1990Y, SN 1991bg, and SN 1993ac, all fitted with mean  $A_V^0 \geq 0.3 \text{ mag}$  in elliptical hosts (although in the case of the very subluminous SN 1991bg, there is a significant correlation between  $\Delta$  and  $A_V^0$ ). The bottom panels of Figure 15 show the residuals after MLCS2k2 calibration of the Hubble flow sample; note the large reduction in the vertical scale, showing the efficacy of corrections for intrinsic luminosity differences and extinction. The Hubble flow SNe Ia do not show any trend in their residuals with respect to host galaxy morphology or projected

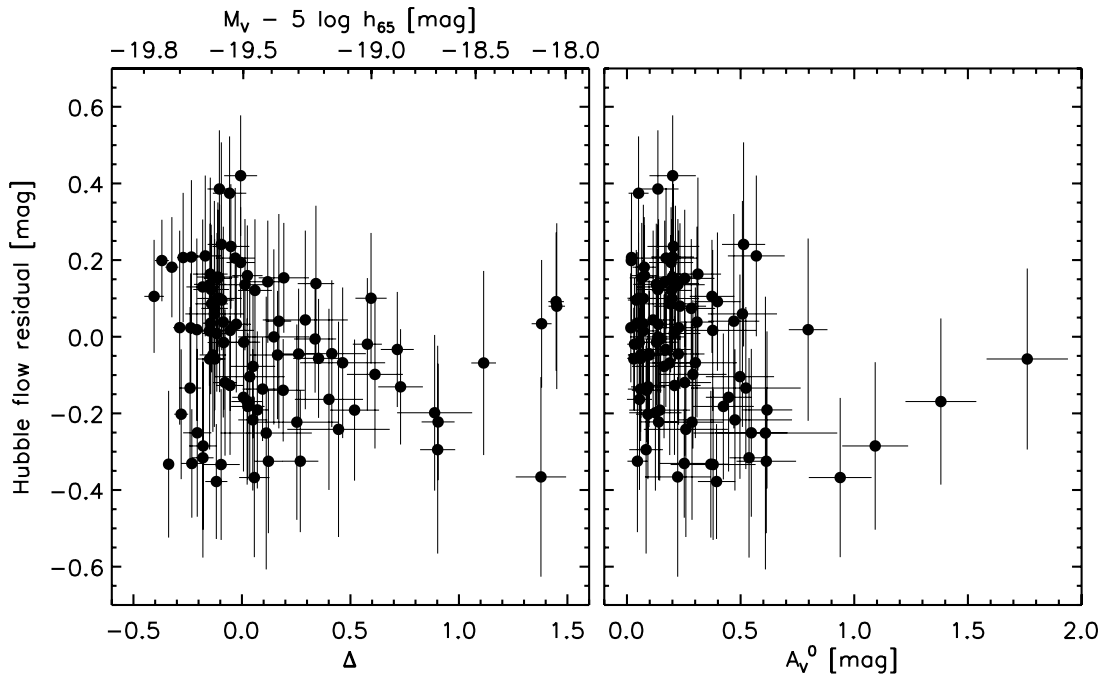


FIG. 14.—MLCS2k2 Hubble flow sample residuals vs. mean values of the light-curve shape parameter  $\Delta$  and host galaxy extinction  $A_V^0$ . The conversion from  $\Delta$  to the peak  $V$  absolute magnitude, given on the top axis of the left panel, is based on eq. (7).

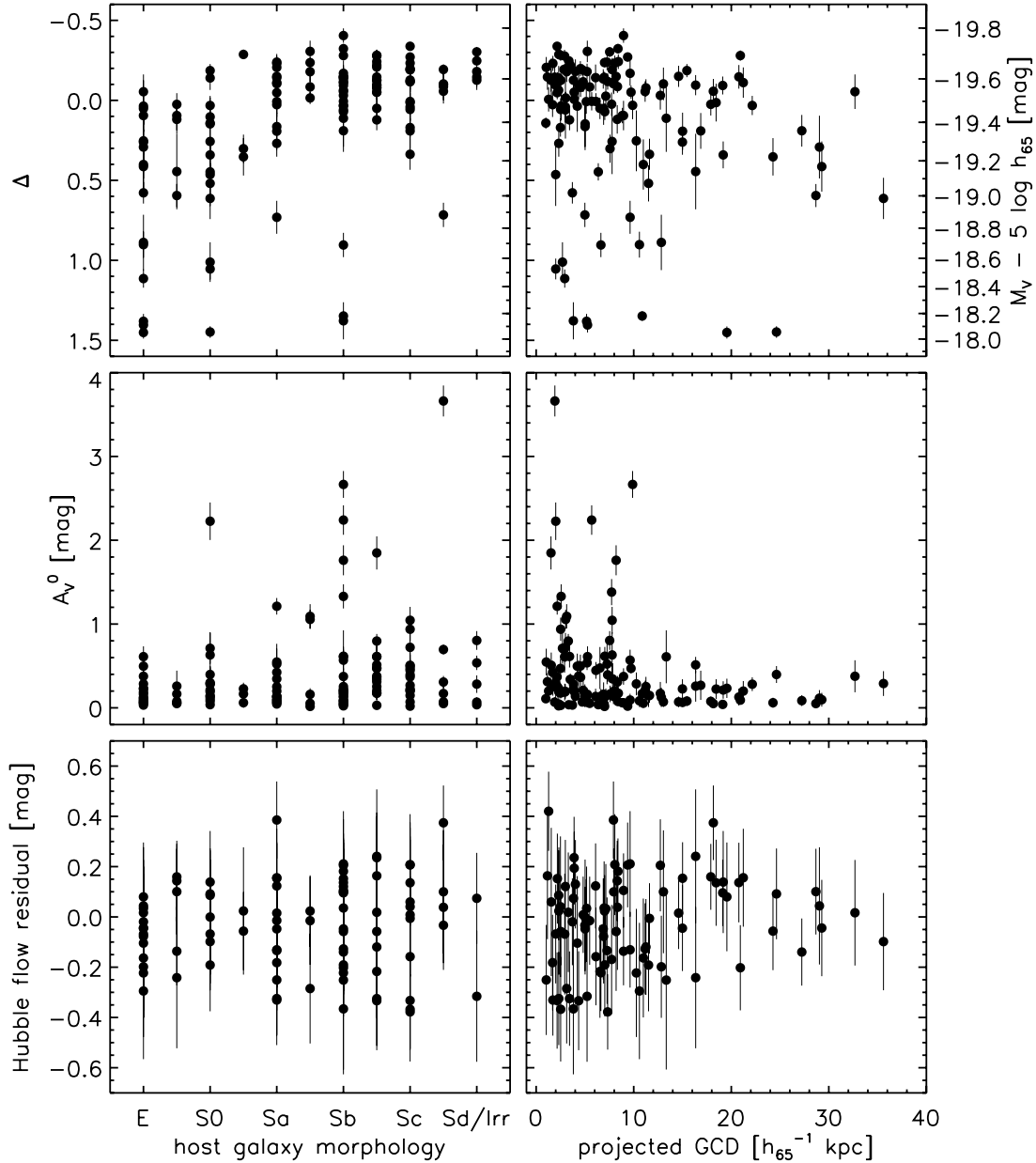


FIG. 15.—Correlations with host galaxy morphology and projected galactocentric distance (GCD). The top panels show mean values of the light-curve shape parameter  $\Delta$  for the full sample, and the middle panels show the distribution of host galaxy extinction  $A_V^0$ . The bottom panels show the residuals relative to the best-fit Hubble line for the Hubble flow sample only (after MLCS2k2 correction for luminosity differences and extinction). Projected GCDs are calculated using the angular offsets presented in Table 1, with angular diameter distances ( $\Omega_M = 0.3$ ,  $\Omega_\Lambda = 0.7$ ) calculated from the redshift for objects with  $cz_{\text{CMB}} \geq 2500$  km s $^{-1}$  and from the MLCS2k2 SN distances for objects with lower recession velocities.

galactocentric distance, although perhaps the residual scatter is decreased at large separations. There is also a hint that SNe Ia in elliptical hosts have slightly negative residuals after MLCS2k2 correction (meaning that they are corrected to be too bright/too nearby); however, the weighted average residual is only  $-0.06 \pm 0.06$  mag, consistent with zero. Grouping together E and E/S0 hosts (which show a similar paucity of slowly declining SNe Ia in the top left panel) yields a weighted mean residual of  $-0.02 \pm 0.04$  mag. The observed scatter in the residuals of the early-type hosts is less than the overall sample, with  $\sigma = 0.11$  mag for elliptical hosts only and  $\sigma = 0.13$  mag for E, E/S0, and S0 hosts; a large fraction of this scatter may be from peculiar velocities, which should contribute  $\sim 0.09$  mag to the dispersion for these galaxies.

Gallagher et al. (2005) have approached these issues in more detail, with integrated spectra of the host galaxies of many of

these SNe Ia, allowing them to correlate SN properties (before and after MLCS2k2 correction) with additional parameters such as host metallicity, star formation rate, and star formation history. Their results suggest no clear correlations with the MLCS2k2 Hubble flow residuals, although there is marginal evidence for a relation between the residuals and host metallicity.

### 6.2. A Hubble Bubble?

Zehavi et al. (1998) presented evidence for a large local void based on SN Ia distances that suggested a monopole in the peculiar velocity field. They found that the Hubble constant estimated from SNe Ia within  $70 h^{-1}$  Mpc was  $6.5\% \pm 2.2\%$  higher than  $H_0$  measured from SNe Ia outside this region, assuming a flat  $\Omega_M = 1$  universe. The significance of this void decreases in the current concordance cosmology ( $\Omega_M = 0.3$ ,  $\Omega_\Lambda = 0.7$ ) to

4.5%  $\pm$  2.1%, but it is still worthwhile to test whether the larger SN Ia sample and updated distances presented here provide evidence for or against a void.

Following Zehavi et al. (1998), it is convenient to work with the SN distances in units of  $\text{km s}^{-1}$ , making them independent of the distance scale. The ambiguity in the zero point of the Hubble diagram disappears if we use the quantity  $H_0 d_{\text{SN}}$ , which can be calculated as

$$H_0 d_{\text{SN}} = 65(10^{0.2(\mu_{65}-25)}) \text{ km s}^{-1}, \quad (10)$$

where we define  $\mu_{65} \equiv \mu_0 + 5 \log h_{65}$ , tabulated in the third column of Table 4. These can be compared to scale-independent luminosity distances: for an object at a cosmological redshift  $z$  in a flat universe,

$$H_0 d_L(z) = c(1+z) \int_0^z [\Omega_M(1+z')^3 + \Omega_\Lambda]^{-1/2} dz', \quad (11)$$

and the difference  $u = H_0 d_L(z) - H_0 d_{\text{SN}}$  is the host galaxy peculiar velocity. The deviation from the Hubble law is given by  $\delta H/H = u/H_0 d_{\text{SN}}$ .

The top panel of Figure 16 shows  $\delta H/H$  for the 95 SNe Ia in the full Hubble flow sample, where we have used our standard assumptions: a peculiar velocity uncertainty of  $\pm 300 \text{ km s}^{-1}$ ,  $\sigma_{\text{add}} = 0.08 \text{ mag}$ , and an  $\Omega_M = 0.3$ ,  $\Omega_\Lambda = 0.7$  cosmology. We then partition the full sample into two parts at each value of  $H_0 d_{\text{SN}}$  (such that there are at least six objects in the smaller subset) and calculate the best-fit Hubble constants  $H_{\text{inner}}$  and  $H_{\text{outer}}$ , as well as their corresponding uncertainties (see eqs. [2] and [3] of Zehavi et al. 1998). We define the void amplitude,  $\delta_H \equiv (H_{\text{inner}} - H_{\text{outer}})/H_{\text{outer}}$ , and display this quantity, with its uncertainty, as a function of the partition radius in the middle panel of Figure 16. We normalize  $\delta_H$  by its uncertainty in the bottom panel to illustrate the void significance.

The full Hubble flow sample clearly shows a void signature; the most significant void is derived when the sample is partitioned at  $H_0 d_{\text{SN}} \simeq 7400 \text{ km s}^{-1}$  (between SN 2000ca and SN 2000bh at  $H_0 d_{\text{SN}} = 7293$  and  $7494 \text{ km s}^{-1}$ , respectively), with  $\delta_H = 6.5\% \pm 1.8\%$ , similar in both location and amplitude to the Zehavi et al. (1998) result. We have performed a number of statistical tests to assess the significance of the result. We created  $3 \times 10^5$  Monte Carlo realizations of the data set with Hubble law deviations drawn from a Gaussian distribution with a standard deviation equal to the uncertainty in each data point and fitted for the most significant void or overdensity at each partition radius. Only 0.2% of the time was there a void as significant as the one seen in the actual data (at any location). Because this result depends on our assumed error distribution, we also created synthetic data sets with the Hubble law deviations randomly resampled from the deviations in the full data set (both with and without resampling of their errors). We have also performed a full bootstrap resampling analysis to determine the distribution of the void amplitude and significance around their best-fit values. In all of these tests a void with the significance as in the actual data was seen at most 1.2% of the time, and typically much less often, depending on the details of the synthetic sample, suggesting that the result is valid at the 2.5–3.5  $\sigma$  level of confidence.

The result also seems robust to jackknife tests; eliminating any one, two, or even three points from the sample does not result in a very large change in the void characteristics. With the three largest outliers removed (without justification; these objects are not peculiar in any way), the void amplitude only decreases

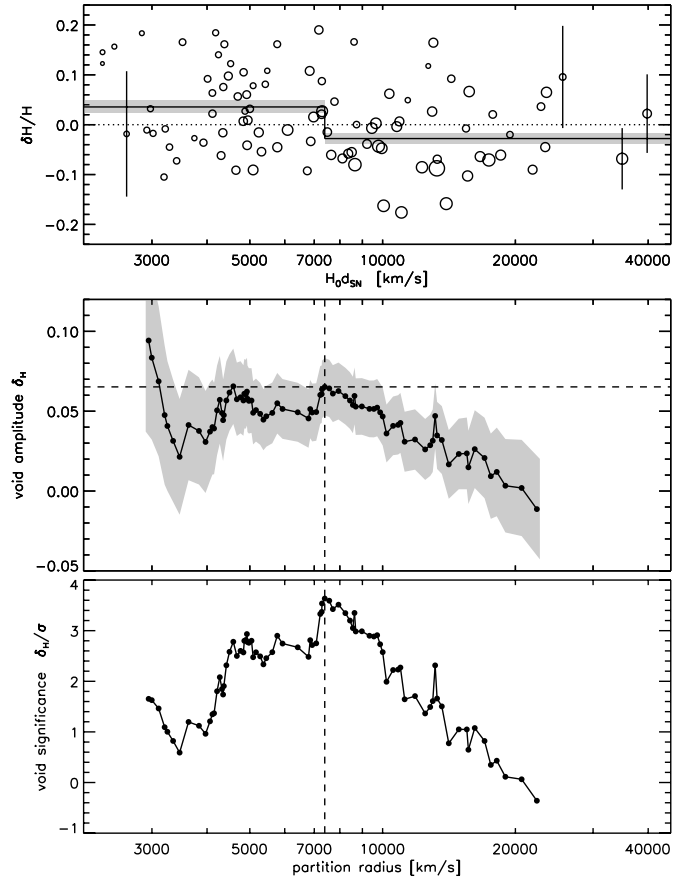


FIG. 16.—Indications of a local void. The top panel shows the deviation from the Hubble law for each object in the full Hubble flow sample. The radius of each circle is inversely proportional to the uncertainty, with several representative points showing the error bars explicitly to calibrate the symbol size. The solid line shows the best-fit Hubble constants in the two-zone model with the most significant void; the shaded regions give the  $1 \sigma$  uncertainty on each of these values. The middle panel shows the void amplitude,  $\delta_H \equiv H_{\text{inner}}/H_{\text{outer}} - 1$ , as a function of the radius at which the sample is partitioned, with the shaded region illustrating the  $1 \sigma$  uncertainty. The bottom panel shows the significance of the void, i.e., the void amplitude divided by its uncertainty. The most significant void occurs when the sample is partitioned at  $H_0 d_{\text{SN}} \simeq 7400 \text{ km s}^{-1}$ , with  $\delta_H = 6.5\% \pm 1.8\%$ .

to  $5.2\% \pm 1.8\%$ . We have also confirmed that the result persists using the 51 SNe Ia from 1997 onward only, an independent sample from Zehavi et al. (1998). The newer data show an even stronger result,  $\delta_H = 9.1\% \pm 2.6\%$  (at the same location), but there are only a handful of recent SNe Ia more distant than  $10,000 \text{ km s}^{-1}$  and the most robust results come from the full sample. Indications of this void can also be seen in other distance estimates to SNe Ia (although with largely overlapping samples), including the “gold” sample of Riess et al. (2004), which used a slightly earlier implementation of MLCS2k2 (Jha 2002), and  $\Delta m_{15}$  distances presented by Prieto et al. (2006), suggesting that it is not an artifact limited to our particular analysis.

The significance of the void at  $7400 \text{ km s}^{-1}$  is high partly because it is near the middle of the sample, such that  $H_{\text{inner}}$  and  $H_{\text{outer}}$  (and thus, their ratio) are most precisely measured. The data suggest that a void of similar amplitude may be present if the sample is partitioned near  $H_0 d_{\text{SN}} \simeq 4800 \text{ km s}^{-1}$ . Indeed, if we attempt to fit a three-zone model, the data support a model with  $\delta_H \simeq 8\%$  closer than  $4600 \text{ km s}^{-1}$ , and  $\delta_H \simeq 5\%$  for  $4600 \text{ km s}^{-1} \lesssim H_0 d_{\text{SN}} \lesssim 7400 \text{ km s}^{-1}$ , both relative to the outer region beyond  $7400 \text{ km s}^{-1}$ . However, another three-zone scenario with nearly the same likelihood has  $\delta_H \simeq 5\%$  nearer

than  $7400 \text{ km s}^{-1}$  and an *overdense* region with  $\delta_H \simeq -2\%$  at  $7400 \text{ km s}^{-1} \lesssim H_0 d_{\text{SN}} \lesssim 14,000 \text{ km s}^{-1}$  relative to the more distant Hubble flow, which is similar to the three-zone infall region model seen by Zehavi et al. (1998). Because there are fewer points in each region, the uncertainties in these numbers are increased to  $\sim 2.5\%$ . Moreover, the data do not favor a three-zone model over a two-zone model (a  $\chi^2$  decrease of less than 1 per new model parameter), unlike the situation for a two-zone model over a one-zone model (a  $\chi^2$  decrease of more than 7 per new parameter).

While it seems likely that this void signature is present in the SN data, is it really present in the universe? The void boundary does occur at a distance comparable to large mass concentrations in the local universe, including the Great Wall and the Southern Wall (Geller 1997 and references therein). A void with  $\delta_H = 6.5\%$  on this scale would imply an underdensity  $\delta\rho/\rho \simeq 20\% - 40\%$  for  $\Omega_M = 0.3$ , depending on our location within the void (Lahav et al. 1991; Turner et al. 1992). Such a large-scale density contrast, while not ruled out, is relatively unlikely in current  $\Lambda$ CDM models; the fraction of mass residing in such a void ranges from  $10^{-4}$  to a few percent, depending on the exact size and underdensity (Furlanetto & Piran 2006). Furthermore, tests of the Hubble bubble using other distance measures have not corroborated the SN Ia result. Using Tully-Fisher distances to galaxy clusters, Giovanelli et al. (1999) find  $\delta_H = 1.0\% \pm 2.2\%$  at  $7000 \text{ km s}^{-1}$ , while Hudson et al. (2004) derive  $\delta_H = 2.3\% \pm 1.9\%$  via fundamental plane cluster distances, both consistent with no void. Each method is subject to various systematic effects that could lead to spurious results. For the SN, these include  $K$ -corrections (but which are unlikely to cause a  $\sim 0.1$  mag error at  $z \simeq 0.03$ ), the effect of higher order multipoles on the monopole signature (but the sky distribution of the Hubble flow objects generally shows the void in all directions), or a possible photometric offset between the Calán/Tololo sample (accounting for most of the more distant objects) and more recent samples such as CfA I and II (making up most of the more nearby objects; Prieto et al. 2006). More data (throughout the nearby redshift range,  $z \lesssim 0.15$ ) and a more thorough analysis are needed to definitively resolve this open issue.

Regardless of whether the Hubble bubble is due to a real local void in the universe or an artifact of SN Ia distances, the feature is present in the Hubble flow SN sample, and this has important implications for using SNe Ia as tools for precision cosmology.<sup>20</sup> The Hubble flow sample is critical to both measurements of  $H_0$  (a differential measurement between the Hubble flow objects and nearby Cepheid-calibrated SNe Ia) and  $\Omega_\Lambda$  or  $w$  (a differential measurement between the Hubble flow objects and high-redshift SNe Ia), and both applications are affected by this result. The effect on  $H_0$  is readily apparent; our derived  $H_0$  will be  $6.5\%$  higher using a Hubble flow sample with  $H_0 d_{\text{SN}} \lesssim 7400 \text{ km s}^{-1}$  compared to a Hubble flow sample with  $H_0 d_{\text{SN}} \gtrsim 7400 \text{ km s}^{-1}$ . This is mitigated if we use the full Hubble flow sample, but that still yields a small but not insignificant effect: the full sample  $H_0$  is larger by  $3\%$  compared to just the subsample beyond  $7400 \text{ km s}^{-1}$  (which gives an intercept of the ridgeline,  $a_V = 0.7015 \pm 0.0049$ ).

<sup>20</sup> This is not to say that the reason for the discrepancy is not important. If the SNe Ia are revealing a true void, one would presumably proceed to measure the global Hubble constant and other cosmological parameters simply using a Hubble flow sample beyond the void region (with  $z \gtrsim 0.025$ ; Riess et al. 2004). However, if the indications for a void are due to an unknown systematic error, the effects on the cosmological utility of SNe Ia could be much more severe.

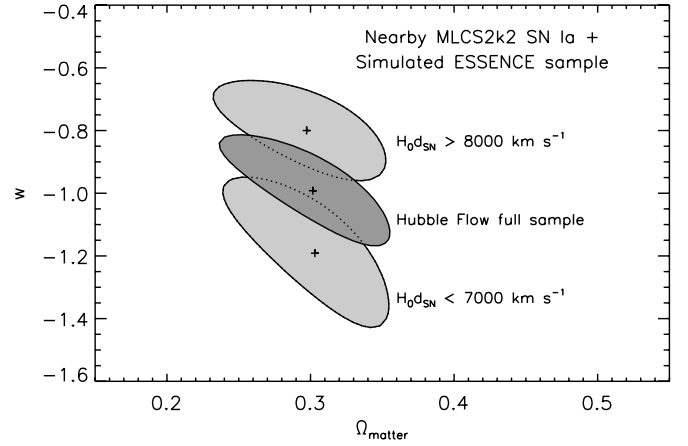


FIG. 17.—Effect of a local void on constraints of the dark energy equation of state, using a simulated sample of 200 SNe Ia with  $0.3 \leq z \leq 0.8$  as expected from the ESSENCE survey (Miknaitis et al. 2007). We perform a cosmological fit using the same simulated high-redshift sample plus three nearby samples: (1) the full MLCS2k2 Hubble flow sample with 95 SNe Ia, (2) the nearby Hubble flow objects with  $H_0 d_{\text{SN}} < 7000 \text{ km s}^{-1}$  (48 SNe Ia), and (3) the distant Hubble flow objects with  $H_0 d_{\text{SN}} > 8000 \text{ km s}^{-1}$  (40 SNe Ia). The figure shows  $68.3\%$  ( $1\sigma$ ) confidence regions (shaded) and the mean values of  $\Omega_M$  and  $w$  (crosses). The input cosmology for the simulated objects is  $\Omega_M = 0.3$ ,  $\Omega_\Lambda = 0.7$  ( $w = -1$ ), with the distance scale set by the full Hubble flow sample. In the cosmological fit, we assume a flat universe and a prior on  $\Omega_M = 0.30 \pm 0.04$ . The different low-redshift samples have a strong effect on the estimation of  $w$ , with  $w = -0.99 \pm 0.12$  for the full Hubble flow sample,  $w = -1.19 \pm 0.17$  for the nearby Hubble flow sample, and  $w = -0.80 \pm 0.11$  for the distant Hubble flow sample.

For high-redshift applications, the void signature can be much more important. Whereas the choice of using the full Hubble flow sample or one just with objects beyond the void region (with  $z \gtrsim 0.025$ ) does not significantly affect the conclusion from SNe Ia that we live in an accelerating universe (Riess et al. 2004), such a choice has a large effect in current efforts to measure the equation of state of the dark energy. In Figure 17 we show constraints on  $w$  from a simulation in which the current Hubble flow sample is used in conjunction with an artificial data set of 200 SNe Ia with  $0.3 \leq z \leq 0.8$ , as expected from the ongoing ESSENCE survey (Miknaitis et al. 2007). The results show a  $\sim 20\%$  difference in the derived value of  $w$  using the full Hubble flow sample compared to one only including objects with  $H_0 d_{\text{SN}} \geq 8000 \text{ km s}^{-1}$ , twice the target statistical uncertainty of the survey. For future surveys with thousands of high-redshift SNe Ia, this single systematic uncertainty in the Hubble flow sample could easily dwarf all other sources of uncertainty combined. Clearly, then, precision cosmology with SNe Ia will require an investment in *nearby* SNe Ia (in both data and analysis) comparable to the immense efforts ongoing and envisioned at high redshift.

### 6.3. The Local Group Motion

The precision of SN Ia distances makes them well suited to measure peculiar velocities of nearby galaxies (e.g., Riess et al. 1995b). Many new SNe Ia are being discovered at redshifts conducive to studying the local flow field ( $z \lesssim 0.03$ ). In Figure 18 we show a clear detection of the motion of the Local Group relative to the frame defined by nearby SNe Ia. We plot the host galaxy peculiar velocities [in the Local Group frame,  $u_{\text{LG}} = H_0 d_L(z_{\text{LG}}) - H_0 d_{\text{SN}}$ ] of 69 SNe Ia with  $1500 \text{ km s}^{-1} \leq H_0 d_{\text{SN}} \leq 7500 \text{ km s}^{-1}$  in Galactic coordinates (excluding the cluster member SN 1999ej and SN 2000cx, which could not be fitted by MLCS2k2). The distance range was chosen to exclude Virgo

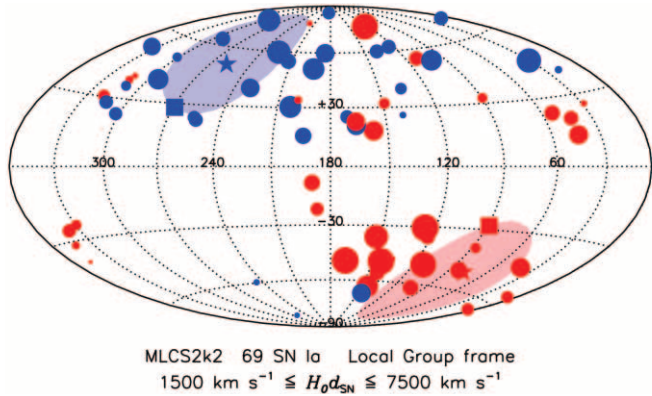


FIG. 18.—Peculiar velocities of 69 SNe Ia with  $1500 \text{ km s}^{-1} \leq H_0 d_{\text{SN}} \leq 7500 \text{ km s}^{-1}$  in the rest frame of the Local Group, plotted in Galactic coordinates (with central meridian  $l = 180^\circ$ ). The blue circles indicate SNe Ia in galaxies with negative peculiar velocities (i.e., approaching us relative to the cosmic expansion). The red circles indicate positive peculiar velocities, objects from which we are moving away. The area of the symbols is proportional to the amplitude of the peculiar velocity. The squares mark the location of the CMB dipole (Fixsen et al. 1996) and are drawn to scale relative to the circles, with the Local Group moving toward  $(269^\circ, +28^\circ)$  at  $635 \text{ km s}^{-1}$ . The stars show the position and amplitude of the best-fit simple dipole model to the SN data, with the shaded area indicating locations within the formal  $2\sigma$  confidence region.

Cluster galaxies at the lower end and be within the void signature discussed above at the upper end (so that monopole deviations are minimized, in addition to excluding objects with increasingly uncertain absolute peculiar velocities).

A dipole signature is clearly present in the data; a simple (naive) dipole fit to these SN data indicates that the Local Group is moving at  $541 \pm 75 \text{ km s}^{-1}$  toward  $(l, b) = (258^\circ \pm 18^\circ, +51^\circ \pm 12^\circ)$ . This is consistent with the position and amplitude of the CMB dipole,  $635 \text{ km s}^{-1}$  toward  $(269^\circ, +28^\circ)$ , at approximately the  $2\sigma$  confidence level. In addition, the paucity of SNe Ia discovered at low Galactic latitude skews the best-fit dipole away from the Galactic plane, suggesting that the SN Ia peculiar velocities are providing evidence for convergence of the local flow field to the CMB dipole at roughly the depths probed by these objects.

The full MLCS2k2 sample is quite amenable to more sophisticated analysis of the flow field (Riess et al. 1997a), such as recently performed by Radburn-Smith et al. (2004), who constrained  $\beta \equiv \Omega_M^{0.6}/b = 0.55 \pm 0.06$  comparing the nearby SN sample of Tonry et al. (2003) with the IRAS PSCz galaxy survey (Saunders et al. 2000). The ever-increasing nearby SN sample should also allow for merging and extension of elaborate local flow models, for example, such as provided by surface brightness fluctuation distances (Tonry et al. 2000). For maximum utility, we strongly encourage nearby SN discovery efforts in the southern hemisphere (which would help fill the empty region in the lower left quadrant of Figure 18).

#### 6.4. Extragalactic Extinction Laws

Extinguished SNe Ia, although less than ideal distance indicators, nevertheless provide one of the few ways to constrain the extinction law along individual lines of sight through distant galaxies (see also, e.g., Muñoz et al. 2004; but note McGough et al. 2005). The traditional method of using SNe Ia to determine the extinction and reddening properties of extragalactic dust (typically parameterized by  $R_V$ ) has been to plot the magnitude residuals (assuming a relative distance, such as from the Hubble law) in a given passband and epoch (for example, in  $B$  or  $V$  at maximum light) versus the SN color at some epoch (for instance,  $B - V$  also at maximum light). Because SNe Ia are not perfect

standard candles, this simple method fails: the magnitude residuals and the intrinsic colors are both functions of intrinsic luminosity. In the calibrated candle framework, the light-curve shape provides the intrinsic luminosity (through a parameterization such as  $\Delta m_{15}$ ). However, SNe Ia with different light-curve shapes have varying luminosities *and* colors, so determination of  $R_V$  depends critically on disentangling the intrinsic variation from the contributions of dust.<sup>21</sup>

By choosing objects in early-type host galaxies, or those that are not located in spiral arms, and using the observations at times when the intrinsic colors are nearly independent of luminosity (e.g., the Lira law for the late-time evolution of  $B - V$ ; § 2.3), it is possible to derive and correct for the relation between intrinsic luminosity and color and construct a sample of magnitude residuals and color excesses that are dominated by the effect of host galaxy dust. From this procedure Phillips et al. (1999) found  $R_V = 2.6 \pm 0.4$ , lower than but roughly consistent with the canonical  $R_V = 3.1$  for Galactic dust. Similarly, Altavilla et al. (2004) find  $R_V = 2.5$  and Reindl et al. (2005) give  $R_V = 2.65 \pm 0.15$ , using generally similar (although different in detail) methods of separating the intrinsic and dust effects on luminosity and color. Using a previous incarnation of MLCS (albeit one with too strong a dependence of intrinsic color on light-curve shape), Riess et al. (1996b) found  $R_V = 2.55 \pm 0.30$ .

Here we present a different method of determining  $R_V$ , individually for each SN Ia, using MLCS2k2. This alternative is discussed by Riess et al. (1996b) and does not require an independent estimate of the SN Ia distance. Rather, we include  $R_V$  directly as an MLCS2k2 fit parameter and make use of the relations between the extinction in different passbands (see Fig. 5 and Table 2). With only two observed passbands, such as  $B$  and  $V$  (and thus only one observed color), the three parameters  $\mu_0$ ,  $A_V^0$ , and  $R_V$  are degenerate, so we require observations in at least three passbands to constrain  $R_V$  directly.<sup>22</sup> Because the distance modulus shifts magnitudes in all passbands uniformly, this approach is effectively the same as constraining  $R_V$  from multiple color excesses [e.g.,  $E(V - I)/E(B - V)$ ; Riess et al. 1996b].

An advantage of this method is that we do not require independent distances; therefore, extinguished SNe Ia with recession velocities too small to give reliable Hubble flow distances can still be used to constrain  $R_V$ . In addition, because MLCS2k2 explicitly utilizes a model covariance matrix, the constraints on  $R_V$  properly account for correlated uncertainties in the data and the model, as well as the effect of the intrinsic dispersion in the luminosities and colors. Furthermore, MLCS2k2 requires the data in all passbands (for one SN) to be fitted by a consistent  $R_V$ , and required constraints such as  $R_B = R_V + 1$  are automatically enforced (not necessarily the case in the alternate method where residuals in  $B$  and  $V$  are independently regressed against the color excess; Phillips et al. 1999; Reindl et al. 2005).

The main disadvantage to this approach is a lack of sensitivity. The intrinsic variation in SN Ia colors, observational

<sup>21</sup> Tripp & Branch (1999) constructed a two-parameter model for SN Ia distances based on fitting SN Ia peak magnitudes as a linear function of  $\Delta m_{15}$  and peak  $B - V$  that explicitly forgoes any attempt at the difficult problem of separating these two causes for faint, red SNe Ia. This model is particularly sensitive to the makeup of the sample and requires care in its application. The same applies to the model of Parodi et al. (2000).

<sup>22</sup> Another approach that would work for Hubble flow SNe Ia with only two observed passbands in the MLCS2k2 framework would be to use the Hubble law to put a prior on  $\mu_0$  and then fit for  $A_V^0$  and  $R_V$ . This would essentially be the same as using magnitude residuals with respect to the Hubble line as discussed above. However, almost all of the nearby SNe Ia presented here have observations in three or more filters, and so we can use the direct method.

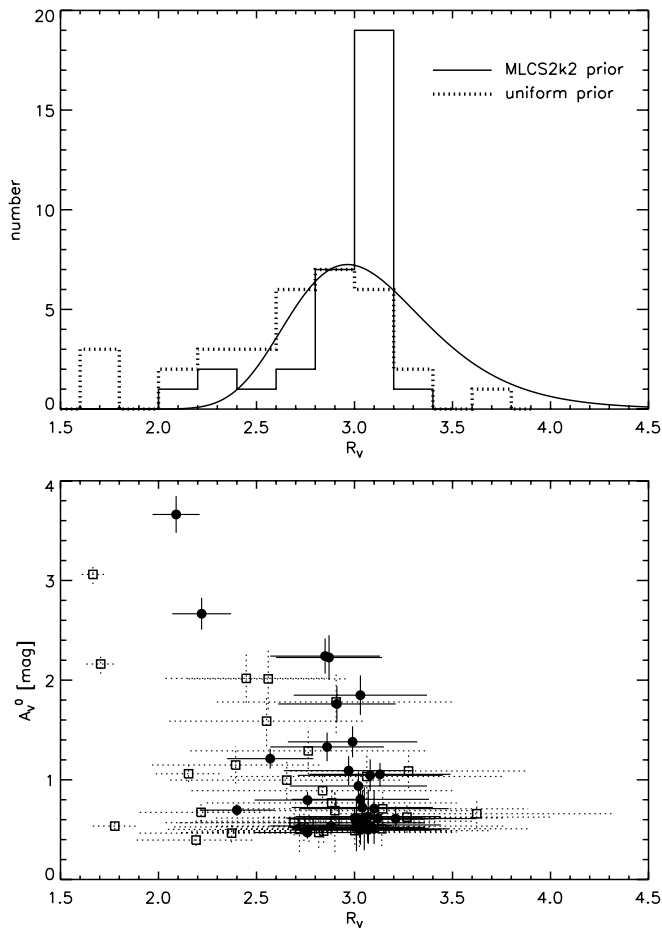


FIG. 19.—Distribution of the host galaxy extinction law parameter,  $R_V$ , and its correlation with the host galaxy extinction  $A_V^0$ . The solid line in the top panel shows the adopted MLCS2k2 prior,  $\hat{p}(R_V)$ , which is a Gaussian in  $R_V^{-1}$  and has a mean  $R_V = 3.1$  with a standard deviation of 0.4. The solid histogram shows the distribution of the mean  $R_V$  for 33 extinguished SNe Ia, using MLCS2k2 and  $\hat{p}(R_V)$ , listed in Table 4. The dotted histogram shows the distribution if a uniform prior for  $R_V \geq 1.6$  is adopted instead. The filled circles in the bottom panel show the mean  $R_V$  and  $A_V^0$  using the MLCS2k2 prior for these 33 objects, while the open squares with dotted error bars correspond to results based on the uniform prior. [See the electronic edition of the Journal for a color version of this figure.]

uncertainties, and the subtle relative color differences (in the optical bands) with changes in the extinction law combine to make the constraints on  $R_V$  relatively weak for individual SNe Ia. Unfortunately, the  $U$  band, which has the most sensitivity to varying  $R_V$ , also has the most intrinsic dispersion (and this is clearly not related to  $R_V$ ; Jha et al. 2006). In the top panel of Figure 19 we plot a histogram of the mean values of  $R_V$  for the sufficiently extinguished SNe Ia tabulated in Table 4, and we show the relation between  $R_V$  and  $A_V^0$  for these objects in the bottom panel.

On first inspection, the data show a clustering near  $R_V \simeq 3.1$ , with a handful of objects with smaller values and hardly any with significantly larger values. However, because of the lack of sensitivity to  $R_V$  even for these moderately extinguished objects, the results turn out to be quite dependent on the choice of prior,  $\hat{p}(R_V)$ . As described in § 5, we have used a prior on  $R_V$  based on its distribution along Galactic lines of sight from CCM89, which is a Gaussian in  $R_V^{-1}$  and is shown as the solid line in the top panel of Figure 19. When data are increasingly informative, the posterior pdf is decreasingly sensitive to the choice of prior, but in this case the data only weakly constrain  $R_V$  and the prior matters. Using the extreme case of a uniform

prior for  $R_V \geq 1.6$  (implying that we are completely ignorant of the relative likelihood of these different kinds of dust distributions) yields the dotted histogram and open squares in Figure 19. Even this is not completely satisfactory because three objects favor  $R_V$  at the (arbitrary) lower limit of the prior, which becomes increasingly unlikely (and perhaps unphysical; Draine 2003 and references therein): lower  $R_V$  corresponds to dust that reddens more and more for a given attenuation, favoring smaller and smaller grains.

Nevertheless, even with this significant dependence on the prior, some results regarding  $R_V$  are robust. The effect of the prior is less important for objects that have very high extinction ( $A_V^0 \gtrsim 2$  mag). In particular, the two most heavily extinguished objects in the sample, SN 1996ai and SN 1999cl, both firmly require  $R_V < 3.1$ . In addition, the posterior pdf has important differences from the prior pdf (which is displayed normalized to the same total area). There is a distinct deficit of SNe Ia that yield  $R_V$  significantly greater than 3.1, whereas many such sight lines exist in the Milky Way (particularly in dense clouds, with  $R_V \simeq 4-5$ ). The SN Ia  $R_V$  distribution may be more similar to lines of sight in the Magellanic Clouds (Gordon & Clayton 1998; Misselt et al. 1999), which typically have lower  $R_V$ , and it might be worthwhile to investigate priors on  $R_V$  derived from more sophisticated models and larger samples of stars, including LMC and SMC lines of sight (Reichart 2001). An important possibility to consider is that the dust around heavily extinguished SNe Ia may be local to the SN environment; SN 1995E, for example, with  $A_V^0 = 2.24 \pm 0.18$  mag, occurred in a relatively face-on host galaxy, suggesting that our line of sight to the SN does not have a large path length in the galaxy disk. If “local” dust plays a significant role, the  $R_V$  distribution could be quite different for moderately and heavily extinguished SNe Ia, and such an effect may be difficult to discern using the method that correlates residuals with color because the most reddened objects have the largest lever arm.

Constraints on  $R_V$  could also be strengthened if we included photometry in other passbands. Observations further in the UV would be increasingly sensitive to variations in  $R_V$ , but they are difficult to obtain (requiring space-based data for nearby extinguished SNe Ia or very deep ground-based data for distant extinguished SNe Ia for which the desired wavelengths redshift past the atmospheric cutoff), and the intrinsic SN Ia magnitudes and dispersions are unexplored at these wavelengths. On the other hand, near-infrared data will be extremely valuable in providing a long-wavelength baseline to constrain both the extinction and the extinction law (e.g., Krisciunas et al. 2006 and references therein). We are currently developing a method to incorporate infrared photometry into MLCS2k2 by using observations in  $JHK$  to provide a joint prior constraint on  $R_V$  and  $A_V^0$ , which is then used to fit the optical data (S. Jha et al. 2007, in preparation).

What are the effects of possible variations in  $R_V$  on our derived MLCS2k2 distances? The results from the extinguished objects with a uniform prior have a mean  $\langle R_V \rangle = 2.7$  (with the default MLCS2k2 prior, the mean is 2.9). The majority of the Hubble flow sample has low extinction, where  $R_V$  variation has nearly negligible effects, and we had fixed  $R_V \equiv 3.1$  for objects with  $A_V^0 < 0.5$  mag. We have refitted the full Hubble flow sample using a new prior with the same shape but  $\langle R_V \rangle = 2.7$ , as well as a fixed  $R_V \equiv 2.7$  for objects with  $A_V^0 < 0.5$  mag. On average, the distance moduli increase by 0.019 mag, with an average increase for the fixed  $R_V$  subsample of 0.014 mag (both corresponding to less than a 1% increase in distance). The effect of a smaller  $R_V$  on differential measurements (such as determining

$H_0$  from the Hubble flow sample and a Cepheid-calibrated sample) would be less because all distances would be slightly increased. At present, we find no compelling evidence to favor a constant  $R_V = 2.7$  over  $R_V = 3.1$  for low-extinction SNe Ia samples such as are typically used in cosmological applications. Allowing for  $R_V$  variations over this range could yield a plausible estimate of the systematic uncertainty, but more problematic for precision cosmology would be a systematic change in the  $R_V$  distribution with redshift.

We thank Alex Filippenko, Weidong Li, Kevin Krisciunas, and Nick Suntzeff for providing access to unpublished spec-

troscopy and photometry. We also thank Peter Challis, Peter Garnavich, Peter Nugent, Steve Furlanetto, and Tom Matheson for helpful discussions, as well as the anonymous referee for useful suggestions. S. J. gratefully acknowledges support at UC Berkeley via a Miller Research Fellowship and NSF grant AST 03-07894 to A. V. Filippenko, as well as the Panofsky Fellowship at KIPAC/SLAC, supported in part by the Department of Energy contract DE-AC02-76SF00515. Research on SNe at Harvard University is supported by NSF grant AST 02-05808.

This research has made use of the NASA/IPAC Extragalactic Database (NED), which is operated by the Jet Propulsion Laboratory, California Institute of Technology, under contract with the National Aeronautics and Space Administration.

## APPENDIX

### EXTINCTION PRIORS

Measurements of the luminosity distances to SNe Ia need to account for the line-of-sight absorption by dust to yield a precise and accurate estimate. The most common approach is to measure the color excess resulting from selective absorption and, with the use of a reddening law, estimate the extinction. Unfortunately, uncertainty in the fiducial color frequently dominates the individual distance uncertainty, arising from the uncertainty (added in quadrature) of two true flux measurements and the intrinsic dispersion of SN Ia colors. Frequent and high-precision monitoring of nearby SNe Ia can remove the contribution of measurement uncertainty, revealing the intrinsic color dispersion to be approximately 0.05 mag for optical colors as shown in Figure 6. Multiplying this intrinsic uncertainty by a standard reddening law,  $R_V = 3.1$ , yields the observed SN Ia distance dispersion of 0.15–0.20 mag. However, failure to measure colors to better precision than the intrinsic dispersion may result in greatly degraded distance precision.

A significant improvement in the extinction estimate can be realized by the use of a Bayesian prior on the extinction parameter because a good deal is known about the likely values of extinction, a priori. The most basic and unassailable truths about extinction are that it cannot be negative<sup>23</sup> and that increasing values are decreasingly likely due to the unlikely viewing angles required for large extinction and, for some surveys, magnitude limits. Models by Hatano et al. (1998), Commins (2004), and Riello & Patat (2005) show that for late-type galaxies, the likelihood distribution for extinguished lines of sight follows an exponential function with a maximum at zero extinction. In Figure 6 we use this function constrained by the a posteriori color distribution to determine a decay constant for the exponential of  $\sim 0.5$  mag in  $A_V$ . The use of such an extinction prior represents great potential improvement to this precision-limiting measure of SN Ia distances. This approach was first used by Riess et al. (1996a) and later by Riess et al. (1998b) and Phillips et al. (1999), as well as in the present work. However, the well-known danger of using a priori information is that it may be in error and thus propagate systematic errors into the final distance estimate. In addition, one must be careful to use an unbiased estimator of extinction from the posterior likelihood distribution to avoid additional systematic error. To weigh the advantages and disadvantages of using extinction priors for realistic measurements of SNe Ia, we have undertaken a set of Monte Carlo simulations.

Our simulations model  $10^4$  SNe Ia, each with a fixed intrinsic  $B - V$  color drawn from a Gaussian distribution (with zero mean and standard deviation  $\sigma_{\text{int}}$ ) and an extinction  $A_V$  drawn from an exponential distribution (with scale length  $\tau$ ). We then simulate  $n_{\text{obs}}$  measurements of the SN  $B - V$  color, each with a Gaussian error  $\sigma_{\text{meas}}$ , and subsequently “fit” for the extinction, determining its posterior pdf with the application of a prior (either the true one describing the input extinction distribution, a more conservative prior, none at all, or an incorrect one). For each posterior pdf we extract both the mean and the mode, calculate the error between the posterior estimate and the input extinction, and analyze this error distribution over the whole simulated sample. These quantities may also be calculated analytically using Bayes’s theorem, but we prefer the numerical approach for ease of the incorporation of a variety of functional forms for the extinction prior.<sup>24</sup>

As an example, we show in Figure 20 the results for  $n_{\text{obs}} = 5$ ,  $\sigma_{\text{meas}} = 0.1$  mag,  $\sigma_{\text{int}} = 0.05$  mag, and  $\tau = 0.5$  mag, parameters chosen to correspond to adequate but minimal color measurements, such as those used in Riess et al. (1998b) for the detection of cosmic acceleration, and we have fitted the simulated sample with both the correct prior [ $\hat{p}(A_V) \propto \exp(-A_V/\tau)$ , with  $\tau = 0.5$  mag] and no prior at all (allowing the fit  $A_V$  to be negative as well).

As shown, use of the mean of the individual extinction likelihoods results in an unbiased estimate of the extinction and an increased precision relative to the absence of an extinction prior. Because the weight of distance estimates for cosmological parameter estimation is proportional to the square of the uncertainty, the precision of 0.18 mag per SN Ia using the prior represents a 50% improvement over the use of no prior for this realistic case. For more poorly measured colors ( $\sigma_{\text{meas}} = 0.2$  mag) or fewer independent measurements, the improvement approaches a factor of 2, akin to doubling the cosmological sample.

Another way extinction priors yield benefits besides improved distance precision is by reining in errors in the knowledge of the intrinsic properties of SNe Ia. The most relevant example is our estimate of the fiducial, unreddened color of an SN Ia, used to estimate the color excess and the net extinction. As an example we consider in Figure 21 the extinction bias resulting from a misestimate of the

<sup>23</sup> For the case of rare light echoes in the presence of excessive quantities of circumstellar dust, scattering can add some additional light to the observer’s view, although the net effect is still positive extinction, albeit with a different ratio of selective to total absorption as discussed by Wang (2005).

<sup>24</sup> The simulation routine is available at <http://astro.berkeley.edu/~saurabh/mlcs2k2/>.

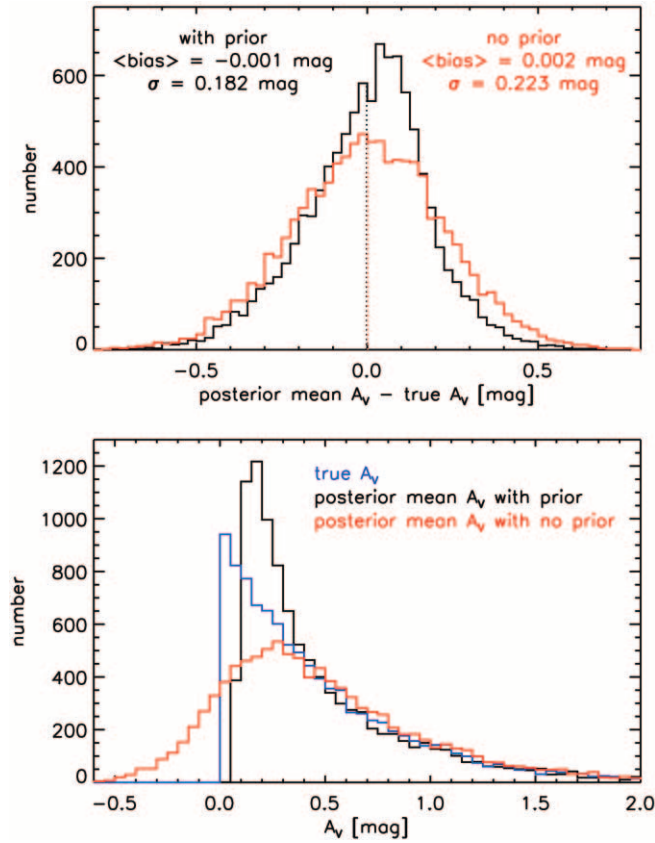


FIG. 20.—Distributions of the extinction bias (*top*) and input and posterior mean extinction (*bottom*) from a simulation of  $10^4$  SNe Ia, with a Gaussian intrinsic  $B - V$  color scatter of  $\sigma_{\text{int}} = 0.05$  mag, “observed” on five epochs with a precision of  $\sigma_{\text{meas}} = 0.1$  mag in each color measurement. The SNe are drawn from an exponential  $A_V$  distribution with a scale length  $\tau = 0.5$  mag (*blue histogram*) and then fitted with a prior matching the extinction distribution (*black histogram*), as well as without any prior (*red histogram*). For each fit, the mean of the posterior extinction distribution (with and without a prior) is used as the extinction estimate, and these distributions are shown in the bottom panel. The top panel then shows the difference between the posterior mean extinction and the true extinction. Use of the correct extinction prior shows no mean bias (*dotted lines*) and improves the precision of the extinction measurement.

unreddened color (with the previous minimal but adequate color measurements). Without a prior the systematic extinction error is exactly the color error multiplied by the reddening law. With the prior, the extinction error becomes smaller because the valuable knowledge about the likely extinction weighs in, reducing the effect of the measurement inaccuracy. Taking a realistic example of a 0.03 mag misestimate in the unreddened color, the bias is reduced from 0.10 mag without a prior to 0.07 mag with the prior. However, the net bias for most cosmological measurements will be negligible if the color error (and extinction distribution) is independent of redshift. For cosmological measurements, this color error may be usefully thought of as a *color evolution*. Again, for such a color evolution, the net bias is reduced by one-third with the use of an extinction prior.

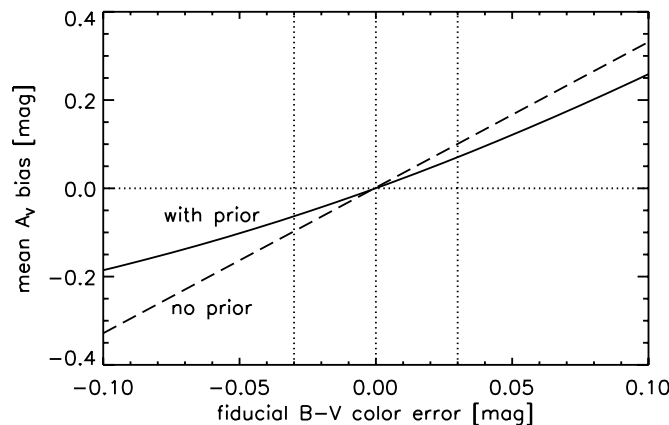


FIG. 21.—Mitigating effect of the extinction prior given an error or evolution in the mean intrinsic color. The use of the prior (*solid line*) reduces the extinction bias by a factor of  $\frac{1}{3}$  relative to no prior (*dashed line*). The dotted lines show a plausible range of  $\pm 0.03$  mag in the mean intrinsic color. [See the electronic edition of the Journal for a color version of this figure.]

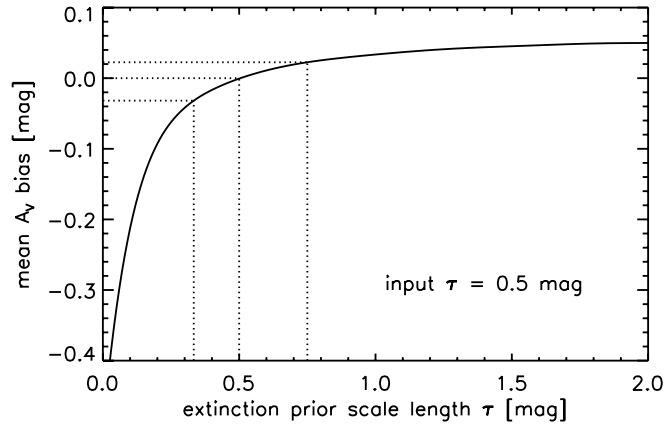


FIG. 22.—Effect of using an incorrect prior. The solid line shows the result of fitting the input distribution (created with  $\tau = 0.5$  mag) with different priors, varying the prior scale length. The dotted lines highlight the results of using the correct prior ( $\tau = 0.5$  mag, no bias) and priors with  $\tau$  larger or smaller by a factor of 1.5. This plausible range of variation (particularly in comparing different SN samples) could lead to a bias of  $\sim 0.03$  mag.

Nonetheless, a basic disadvantage of using priors is that biases may result from the use of an incorrect prior.<sup>25</sup> As an example we show in Figure 22 the extinction bias as a function of the exponential decay scale length assumed for the prior. Values differing from the input of  $\tau = 0.5$  mag result in an under- or overestimate of the mean extinction. Using the results from Riello & Patat (2005), we can guess the approximate size of an error in  $\tau$  by imagining it was determined from galaxy-based simulations, and in so doing we have misestimated the relative importance of the bulge to the total luminosity in late-type galaxies. The dotted lines show that a 30% error in this ratio (and thus reducing or augmenting the scale length by a factor of 1.5) results in a  $\sim 0.03$  mag bias. In practice (i.e., for cosmological applications), a net bias would only result from unaccounted for differences in  $\tau$  between high and low redshift such as may result from evolution or sample selection. Interestingly, we also find that the effect of taking a so-called weak prior, such as  $\hat{p}(A_V)$  constant for  $A_V \geq 0$  and zero for  $A_V < 0$ , is a worse choice, resulting in a bias of 0.07 mag. The reason is that the mean of such a prior is unnaturally large, biasing the extinction estimate in that direction. Likewise, assuming negligible extinction will result in an underestimate, equal to the mean of the true distribution (which, for an exponential, is the value of the scale length itself). The lesson is intuitively clear: when using a prior it is important to take the best estimate (and estimate a systematic error from the range of good guesses) as a seemingly “conservative” or “weak” version can be worse.

For a specific SN sample it is probably best to simulate the sources and sizes of uncertainty depending on the data quality before determining whether the use of an extinction prior offers more to gain than to lose. Our simulations reveal nothing that intuition does not: a good measurement is better than a bad prior, and a good prior will improve imperfect measurements.

<sup>25</sup> A bias can also occur when a moment other than the mean of the individual extinction likelihood function is used as discussed by Perlmutter et al. (1999). For example, in Riess et al. (1998b) the maximum likelihood (i.e., the mode of posterior distribution) was initially used, which results in a 0.06 mag bias as determined from our simulation. However, because the bias occurs for both low- and high-redshift SNe Ia similarly, the net bias (i.e., in the difference) was much smaller. Modeling the low-redshift SNe Ia as having twice as many observations each with twice the individual precision ( $n_{\text{obs}} = 10$ ,  $\sigma_{\text{meas}} = 0.05$  mag) shows that the net bias is 0.02 mag in the distance difference at low and high redshifts, much smaller than the 0.05 mag error in the mean of the high-redshift sample.

#### REFERENCES

- Altavilla, G., et al. 2004, *MNRAS*, 349, 1344  
 Benetti, S., et al. 2004, *MNRAS*, 348, 261  
 Bessell, M. S. 1990, *PASP*, 102, 1181  
 Buta, R. J., & Turner, A. 1983, *PASP*, 95, 72  
 Candia, P., et al. 2003, *PASP*, 115, 277  
 Cardelli, J. A., Clayton, G. C., & Mathis, J. S. 1989, *ApJ*, 345, 245 (CCM89)  
 Commins, E. D. 2004, *NewA Rev.*, 48, 567  
 Draine, B. T. 2003, *ARA&A*, 41, 241  
 Filippenko, A. V. 1997, *ARA&A*, 35, 309  
 Filippenko, A. V., et al. 1992, *AJ*, 104, 1543  
 Fitzpatrick, E. L. 1999, *PASP*, 111, 63  
 Fixsen, D. J., Cheng, E. S., Gales, J. M., Mather, J. C., Shafer, R. A., & Wright, E. L. 1996, *ApJ*, 473, 576  
 Ford, C. H., Herbst, W., Richmond, M. W., Baker, M. L., Filippenko, A. V., Treffers, R. R., Paik, Y., & Benson, P. J. 1993, *AJ*, 106, 1101  
 Freedman, W. L., et al. 2001, *ApJ*, 553, 47  
 Friedman, A., King, J. Y., & Li, W. D. 1999, *IAU Circ.*, 7286, 1  
 Furlanetto, S., & Piran, T. 2006, *MNRAS*, 366, 467  
 Gallagher, J. S., Garnavich, P. M., Berlind, P., Challis, P., Jha, S., & Kirshner, R. P. 2005, *ApJ*, 634, 210  
 Garnavich, P. M., et al. 2004, *ApJ*, 613, 1120  
 Geller, M. J. 1997, *Rev. Mod. Astron.*, 10, 159  
 Germany, L. M., Riess, D. J., Schmidt, B. P., Stubbs, C. W., & Suntzeff, N. B. 2004, *A&A*, 415, 863  
 Giovanelli, R., Dale, D. A., Haynes, M. P., Hardy, E., & Campusano, L. E. 1999, *ApJ*, 525, 25  
 Goldhaber, G., et al. 2001, *ApJ*, 558, 359  
 Gordon, K. D., & Clayton, G. C. 1998, *ApJ*, 500, 816  
 Guy, J., Astier, P., Nobili, S., Regnault, N., & Pain, R. 2005, *A&A*, 443, 781  
 Hamuy, M., Phillips, M. M., Maza, J., Suntzeff, N. B., Schommer, R. A., & Avilés, R. 1995, *AJ*, 109, 1  
 Hamuy, M., Phillips, M. M., Maza, J., Wischnjewsky, M., Uomoto, A., Landolt, A. U., & Khatwani, R. 1991, *AJ*, 102, 208  
 Hamuy, M., Phillips, M. M., Suntzeff, N. B., Schommer, R. A., Maza, J., Smith, R. C., Lira, P., & Avilés, R. 1996a, *AJ*, 112, 2438  
 Hamuy, M., Phillips, M. M., Wells, L., & Maza, J. 1993, *PASP*, 105, 787  
 Hamuy, M., Trager, S. C., Pinto, P. A., Phillips, M. M., Schommer, R. A., Ivanov, V., & Suntzeff, N. B. 2000, *AJ*, 120, 1479  
 Hamuy, M., et al. 1996b, *AJ*, 112, 2408  
 Hatano, K., Branch, D., & Deaton, J. 1998, *ApJ*, 502, 177  
 Hubble, E. P. 1929, *Proc. Natl. Acad. Sci.*, 15, 168  
 Hudson, M. J., Smith, R. J., Lucey, J. R., & Branchini, E. 2004, *MNRAS*, 352, 61  
 Jha, S. 2002, Ph.D. thesis, Harvard Univ.  
 Jha, S., Challis, P., Garnavich, P., Kirshner, R., & Calkins, M. 1999a, *IAU Circ.*, 7298, 2  
 Jha, S., et al. 1999b, *ApJS*, 125, 73  
 ———. 2006, *AJ*, 131, 527

- Kim, A., Goobar, A., & Perlmutter, S. 1996, *PASP*, 108, 190
- Kirshner, R. P. 2004, *Proc. Natl. Acad. Sci.*, 101, 8
- Knop, R. A., et al. 2003, *ApJ*, 598, 102
- Krisciunas, K., Hastings, N. C., Loomis, K., McMillan, R., Rest, A., Riess, A. G., & Stubbs, C. 2000, *ApJ*, 539, 658
- Krisciunas, K., Prieto, J. L., Garnavich, P. M., Riley, J.-L. G., Rest, A., Stubbs, C., & McMillan, R. 2006, *AJ*, 131, 1639
- Krisciunas, K., et al. 2001, *AJ*, 122, 1616
- . 2003, *AJ*, 125, 166
- . 2004a, *AJ*, 127, 1664
- . 2004b, *AJ*, 128, 3034
- Lahav, O., Lilje, P. B., Primack, J. R., & Rees, M. J. 1991, *MNRAS*, 251, 128
- Leibundgut, B., Tammann, G. A., Cadonau, R., & Cerrito, D. 1991, *A&AS*, 89, 537
- Leibundgut, B., et al. 1993, *AJ*, 105, 301
- Leonard, D. C., Li, W., Filippenko, A. V., Foley, R. J., & Chornock, R. 2005, *ApJ*, 632, 450
- Li, W., et al. 1999, *AJ*, 117, 2709
- . 2001, *PASP*, 113, 1178
- . 2003, *PASP*, 115, 453
- Lira, P. 1995, M.S. thesis, Univ. Chile
- Lira, P., et al. 1998, *AJ*, 115, 234
- McGough, C., Clayton, G. C., Gordon, K. D., & Wolff, M. J. 2005, *ApJ*, 624, 118
- Meikle, W. P. S., et al. 1996, *MNRAS*, 281, 263
- Miknaitis, G., et al. 2007, *ApJ*, submitted (astro-ph/0701043)
- Miller, N. A., Ledlow, M. J., Owen, F. N., & Hill, J. M. 2002, *AJ*, 123, 3018
- Misselt, K. A., Clayton, G. C., & Gordon, K. D. 1999, *ApJ*, 515, 128
- Modjaz, M., Li, W. D., Filippenko, A. V., King, J. Y., Leonard, D. C., Matheson, T., & Treffers, R. R. 2001, *PASP*, 113, 308
- Muñoz, J. A., Falco, E. E., Kochanek, C. S., McLeod, B. A., & Mediavilla, E. 2004, *ApJ*, 605, 614
- Nobili, S., Goobar, A., Knop, R., & Nugent, P. 2003, *A&A*, 404, 901
- Nobili, S., et al. 2005, *A&A*, 437, 789
- Nugent, P., Kim, A., & Perlmutter, S. 2002, *PASP*, 114, 803
- O'Donnell, J. E. 1994, *ApJ*, 422, 158
- Parodi, B. R., Saha, A., Sandage, A., & Tammann, G. A. 2000, *ApJ*, 540, 634
- Patat, F., Benetti, S., Cappellaro, E., Danziger, I. J., Della Valle, M., Mazzali, P. A., & Turatto, M. 1996, *MNRAS*, 278, 111
- Perlmutter, S., et al. 1997, *ApJ*, 483, 565
- . 1999, *ApJ*, 517, 565
- Phillips, M. M. 1993, *ApJ*, 413, L105
- Phillips, M. M., Lira, P., Suntzeff, N. B., Schommer, R. A., Hamuy, M., & Maza, J. 1999, *AJ*, 118, 1766
- Phillips, M. M., et al. 1987, *PASP*, 99, 592
- Pignata, G., et al. 2004, *MNRAS*, 355, 178
- Press, W. H., Teukolsky, S. A., Vetterling, W. T., & Flannery, B. P. 1992, *Numerical Recipes in C* (2nd ed.; New York: Cambridge Univ. Press)
- Prieto, J. L., Rest, A., & Suntzeff, N. B. 2006, *ApJ*, 647, 501
- Radburn-Smith, D. J., Lucey, J. R., & Hudson, M. J. 2004, *MNRAS*, 355, 1378
- Ramella, M., Geller, M. J., Pisani, A., & da Costa, L. N. 2002, *AJ*, 123, 2976
- Reichart, D. E. 2001, *ApJ*, 553, 235
- Reindl, B., Tammann, G. A., Sandage, A., & Saha, A. 2005, *ApJ*, 624, 532
- Richmond, M. W., et al. 1995, *AJ*, 109, 2121
- Riello, M., & Patat, F. 2005, *MNRAS*, 362, 671
- Riess, A. G., Davis, M., Baker, J., & Kirshner, R. P. 1997a, *ApJ*, 488, L1
- Riess, A. G., Nugent, P., Filippenko, A. V., Kirshner, R. P., & Perlmutter, S. 1998a, *ApJ*, 504, 935
- Riess, A. G., Press, W. H., & Kirshner, R. P. 1995a, *ApJ*, 438, L17
- . 1995b, *ApJ*, 445, L91
- . 1996a, *ApJ*, 473, 88
- . 1996b, *ApJ*, 473, 588
- Riess, A. G., et al. 1997b, *AJ*, 114, 722
- . 1998b, *AJ*, 116, 1009
- . 1999, *AJ*, 117, 707
- . 2004, *ApJ*, 607, 665
- . 2005, *ApJ*, 627, 579
- Salvo, M. E., Cappellaro, E., Mazzali, P. A., Benetti, S., Danziger, I. J., Patat, F., & Turatto, M. 2001, *MNRAS*, 321, 254
- Sandage, A., Tammann, G. A., Saha, A., Reindl, B., Macchetto, F. D., & Panagia, N. 2006, *ApJ*, 653, 843
- Saunders, W., et al. 2000, *MNRAS*, 317, 55
- Schlegel, D. J., Finkbeiner, D. P., & Davis, M. 1998, *ApJ*, 500, 525
- Stritzinger, M., et al. 2002, *AJ*, 124, 2100
- Strolger, L.-G., et al. 2002, *AJ*, 124, 2905
- Suntzeff, N. B., et al. 1999, *AJ*, 117, 1175
- Szabó, Gy. M., Sárneczky, K., Vinkó, J., Csák, B., Mészáros, Sz., Székely, P., & Bebesi, Zs. 2003, *A&A*, 408, 915
- Tonry, J. L., Blakeslee, J. P., Ajhar, E. A., & Dressler, A. 2000, *ApJ*, 530, 625
- Tonry, J. L., et al. 2003, *ApJ*, 594, 1
- Tripp, R., & Branch, D. 1999, *ApJ*, 525, 209
- Tsvetkov, D. Yu. 1982, *Soviet Astron. Lett.*, 8, 115
- Turatto, M., Benetti, S., Cappellaro, E., Danziger, I. J., Della Valle, M., Gouiffes, C., Mazzali, P. A., & Patat, F. 1996, *MNRAS*, 283, 1
- Turatto, M., Piemonte, A., Benetti, S., Cappellaro, E., Mazzali, P. A., Danziger, I. J., & Patat, F. 1998, *AJ*, 116, 2431
- Turner, E. L., Cen, R., & Ostriker, J. P. 1992, *AJ*, 103, 1427
- Valentini, G., et al. 2003, *ApJ*, 595, 779
- Wang, L. 2005, *ApJ*, 635, L33
- Wang, L., Goldhaber, G., Aldering, G., & Perlmutter, S. 2003, *ApJ*, 590, 944
- Wang, X., Wang, L., Zhou, X., Lou, Y.-Q., & Li, Z. 2005, *ApJ*, 620, L87
- Wells, L. A., et al. 1994, *AJ*, 108, 2233
- Zehavi, I., Riess, A. G., Kirshner, R. P., & Dekel, A. 1998, *ApJ*, 503, 483